KfK 3701 e
Dezember 1990

Triggered Fragmentation Experiment with Sodium, Silicone Oil, and Pentane

T. Morita
Institut für Reaktorentwicklung

Kernforschungszentrum Karlsruhe

KERNFORSCHUNGSZENTRUM KARLSRUHE
Institut für Reaktorentwicklung

KfK 3701 e

Triggered Fragmentation Experiment with Sodium, Silicone Oil and Pentane

T. Morita

Kernforschungszentrum Karlsruhe GmbH, Karlsruhe

Als Manuskript gedruckt

Kernforschungszentrum Karlsruhe GmbH
Postfach 3640, 7500 Karlsruhe 1

ISSN 0303-4003

Triggered Fragmentation Experiment with Sodium, Silicone Oil and Pentane *

Summary

Within the analysis of severe hypothetical fast breeder accidents the consequences of a fuel-coolant-interaction have to be considered, i. e. the thermal interaction between hot molten fuel and sodium. For the detailed understanding of the fragmentation during the thermal interaction of a hot liquid droplet with a cold fluid a series of experiments was performed with sodium and silicone oil as a hot liquid and pentane as cold easily volatile fluid. For the precise observation of the reaction an efficient high speed camera with a maximum recording frequency of $1 \cdot 10^5$ f/s was used. So the fragmentation caused by boiling phenomena could be observed. The pictures were used to estimate quantitatively e. g. the volume of the reaction zone and its expansion rate. By a special measuring device for the first time results on the time dependent portion of the liquid within the reaction zone could be gained. Based on the measured results of the experiments the course of a typical reaction, which can be devided into six phases, is presented and physically explained in this report. The influence of experimental parameters, as pressure of the external trigger and temperature of the hot liquid droplet, was investigated and from this the role of both the homogeneous nucleation temperature and the external trigger for the reaction was deduced. A model for the fragmentation is presented too. By this model the fragmentation of the hot droplet and its mixing with the surrounding fluid are explained by the instability of the boundaries due to the high pressure build up at local direct contact. Based on the fragmentation model two numbers are deduced, which characterize the violence of the boiling fragmentation to be expected. These numbers are applied on UO_2 and sodium. These materials are in contact during a real fuel-coolant interaction. Hence these materials tend to a mild boiling fragmentation only.

* English translation of KfK 3701, April 1984

Getriggertes Fragmentationsexperiment mit Natrium, Silikonöl und Pentan

Zusammenfassung

Bei der Analyse von schweren, hypothetischen Schnellbrüterstörfällen sind die Auswirkungen einer BNR, d. h. thermischen Reaktion des heißen Brennstoffs mit Natrium zu berücksichtigen. Zum detaillierten Verständnis des entscheidenden Fragmentationsvorgangs bei der thermischen Wechselwirkung eines heißen Flüssigkeitstropfens mit einer kalten Flüssigkeit wurden Versuchsreihen mit Natrium und Silikonöl als heiße Flüssigkeit und Pentan als kalte leichtflüchtige Flüssigkeit durchgeführt. Zur genauen Beobachtung des Reaktionsvorgangs, die durch Siedevorgänge bedingte Fragmentation eingeschlossen, was bei bisherigen Arbeiten nicht gegeben war, wurde eine leistungsfähige Hochgeschwindigkeitskamera mit einer maximalen Aufnahmegeschwindigkeit von $1 \cdot 10^5$ B/s eingesetzt. Diese Aufnahmen wurden zu verschiedenen quantitativen Abschätzungen wie Volumen der Reaktionszone sowie deren Wachstumsrate verwendet. Mit einer besonderen Methode konnten zum ersten Mal Ergebnisse zum zeitabhängigen Flüssigkeitsanteil in der Reaktionszone gewonnen werden. Basierend auf den Meßergebnissen wird in diesem Bericht ein typischer Reaktionsvorgang, der in sechs Phasen unterteilt werden kann, dargestellt und physikalisch begründet. Die Einflüsse von Versuchsparametern, wie externer Triggerdruck und Temperatur des heißen Tropfens, wurden untersucht und daraus die Rolle der homogenen Keimbildungstemperatur und des externen Triggers bei der Reaktion klargestellt. Ein Fragmentationsmodell wird ebenfalls vorgestellt. Nach diesem Modell sind Fragmentation des heißen Tropfens und Vermischung mit der umgebenden Flüssigkeit durch Grenzflächeninstabilitäten aufgrund des hohen örtlichen Dampfdruckaufbaus an Direktkontaktstellen zu erklären. Basierend auf dem Fragmentationsmodell werden zwei Kennzahlen über die zu erwartende Heftigkeit der Siedetemperaturen abgeleitet. Diese Kennzahlen werden auf die bei einer BNR vorliegende Materialpaarung UO_2-Na angewendet. Demnach neigt diese Materialpaarung nur zu einer milden Siedefragmentation.

Table of Contents

1. Introduction 1

2. Review of Important Earlier Studies, and Goals of these Studies 2

2.1 Vapour Explosion 2

2.1.1 Theoretical Models of the Vapour Explosion Process 4

2.1.2 General Results of Vapour Explosion Experiments 7

2.2 Fragmentation Models and Experiments 8

2.2.1 Hydrodynamic Fragmentation 8

2.2.2 Boiling Fragmentation (Thermodynamic Fragmentation) 10

2.3 Problem Definition and Goals of the Present Study 11

3. Conduct of Experiments 13

3.1 Conception of Experimental Set-Up 13

3.1.1 Selection of Experimental Materials 13

3.1.2 Experimental Set-Up 14

3.2 Measuring System 15

3.2.1 Temperature, Pressure, and Film Recording 15

3.2.2 Determination of the Liquid Fraction in the Reaction Zone 16

3.2.3 Fragment Size 17

3.3 Experimental Parameters 17

3.4 Experimental Procedure 19

3.5 Error Assessment 20

4. Experimental Results 23

4.1 General Remarks 23

4.1.1 Boiling Pattern 23

4.1.2 Characteristic Trigger Pressure Curve 23

4.1.3 Description of the Experiments 24

4.2 Reaction Process 25
4.2.1 Reaction Pressure Curve 25
4.2.2 Reaction Process According to the High-Speed Films 27
4.2.3 Summary 31
4.3 Influence of Experimental Parameters 32
4.3.1 Time Curves for Different Experimental Parameters 32
4.3.2 Reaction Pressure and Delay Time 33
4.3.3 Summary 35
4.4 Energetic Aspects of the Trigger and the Reaction 35
4.5 Analysis of Sodium Droplet Fragments 36
5. Discussion of the Experimental Findings 37
5.1 Physical Explanation of the Reaction Process 37
5.1.1 Trigger Front Propagation and Kinetics of Vapour Film Collapse (Phase II) 37
5.1.2 Boundary Surface Instabilities (Phase III) 41
5.1.3 Transition Phase and Slow Mixing (Phases IV,V) 46
5.1.4 Estimation of Minimum Mixing Energies 47
5.1.5 Internal Energy Balance of the Reaction Zone 48
5.2 Influence of the Homogeneous Nucleation Temperature (T_{HN} Criterion) 49
5.3 Influence of the External Trigger Pressure 50
5.4 Influence of the Main Material Characteristics on the Fragmentation Process 54
6. Summary and Conclusions 57
7. Appendix A 61
8. Appendix B 65
9. Nomenclature 66
10. Bibliography 70
11. List of Tables and Figures

1. Introduction

Nuclear reactor safety has been a subject of investigation for many years. This included research on the problem of hypothetical core meltdown accidents (HCDA), i.e. accidents during which hot, molten fuel and fuel element material (corium), with a temperature far above the boiling point of the coolant (sodium, water), may come into contact with the coolant. Any contact between a hot liquid and a cooler, volatile liquid may induce violent, coherent vapour explosions releasing large amounts of energy which may cause the reactor tank to fail.

Serious vapour explosion accidents involving the killing or wounding of humans and loss of costly equipment are known to have occurred in the metal industry, the paper industry, and in liquid natural gas handling.

In a nuclear reactor, the consequences of a coherent vapour explosion would be serious, as large amounts of radioactive materials would be released into the environment in case of reactor tank failure. A HCDA involving a coherent vapour explosion might be caused by

- uncontrolled increase of reactivity
- failure of the cooling and emergency shutdown systems.

In order to prevent these initiating events from happening and from developing into a HCDA, nuclear reactors are equipped with redundant and diversified safety systems /1/. For a better understanding of the risks involved in a reactor accident, safety analyses like WASH 1400 and the "German Risk Study" were carried out. The German Risk Study showed, e.g., that the probability of a vapour explosion occurring in a LWR is less than 2×10^{-6} per annum, i.e. the occurrence of a coherent vapour explosion during a reactor accident cannot be totally excluded although it is highly improbable /2/.

For these reasons, there have been many experimental studies on vapour explosions, and a number of theories for their physical interpretation have been forwarded. In spite of this, the basic mechanisms and influencing parameters of a vapour explosion still are not completely understood.

A vapour explosion is defined as a sudden evaporation of a cool liquid by fast heat transfer from a very hot liquid, accompanied by high pressure build-up. It is also referred to as "thermal explosion" or "fuel-sodium interaction". A sudden evaporation process with high pressure build-up takes place only if the time of

heat transfer is shorter than the expansion time of the vapour/liquid mixture. This intensive mixing, i.e. the fragmentation of the hot liquid, is a key factor in a vapour explosion.

In the present study, the fragmentation mechanism will be investigated experimentally, and the results will be analyzed and discussed. Chapter 2 will start with a survey of important experimental and theoretical studies on fragmentation and vapour explosion and an outline of the present state of knowledge. The problems to be solved will be defined, and the goals of the present investigation will be stated. Chapter 3 will describe the experimental set-up and methodology, while Chapter 4 will present the experimental findings and Chapter 5 the discussions and physical explanations of the main results based on the records of fragmentation as filmed by a high-speed camera. The influence of the main experimental parameters and material characteristics will be discussed. Chapter 6 will present the main results of this investigation and the conclusions drawn therefrom.

2. Review of Important Earlier Studies, and Goals of these Studies

2.1 Vapour Explosion

A vapour explosion is caused by a process of extremely fast heat transfer between a hot and a cold liquid, leading to sudden evaporation of the superheated cold liquid. It may comprise several events. Bankoff /3/ and Cronenberg /4/ proposed the following chains of events for the initiation of a vapour explosion, which are generally accepted today:

- First, coarse premixing of the two liquids without rapid heat transfer in a stable film boiling phase (initial phase).
- Collapse of the vapour film causing direct contact between the two liquids (trigger phase).
- Intensive mixing of the two components, so-called fragmentation, followed by rapid heat transfer with violent evaporation of the cold liquid and pressure build-up (escalation phase).
- Propagation of the reaction across the whole premixed region (propagation phase).

In the initial phase, there is a quasi-thermal insulation effect of film boiling, enabling the hot liquid to penetrate deeply into the cold liquid without being

cooled down noticeably. This penetration causes an inclusion effect (constraint of vapour expansion) which may prevent fast pressure relief. Without this constraint high pressure build-up due to evaporation of the cold liquid is impossible. Coarse pre-mixing therefore is a precondition for subsequent propagation of the reaction, i.e. for the occurrence of a coherent vapour explosion.

The vapour film collapses as a result of an external disturbance and a spontaneous film boiling instability. During film boiling at low temperature, i.e. near the minimum film boiling temperature, spontaneous local direct contact occurs more frequently /5,6/. On the other hand, an external shock wave or an intensive flow is required for making a vapour film collapse during film boiling, where the temperature of the hot liquid is far above the critical temperature of the cold liquid. There is uncertainty as yet over whether the direct contact between the two liquids may in itself initiate the further reaction.

The following two processes are possible after direct contact:

- Heat transfer during direct contact may heat the cold liquid to above its boiling point, causing sudden evaporation and fragmentation of the hot liquid (boiling fragmentation).

- With an external shock wave acting as trigger, a relative velocity or acceleration are induced between the two liquids as a result of their different densities. This relative velocity and acceleration may cause a so-called hydrodynamic instability, leading to fine fragmentation of the hot liquid. This way, the surface available for direct contact is considerably increased, and fast heat transfer to the cold liquid becomes possible. The shock wave may be further enhanced by rapid evaporation (hydrodynamic fragmentation).

The result in both cases is a high pressure build-up in the escalation phase, which disturbs the still uninterrupted film boiling process and thus maintains the reaction.

Fig. 1 shows a simplified representation of the sequences of events according to Cronenberg /4/. General necessary and sufficient conditions in which a thermal interaction will induce a vapour explosion can be derived from this:

- First, thermal energy must be available, with the hot liquid having a temperature higher than the boiling temperature of the cold liquid in order to cause evaporation.

- Coarse mixing must take place, with both components separated by a vapour film.

- Direct liquid-to-liquid contact must take place as a result of a mechanical or thermal perturbance.

- The reaction mixture must be prevented from expanding by an inclusion effect in order to cause a feedback followed by escalation of the vapour explosion.

These processes and conditions have been investigated in many experimental and theoretical studies. The main results of studies will be presented in the following chapters.

2.1.1 Theoretical Models of the Vapour Explosion Process

Hicks and Menzies /7/ presented an upper limit, i.e. a conservative estimate of the mechanical work potentially released during a vapour explosion. This model assumes spontaneous complete thermal equilibrium between the hot and cold liquid, and isentropic expansion of this mixture to a given final pressure, releasing mechanical work. During the expansion process, all components are assumed to be in thermodynamic equilibrium at any time; the model is therefore known as "equilibrium model".

The calculations show:

- There is a mass ratio of hot liquid to cold liquid at which maximum mechanical work is released, e.g. 0.1 for UO_2/Na.

- The maximum releaseable mechanical work is a function of the final pressure of the system. A lower final pressure, of course, means higher efficiency. For UO_2/Na and a final pressure of 1 bar, the efficiency is 30 %.

This model has many variations: In the "adiabatic model" of Anderson and Armstrong /8/, instead of the thermal equilibrium the thermal insulation resulting from the vapour film forming between the two liquids is considered. Results show that the mechanical work will be lower by up to 50 %. In a real reactor, cold structures or other materials may act as a heat sink and reduce the mechanical work released still further.

If the processes of fragmentation and heat exchange during the reaction are considered as well, an even more realistic estimate is obtained. For example, Caldarola /9/ presented a model in which these processes are described by given fragmentation and heat exchange times. However, this model requires specific experimental data to permit a reliable prediction of the processes, as its results are largely dependent on the two time parameters.

In other vapour explosion models, the processes of fragmentation and/or rapid vapour generation are considered as well.

The coherent vapour explosion model presented by Board, Hall, and Hall /10/ states an analogy to chemical detonations. The reaction mechanisms are described as follows: In a reactive mixture consisting of a hot and a cold liquid, the hot liquid is finely fragmented by a shock wave, thus increasing the contact surface of the two liquids to such an extent that extremely rapid heat-up (10^{-5} s) of the cold liquid takes place. Sudden evaporation of the superheated cold liquid follows, causing a pressure increase, which in turn feeds the shock wave, i.e. the reaction may propagate through the whole mixture without losing force.

In analogy to the chemical detonation, in which energy is released by combustion, this model replaces heat supply to the cold liquid by a fragmentation process, i.e. the hot liquid is fragmented independent of heat transfer. Board and Hall thus presented a type of hydrodynamic fragmentation mechanism, with a relative velocity between the two liquids behind the shock front. The important fact is that the fragmentation takes place faster than the slowing-down of the relative motion under the effect of two-phase frictional forces.

Results of calculations with this detonation model show that the energy conversion efficiency may be higher than assumed in the equilibrium model. However, this requires a very high trigger pressure up to 700 bar and a reaction pressure of 15,000 bar for the UO_2/Na system.

The detonation model first presented by Board and Hall is limited to steady shock waves. For this reason, more recent models based on transient processes are to determine the minimum trigger required for initiating a detonation.

The calculations show:

- A trigger of 10 bar is sufficient for initiating a detonation wave in the Al/H_2O system /11/.

- In the UO_2/Na system, a vapour explosion cannot be excluded in case of premixing with stable film boiling /11/.

- If the trigger pressure is very low, the length of the premixed region may not be sufficient for a significant pressure increase /12/.

These results still depend strongly on the fragmentation models used. Fauske /13,14,15/ presented a physical explanation of some vapour explosion experiments in a model assuming the following sequence of events:

- Initially, coarse mixing of the hot and cold liquid takes place while the hot phase is in the film boiling state (initial phase).

- The hot and cold liquid are made to directly interact by a disturbance (trigger phase).

- If the contact temperature is higher than the spontaneous nucleation temperature, sudden evaporation of the cold liquid in the superheated state may take place, with simultaneous fragmentation of the hot liquid (escalation phase).

- Fast relief of the built-up reaction pressure must be prevented by inclusion so that local pressure increase will cause large-area collapse of the vapour film. This induces a chain reaction of rapid heat transfer, evaporation and enhanced pressure build-up with enhanced fragmentation (propagation phase).

According to this so-called "spontaneous nucleation model", the UO_2/Na system is not susceptible to violent vapour explosions as its contact temperature is too low /14/. Fauske's model is criticized on the following grounds:

- The model comprises no quantitative assessment of the expected energy release.

- There is no detailed description of the expected fragmentation mechanism.

- The model is not valid for some experimental findings, e.g. of water/freon experiments /24/.

Ochiai /16/ and Anderson /17/ presented further, illustrative models which stress the contribution of spontaneous instabilities during the escalation phase. So far,

however, there was nothing to prove the importance of the spontaneous nucleation temperature during vapour explosion or fragmentation.

2.1.2 General Results of Vapour Explosion Experiments

Many vapour explosion experiments have been carried out so far. Most of them can be classified in three categories:

-Pouring experiments, both droplet-scale and large-scale,

- Shock tube and injection experiments,

- Simulation experiments inside and outside the reactor.

The following results were obtained:

(1) Al/water and tin/water pouring experiments /18,19,20,21/.

- All experiments leading to violent vapour explosions started with film boiling in the coarse mixing phase.

- Violent vapour explosions appear to be triggered by the collapse of the vapour film.

- A vapour explosion propagates like a detonation, with a propagation rate in the order of 100 - 200 m/s.

- There is a so-called "thermal interaction zone" (TIZ), a well defined region comprising combinations of temperatures of the two components at which a violent explosion may take place. The upper limit may be extended by applying an external trigger.

- In the THERMIR experiments /22/, apart from the coherent reactions also incoherent and local reactions were observed.

- The Al/water system always reacts more violently than the tin/ water system.

(2) The existence of a TIZ was proved by water/freon and oil/freon experiments. In the oil/freon system /23/, the TIZ is clearly located between the homogeneous nucleation temperature T_{HN} and the critical temperature. On the other hand, violent reactions were observed in the water/freon system also at contact temperatures lower than T_{HN} /17,24/.

(3) If small volumes of Na were introduced into molten UO_2, reaction energies were higher than vice versa /25/.

(4) In the shock tube experiment /26/, a higher reaction pressure was measured once in the UO_2/Na systems, but the rise time was much lower than expected from the detonation model.

(5) Violent reactions in the corium*/water and in the UO_2/water systems cannot be excluded, although the contact temperature may be far from the TIZ /27/.

(6) Simulation experiments with UO_2 (fuel) and Na (coolant) had different results. In some cases, the reaction pressures were very high, i.e. up to 600 bar /28/ or 200 bar /29/. It is uncertain whether a vapour explosion really did take place. The high pressure may be due to the high vapour pressure of the fuel.

In spite of the many large-scale pouring experiments and simulation experiments, practically no clear answer is given on what fragmentation and heat transfer mechanisms prevailed behind the shock front during propagation of the reaction. Further selective and costly experiments will be required for this.

2.2 Fragmentation Models and Experiments

The fragmentation process is the most important of all processes of a vapour explosion. It was investigated in a number of experimental and theoretical studies, some of which will be described in the following chapter.

2.2.1 Hydrodynamic Fragmentation

This model was introduced for explaining the initiation of the thermal detonation. If a shock wave passing through the surrounding fluid (gas or liquid) impacts on a droplet, the droplet may be fragmented due to the following interactions with the shock wave:

- The distribution of dynamic pressure on the droplet surface may cause deformation of the droplet. If the droplet is deformed beyond a given point, with the surface tension acting in the opposite direction, fragmentation may occur (impact fragmentation).

*molten mixture of reactor structural materials and UO_2

- Under the effect of viscosity, the tangential component of the flow at the droplet surface induces a transverse force which moves the boundary layer of the droplet. As a result, the boundary layer may disintegrate into droplets (boundary layer stripping).

- Various hydrodynamic instabilities may generate waves at the droplet surface causing droplet fragmentation:

  i) Rayleigh-Taylor instability due to high acceleration from the lighter to the heavier component

  ii) Kelvin-Helmholtz instability due to relative velocity at the boundary layers

  iii) Capillary waves resulting from the combined effect of flow pressure and surface tension.

The relative velocity between the two components and the droplet acceleration caused by the drag force resulting from the relative velocity have decisive influence on these effects. As the relative motion between the two components behind the shock front results from the difference in density or, more precisely, from the acoustic impedance ($\rho \times C$), this theory is frequently applied to droplet fragmentation in a gas flow, where the density ratio may be quite high.

There is the problem of whether this droplet fragmentation mechanism also applies in a system of two liquids, as stated by Board and Hall. To answer this question, Patel and Theofanous /30,31/ carried out a number of experiments in which a mercury droplet was fragmented in a water-filled shock tube. They found that the droplet was fragmented in about a tenth of the time as predicted even by the theory based on the Rayleigh-Taylor instability for the water droplet/air system. Bains /32/ reported similar results for mercury and water, although his droplet fragmentation times differed from those of Patel and Theofanous.

On the other hand, the theoretical study of Schriewer /33/ on hydrodynamic fragmentation points out that the processes characterized by Rayleigh-Taylor and Kelvin-Helmholtz instabilities as well as by boundary layer stripping alone are too slow for fragmentation in liquid/liquid systems for certain triggers. Therefore, a valid physical explanation of the results obtained by Patel and Theofanous or Bains is still lacking.

2.2.2 *Boiling Fragmentation (Thermodynamic Fragmentation)*

Sudden evaporation of the superheated cold liquid in the point of direct contact may cause fragmentation of the hot liquid. Two evaporation patterns are possible, i.e. violent transition boiling /34,35/ or spontaneous nucleation /36/. Fauske's vapour explosion model combines spontaneous nucleation with the contact temperature hypothesis. Recently, Wey /37/ showed in an experiment with tin and water that bubble regions existed on the contact surfaces already 1 ms before pressure build-up. In his interpretation, this suggests that the dynamic effect inducing a disturbance of the surface, i.e. fragmentation, is not caused by spontaneous nucleation but rather by normal bubble growth.

Colgate /38/ speculated that the Kelvin-Helmholtz instability caused by vapour flow in the region of bubble growth may contribute to fragmentation. Corradini /39/ combined boiling fragmentation with hydrodynamic effects. In his model, fragmentation is described by the following sequence of events:

- Non-symmetrical collapse of the vapour film
- Acceleration of the hot liquid by pressure build-up due to sudden evaporation in the contact region
- Rayleigh-Taylor instability as a result of this acceleration
- Mixing of the two liquids and further escalation of the reaction.

Although it may be speculative in character, this model is the first quantitative description of boiling fragmentation processes as influenced by thermal effects.

A number of the models proposed are of the "bubble collapse" type, in which the kinetic energy of a jet of the cold liquid, which may be generated during collapse of a full-grown bubble, contributes to fragmentation /40/. Caldarola /41/ assumed a similar mechanism for quantitative modelling of fragmentation due to bubble collapse. So far, this model has not been validated by experiments.

Other fragmentation models are based on different effects, e.g. entrainment of cold liquid in the hot liquid, thermal stresses due to solidification of the hot liquid, gas release, etc. Although they may help to explain some of the experimental findings, it is difficult to accept these models for a general explanation of the fragmentation process.

2.3 *Problem Definition and Goals of the Present Study*

The many studies on fragmentation and vapour explosion have raised new problems. Not all of these can be answered here, but some points for further research will be mentioned which are the subject of this investigation.

- Full-scale hydrodynamic fragmentation requires a certain degree of relative velocity between the two components. This relative velocity cannot be provided by external triggers alone, that are frequently used in vapour explosion experiments. At least in the early phase of the explosion, in which the shock wave has not yet developed sufficiently, a boiling fragmentation mechanism must be dominant.

- Vapour explosions in oil/freon and water/freon systems cannot be explained by hydrodynamic fragmentation alone, as the density ratio, or rather the ratio of acoustic impedance, is nearly unity. Boiling fragmentation must be dominant here.

- In the most recent results presented by Ando /42/ of his experiments with Cu droplets in water using a high-speed camera, neither non-symmetrical bubble collapse nor water jets were observed, but white spots and eruptions were visible on the surface of the Cu droplet.

These findings prove the possibility of boiling fragmentation taking place, but the following problems remain unresolved:

- An accurate description of the fragmentation process on the basis of visual observations is not available.

- The criterion of the spontaneous nucleation temperature has not been verified by visual observations.

- There is a threshold for external triggers beyond which fragmentation may take place /42/. This raises the question of the function of the external trigger. For example, the trigger may serve only to cause direct contact between the two liquids, or it may have other effects as well.

- To transfer the results to real reactor conditions, it is very important to know the materials' main thermophysical properties characteristics influencing fragmentation. Experiments so far have been unable to answer this question.

These problems define the goals of the present experimental investigation, which is to provide fundamental information on the interaction between the hot and cold liquid:

- Description of the thermal reaction process under the aspect of pure boiling fragmentation .

Above all, the use of an efficient high-speed camera will enable visual observations of fragmentation processes. The experimental geometry, with a single hot droplet in a cold liquid, facilitates evaluation. Among the data evaluated will be the reaction pressure, the volume, the growth rate of the reaction zone, the rate of mixing with the cold liquid, and the liquid fraction in the reaction zone. For the last-mentioned parameter, the present investigation was the first to provide results. The time curve of the liquid fraction characterizes the reaction process. A physical explanation of the process is given on the basis of visual observations. The density ratio of the two liquids should be near 1 in order to minimize the hydrodynamic instabilities acting between the liquids.

- Proof of the validity of the spontaneous nucleation temperature criterion

So far, this criterion has been discussed only on the basis of recorded pressure signals. In the present study, it will be investigated also by visual observations using a high-speed camera.

- Investigation of the parameters influencing fragmentation.

Not only the temperature conditions but also external disturbances appear to be an important influencing factor in fragmentation. An external trigger is required for a parametric investigation of this influence. Due to the use of different combinations of liquids with different thermophysical properties, the effects of these on the boiling fragmentation process can be investigated. The findings and discussions of our study will be compared with earlier investigations.

3. Conduct of Experiments

3.1 Conception of Experimental Set-Up

3.1.1 Selection of Experimental Materials

The experimental materials were selected with a view to the following requirements:

- The cold, volatile liquid simulating the reactor coolant should have a critical temperature as low as possible but should remain in the liquid state also at room temperature.

- The cold liquid must be transparent in order to permit filming.

- The hot liquid simulating the molten fuel must be capable of being heated up without noticeable evaporation to a temperature level high enough to have a temperature at contact with the cold liquid close to, or higher than, the critical temperature of the cold liquid.

- The hot and cold liquids should have similar densities.

- No chemical reaction must take place between the two liquids.

In view of these requirements, the following systems were selected:

Cold liquid: Pentane (C_5H_{12})

Hot liquid: Sodium (molten) or silicone oil (DC710)

Table 1 lists the main thermophysical properties. Sodium is particularly advantageous as it permits experiments in a wide temperature range; it is stable even at high temperatures and has good thermal properties. Post test examinations and analyses can be carried out on the fragments. The experiments must be carried out in the absence of oxygen, which makes the sodium experiments more difficult than the silicone oil experiments. On the other hand, the silicone oil/pentane system is frequently chosen for experiments of this type /15/; it is similar to the well-known oil/freon system.

Preliminary experiments proved that no chemical reaction takes place between the selected substances.

3.1.2 Experimental Set-Up

Fig. 2 shows the experimental set-up for sodium droplets. A plexiglass vessel (1) of 30 x 30 x 200 mm is filled with pentane. The upper gas plenum (2) is filled with argon or helium. The sodium is introduced into the heating tube (3) by distillation and heated to the desired temperature by an electric heater. Single sodium droplets are separated by pressing them through a sintered metal disk (4) using argon gas of about 10 bar. The arrival of the droplet in the recording field of the high-speed camera is determined by laser photocell switchoff (5). Via two adjustable lag elements (6,7), first the flashlights (8) for the camera are connected, which need about 60 s to reach full power, and then the trigger for generating the shock wave. The external trigger was generated by an exploding wire: a suspended silver wire with a diameter of 0.025 mm (9) was made to evaporate by a sudden condenser discharge. Depending on the desired trigger size, the condenser capacity was between 1 and 2 μF and the voltage between 1 and 2 kV. The trigger time for the fast electric circuitry (Ignitron) (10) is less than 2 μs.

Fig. 3 gives a detailed picture of the recording field of the sodium/pentane experiment. The experimental vessel has a size of 30 x 30 mm. One of the two pressure transducers (A) protrudes into the experimental vessel, while the other is mounted directly on its wall. The distance between the envisaged droplet center and the pressure transducer is 7.5 mm for transducer A and 15 mm for transducer B. The wire for the wire explosion is suspended 20 mm below the horizontal center line of the pressure transducers. The wire is about 10 mm long. The droplet diameter is between 6 mm and 8 mm depending on the experiment; in most cases, it is around 7 mm. The pentane column above the droplet is 25 mm.

The silicone oil/pentane experiment has smaller dimensions, with an experimental vessel of 20 x 20 mm. Transducers A and B are located at 5 mm resp. 10 mm from the droplet center. The wire for generating the trigger pressure is 15 mm below the horizontal center line of the pressure transducers and has a length of about 10 mm. The droplet diameter is 3 to 4 mm. The pentane column above the droplet is about 15 mm high.

Fig.4 shows the sodium distillation and gas supply system. There are valves for evacuating the whole system and filling it with argon. The sodium distillation system consists of the sodium container (1), the supply tube (2), and the valve and the sodium heating tube (3). The system has autonomous electric heaters, so that

each section can be heated as desired. This facilitates sodium distillation and transport from the sodium container into the heating tube.

The experimental set-up of the silicone oil droplet system follows the same principle. The experimental vessel is slightly smaller, i.e. 20 x 20 x 150 mm, and the droplets are smaller than the sodium droplets. Instead of using a laser, the arrival of the droplet in the recording field is indicated by an ultrasonic barrier (Viscolux USG 3).

3.2 Measuring System

3.2.1 Temperature, Pressure and Film Recording

The temperature of the hot liquid was measured by two thermoelements, one of which was installed on the inner wall of the heating tube and the other on the outer wall of the sintered metal disk. In the sodium experiments, the two measured values differed by only a few degree C. In the silicone oil experiments, an additional thermoelement was installed on the inner wall of the sintered metal disk. The temperature difference across the disk was less than one degree C. As the reaction temperature could not be measured accurately, it was approximated analytically after the experiment (see Appendix A).

The dynamic pressure curves of the trigger and the fragmentation process were recorded by two pressure transducers (Kistler 603 B) installed on the wall of the experimental vessel. The curves were recorded by an oscillograph and photographed after the experiment. The two pressure transducers were arranged at different distances from the projected reaction site. If the measured values of a reaction pressure event were to differ, the actual reaction pressure was to be derived by an analytical procedure (Appendix B).

The high-speed camera used was a Cordin Daynafax 374 A, with a maximum taking speed of 10^5 pictures per second. The total recording time is 4 ms for 1 x 10^5 pictures per second. The high-speed films provide valuable information, e.g. time curves of the reaction zone volume, its growth rate, and the acceleration of the two-phase boundary. In the experiments, the exploding wire was arranged in the recording field in order to record the explosion time.

3.2.2 Determination of the Liquid Fraction in the Reaction Zone

By measuring the movement of the liquid around the reaction zone, the liquid volume confined in the reaction zone can be determined at any given time. This was done as follows:

As shown in Fig. 5, a mobile, thin aluminium foil or a silver wire coil is suspended near the envisaged reaction site. This foil or coil follows the motion of the surrounding liquid. Assuming that the inertia of the foil equals the inertia of the liquid, the motion of the foil or coil will equal the motion of the liquid.

By measuring the motion of the liquid surrounding the reaction zone, a quantitative assessment of the liquid volume inside the reaction zone is possible. A spherically symmetrical expansion zone is assumed:

$$\Delta V_V = 4\,\pi/3\,(R^3_{V2} - R^3_{V1}) \qquad (1)$$

$$\Delta V_L = 4\,\pi/3\,[\,(R_L + X)^3 - R^3_L], \qquad (2)$$

where

R_{V1}: Initial droplet radius

R_{V2}: Radius of the reaction zone after a given time

R_L: Initial radius of the sphere, characterized by the distance of the foil or coil from the center of the reaction zone

X: Motion of the liquid.

If the two volumes ΔV_V and ΔV_L differ, the difference must be identical with the volume of the cold liquid participating in the reaction. The result is the liquid volume in the reaction zone:

$$V_F = \Delta V_V - \Delta V_L. \qquad (3)$$

The liquid fraction is

$$F_F = V_F / \Delta V_V. \qquad (4)$$

The possibility of a liquid volume being confined in the rapidly expanding reaction zone was predicted theoretically by Beirak /43/.

3.2.3 *Fragment Size*

Post-test investigations were carried out on fragments of the sodium droplet. As sodium fragments tend to oxidize rapidly, only the fragment size and number were determined. The fragments removed from the vessel after the experiment were poured into a glass dish and distributed evenly. They were then photographed from above. From the enlarged picture, the diameters of the fragments were measured, and the fragments were counted.

3.3 *Experimental Parameters*

The most important experimental parameters are the contact temperature resulting from the droplet temperature and the external trigger pressure. The contact temperature is calculated according to /14/:

$$T_K = \frac{\beta_T T_T + \beta_F T_F}{\beta_T + \beta_F} \tag{5}$$

with $\beta = \sqrt{\rho c_p k}$ representing the thermal effusivity. T_T and T_F are the temperatures of the droplet and the cold liquid, respectively. T_F was kept constant.

There is no generally applicable value of the spontaneous nucleation temperature. As Fauske showed in /13/, it is a function of the surface characteristics of the two liquids. In a liquid-to-liquid contact, especially between liquids soluble in each other, it is often substituted by the homogeneous nucleation temperature T_{HN}, which is a purely physical property of the cold liquid.

The modified Berthelot equation of state and thermodynamic considerations lead to

$$T_{HN} = (27/32)^{2/3}\, T_{Kr} \tag{6}$$

Beyond this temperature limit, no metastable state can exist.

The homogeneous nucleation temperature can also be determined using molecular kinetics. Molecular fluctuations are assumed to destabilize the superheated liquid, i.e. above a given temperature T_{HN} so many growing nuclei are formed that rapid transition from the metastable state to the stable two-phase state will take place.

The nucleation rate J can be approximated as

$$J \propto N \exp(-W/kT) \qquad (7)$$

N: Number of molecules per unit volume

W: The reversible work required for bubble formation

k: Boltzmann constant (1.3804×23^{-10} J/K)

If W/kT, i.e. the so-called "Gibs number", exceeds a given value (about 11.5 according to /44/), the nucleation rate will increase rapidly. W is practically a function of the temperature, so that the homogeneous nucleation temperature can be calculated from the Gibs number. The two homogeneous nucleation temperatures resulting from these different approaches are nearly identical, e.g. 145 °C for pentane.

To meet Fauske's criterion, the hot liquid must be heated to a temperature high enough to ensure a contact temperature higher than T_{HN}. The experimental range for the hot droplet temperature was determined on this basis:

(1) 120 °C < sodium-temperature < 400 °C

Using equation (5) and the physical properties compiled in Table 1 contact temperatures of the Na/pentane system are approximated by $T_K \approx 0.95 \cdot T_T$..

(2) 200 °C < silicone oil temperature < 350 °C

resp. 110 °C < contact temperature < 180 °C

The temperature of pentane is always assumed to equal room temperature, i.e. around 20 °C.

Some preliminary experiments were necessary for determining the external trigger pressure required. The result for the sodium/pentane system is

(3) 2 bar < trigger pressure P_{Tr} < 15 bar

In the silicone oil/pentane system, the reaction can be initiated by a small trigger pressure, e.g. 1 bar.

3.4 *Experimental Procedure*

The experiments were carried out as follows:

- The whole system is filled with argon gas or partly evacuated.
- Sodium is transferred from the sodium container into the sodium heating tube by distillation. Silicone oil is filled into the heating tube by hand.
- The vessel is filled with pentane.
- The hot liquid is heated up in the heating tube to the desired temperature level, at which the temperature is kept constant.
- The film drum of the camera is set at the desired taking speed, normally 80 000 pictures per second.
- The condensers for exposure and for initiating the wire explosion are charged. Other elements, e.g. the laser barrier, the retarding elements and the oscillograph are set in ready position.
- The aperture of the camera is opened. (The camera drum rotates too fast for film exposure with normal light)
- By opening the electromagnetic valve 1, see Fig. 2, a single droplet is pressed through the sintered metal disk.
- Immediately after the droplet has fallen, the electromagnetic valve 2 is opened in order to relieve the pressure in the heating tube and prevent further droplet formation.

The subsequent experimental process is controlled automatically by the electronic control system. Fig. 6 gives a schematic representation of the sequence of events.

- As soon as the droplet has reached the envisaged reaction site, the flashlights are switched on, and after a certain delay the wire explosion is initiated and the oscillograph is triggered.
- A series of pictures is taken during a recording time of about 4 ms, which equals the flash exposure time.

- The reaction pressure curve is measured by pressure transducers, recorded by the oscillograph, and photographed.

- After a number of experiments with identical experimental parameters, the fragments are removed via the valve arranged below the experimental vessel.

3.5 Error Assessment

The physical data determined in this experimental study are bound to have some uncertainties, owing to the limited accuracy of the instruments and amplifiers used. In addition to these systematic measuring errors, there are subjective errors made by the observer during evaluation due to the incapability of interpolation of the human eye and to blurring of the film. These two sources of errors are discussed in the following estimate without making a clear distinction between them.

(1) Temperature T_T

Systematic errors in temperature measurements result from

- deviations from linearity of the thermocouples in the measuring range, $< 1\,°C$
- inaccuracy of the digital reading, $< 0.8\,°C$

Total error $/\delta T/ < 1.8\,°C$

(2) Pressure P

The error in pressure measurement comprises the following components:

- deviation from linearity of the pressure transducer $< 0.3\,\%$
- deviation from linearity of the amplifier $< 1\,\%$
- reading error on the recorded picture < 0.25 mm

This corresponds to $< 2.5\,\%$

Total error $/ \delta p/p /$ $< 3.8\,\%$

The distance between the measuring site and the reaction site will, of course, make the measured value differ to some extent from the real reaction pressure. The discussion in Appendix B will enable a comparison between the measured value and the actual reaction pressure. According to this the actual reaction

pressure should be higher by a factor of 1.2 than the value measured by transducer A.

(3) Synchronisation

There are two common causes of errors in the synchronisation of the recorded pressure curve and the pictures of the high-speed camera:

- the time resolution of the high-speed films
  $0 < t_o < 12.5$ µs (at 80 000 pictures per second)
- the reading error on the pictures of the pressure curve, $/t_o/ < 3.1$ µs.
  Total error: -3.1 µs $< t_o < 15.6$ µs.

The error resulting from the deviation of the sound velocity is negligible as the distance between the exploding wire and the pressure measuring site is very short (about 10 mm).

(4) Evaluation of the high-speed films

The high-speed films were projected onto a surface with a millimeter grid and then evaluated. The picture is enlarged four times as compared with the film. The main source of error is in reading. The maximum reading error of the enlarged picture is 0.2 mm, i.e. $\delta x = 0.05$ mm, on the original film.

The average error of a function f of a number of measured values x_K can be approximated by /45/:

$$SF = \sqrt{\sum_{k=1}^{n} \left(\frac{\partial f}{\partial x_k}\right)^2 \delta x_k^2} \qquad (8)$$

The relative errors are:

- Total volume of the reaction zone (after 100 µs)

$$\widetilde{\delta V_V} = \frac{\pi/2\, D_V^2\, \delta D_V}{V_V} = 3\,\frac{\delta f}{D_V} \qquad (1.75\ \%) \qquad (9)$$

- Growth rate of the reaction zone (after 100 µs)

$$\widetilde{\delta \dot{R}_V} = \frac{\sqrt{2}\,\delta f}{D_{Vi+1} - D_{Vi}} \qquad (13.2\ \%) \qquad (10)$$

- Acceleration of the interface of the cold liquid in the reaction zone (after 100 µs)

$$\widetilde{\delta \ddot{R}_V} = \frac{R_V \sqrt{R_{Vi+1}^2 + R_{Vi}^2}}{R_{Vi+1} - R_{Vi}} \qquad (23.4\ \%) \qquad (11)$$

- Volume of cold liquid in the reaction zone. Application of equation (8) to equation (3) results in

$$\widetilde{\delta V_F} = \frac{\pi \delta f \sqrt{1/4\,(D_{V2}^4 + D_{V1}^4) + 16\,[(R_L + x)^4 + R_L^4]}}{\pi/6\,(D_{V2}^3 - D_{V1}^3) - 4\pi/3\,[(R_L + x)^3 - R_L^3]} \qquad (12)$$

After 150 µs, the result is 33.6 %.

-Liquid fraction F_F. Equation (4) results in

$$F_F = \frac{V_F}{\Delta V_V}\left[1 \pm \left(\widetilde{\delta V_F} + \widetilde{\delta \Delta V_V}\right)\right] \qquad (13)$$

The derivation with equation (8) is

$$\widetilde{\delta F_F} = \widetilde{\delta V_F} + \widetilde{\delta \Delta V_V} = \widetilde{\delta V_F} + 2\,\widetilde{\delta V_V} \qquad (14)$$

After 150 µs, the result is 36 % .

The diameters and liquid motion values used here were derived from the experimental data for sodium/pentane, see Fig. 12. Both the growth rate and the

acceleration reach a peak value after 100 µs, while the liquid fraction F_F has a peak after 150 µs. After this peak value, all relative errors decrease; for example, the relative errors of the liquid volume V_F and the liquid fraction F_F after 500 µs have decreased to 10.5 % resp. 12.7 %. The time curves of the reactions indicate such clear trends, as the subsequent experimental results will show, that conclusions from, and interpretations of, the experimental findings are possible in spite of these errors.

4. Experimental Results

4.1 General Remarks

4.1.1 Boiling Pattern

Two different boiling patterns were observed in the experiments without external trigger and during immersion of the sodium droplet into pentane: If the droplet temperature is above a given value - here, about 140 °C -, the vapour-liquid interface and the droplet surface have a smooth look. Before the droplet reaches the bottom of the vessel, some vapour bubbles are separated which are about equal in size to the droplet itself. These observations suggest film boiling.

Below 140 °C, the droplet is surrounded by a thicker multi-bubble region, so that its contour becomes blurred. Bubbles are formed and separated more frequently than in the former case. This observation is interpreted as a typical sign of some type of pool boiling or transition boiling.

These two boiling patterns are proved by observations with the high-speed camera, see Chapter 4.2.2. The minimum film boiling temperature of 140 °C is compatible with the result of Spiegler's film boiling experiment using pentane /46/.

In case of silicone oil droplets, only film boiling was observed. It should be noted, however, that the bulk temperature of the silicone oil droplet was always higher than the minimum film boiling temperature, although the contact temperature was lower in some instances. The thickness of the vapour film is 0.1 to 0.2 mm as estimated by the high-speed films (taking speed 3000 pictures per second).

4.1.2 Characteristic Trigger Pressure Curve

The external trigger is one of the most important experimental parameters. Therefore, the characteristic features of the trigger pressure had to be known

before carrying out the experiments. As the trigger pressure wave is generated in our experiments by an exploding wire, the trigger pressure level can be altered by modifying the electrical energy applied to the wire, i.e. the condenser voltage. Fig.9 shows a typical trigger pressure signal curve. A trigger pressure wave normally has several peaks. The first peak is recorded after a rise time of a few microseconds, followed by a second peak. The natural frequency of the pressure transducer is 400 kHz, so that rise times shorter than 2.5 μs cannot be measured accurately. This event of two high peaks, lasting around 30 μs in all, is viewed as a "trigger pressure pulse". After this, the pressure drops to nearly system pressure. At 50 μs after the first peak, there is a third peak amounting to nearly one third of the first peak and lasting for about 10 μs. This pressure peak is viewed as being caused by reflection of the first peak from the pentane surface, as it takes about 50 μs for the first peak to return to the measuring site after reflection from the pentane surface. After a still smaller fourth peak, there is a phase of negative pressure whose absolute value equals the fourth positive peak. The negative pressure lasts for about 80 μs, while the absolute pressure keeps decreasing. The subsequent pressure up to 0.8 ms after the onset of the trigger pressure wave is several times lower than the first "trigger pressure pulse" and assumes negative values.

As the external trigger is an experimental parameter, it should be characterized by one or several variables. Table 2 presents a number of trigger pressure pulses as characterized by important parameters. "Pressure" means the height of the trigger pressure pulse, "Impulse" the time integration, $\int Pdt$, and $\int PdV$ the mechanical work produced by the wire explosion as estimated by evaluation of the high-speed films. These four values are proportional. The qualitative curves of the different trigger pressures are similar.

4.1.3 Description of the Experiments

Tables 3 and 4 show the experiments and the main experimental parameters for the sodium/pentane and silicone oil/pentane systems. "Temp." is the measured temperature of the sodium droplet resp. the estimated temperature of the silicone oil droplet. "Trigger pressure" is the height of the so-called "trigger pressure pulse", see Chapter 4.1.2. "Reaction pressure" is the maximum reaction pressure, and "Delay" the delay between the first trigger pressure peak and the reaction pressure peak, see Chapter 4.2.1. "Impulse ratio" is the ratio between the impulse of the reaction pressure pulse and the impulse of the trigger pressure pulse. These three values were estimated from the recorded pressure signals,

while "Fragmentation" was derived from observations of the high-speed films. "analyzed" indicates that a high-speed film was evaluated. A detailed evaluation of the high-speed films for the purpose of determining the time curves of the reaction was carried out only for the sodium/pentane system. Apart from the experiments listed in the tables, further series of experiments were carried out on both systems; in most of these cases only the reaction pressures were recorded. The values of Tables 3 and 4 lead to the following general statements:

- There is a lower threshold of the external trigger for initiating a reaction or droplet fragmentation.
- The reaction process is determined both by the droplet temperature and the trigger pressure.
- In the silicone oil/pentane system, always smaller external triggers are required for initiating a reaction.
- The impulse ratios of the silicone oil/pentane system are several times higher than those of the sodium/pentane system.

To explain the first statement, the experimental points of the two parameters "droplet temperature" and "external trigger pressure" are shown in Figs. 7 and 8. The two pictures show: There is a minimum trigger pressure, $P_{Tr,min}$, which must be reached in order to initiate a reaction. $P_{Tr,min}$ in both systems is seen to depend on the droplet temperature resp. the contact temperature which is a function of the droplet temperature (cf. equation 5). The minimum value of $P_{Tr,min}$ is obtained around $T_l = T_{HN}$, i.e. the homogeneous nucleation temperature of pentane. $P_{Tr,min}$ increases in both directions of the droplet temperature. The results obtained with the different experimental parameters and their discussions will be presented in more detail in Chapter 4.3.

4.2 Reaction Process

4.2.1 Reaction Pressure Curve

The measured pressure curves of the reaction show important characteristics of the reaction process. Fig.10 compares the pressure curve of the reaction of the sodium/pentane system, taking test V15 as an example, with the trigger pressure curve (without reaction). Curves A and B were measured by the corresponding pressure transducers (Fig.3). As seen in Fig. 10, the first pressure peak has a rise time of 2 - 3 µs which is due to the natural frequency of the transducer (400 kHz).

The first pressure pulse, with 2 peaks, lasts for about 30 µs. During this time, the curves for the trigger pressure plus reaction and for the trigger pressure alone are completely synchronized. This pressure pulse therefore is called "trigger pressure pulse" or "trigger pressure range". After this, the curve including the reaction has another pressure peak with a longer rise time of 20 µs and a total time of 60 to 80 µs, i.e. several times longer than the trigger pressure pulse itself. This longer time is the feature that clearly distinguishes the trigger pressure pulse from the pressure generated by the thermal reaction between droplet and liquid. This second result is referred to as "reaction pressure". It should be noted that the peak of the reaction pressure is higher in Curve A than in Curve B owing to the geometric arrangement of the pressure transducers. As shown in Fig. 3, transducer A is closer to the expected reaction site than transducer B. Using both signals and the computer code SING /54/ (cf. Appendix B), the real reaction pressure in the reaction site can be approximated. It is deduced from Fig. B-1 that the reaction pressure in the reaction site should be higher by only a factor of 1.2 than the value measured by transducer A, i.e. the pressure pulse recorded by transducer A is a good representation of the reaction pressure at the droplet surface.

The delay time of the reaction pressure peak related to the first trigger pressure pulse peak is about 50 µs. No delay times in the millisecond range were observed, i.e. the reaction of the sodium/pentane system should correspond in all cases to Ando's /42/ "prompt fragmentation" pattern. The impulse ratio in test V15 is around 1.5 (cf. Table 3), the impulse ratios in the tests with different experimental parameters vary between 0.4 and 1.7.

Fig. 11 shows typical pressure curves of a reaction with silicone oil and of a trigger alone of nearly the same size. In the trigger curve there is a pressure peak of several microseconds, followed by a pressure pulse of about 20 µs which is only half as high as the first peak. These two result from the wire explosion. In the pressure curve of the reaction, the first pulse (trigger pressure pulse) is followed by a pressure increase with several free peaks, with maximum pressure after about 40 µs. The pressure then decreases during more than 250 µs. The two pressure curves comprising and excluding the reaction are distinguished by this pressure increase, which is identical with the reaction pressure in the silicone oil experiment. "Delayed Fragmentation" with delays in the milliseconds range was not observed for silicone droplets either.

A direct comparison of the pressure curves of sodium droplets and silicon oil droplets is impossible, owing to the different droplet sizes and to the different geometries of the experimental vessels. It can be stated, however, that the pulse ratio of the reaction pressure to the trigger pressure pulse is several times higher in the silicon oil/pentane system than in the sodium/pentane system, see Tables 3 and 4.

4.2.2 Reaction Process According to the High-Speed Films

Fig. 12 shows the time curves of a typical fragmentation experiment for sodium droplets at T_1 = 150 °C, P_{Tr} = 10 bar. All values except the pressure curve were obtained by direct evaluation of the high-speed film. The top diagram shows the time curves of the reaction pressure and the total volume of the reaction zone, $V_t = (4/3)\,\pi\,R^3_{V2}$ the central diagram the time curves of the velocity and acceleration of the boundary of the reaction zone, and the bottom diagram those of the liquid fraction and the mixing rate in the reaction zone. The reaction zone is defined as the net expanding volume, ΔV_V, cf. equation (1) and Fig. 5. The values in the bottom diagram were estimated by the method described in Chapter 3.2.2.

Fig. 13 presents a series of pictures of this high-speed film. The taking speed was 8000 pictures per second. Pictures No.1-13 are in the original order, while the pictures beyond No.14 were selected. The times refer to the period after the arrival of the trigger pressure pulse at the droplet.

Fig. 14 is an idealized representation of the growth of the reaction zone volume during the reaction as observed on the pictures. It also shows the liquid volume in the reaction zone. These diagrams and the series of pictures help to divide the reaction process into the following six phases, each of which is marked by a Roman numeral (see Fig. 12).

(I) Film boiling

- Time: about 1 ms before arrival of the trigger pressure pulse
- Pictures : Picture No. 1 on Fig. 13

The picture is described as follows: The contour of the droplet surface is dark but smooth. Although the vapour film is not visible, film boiling is assumed to occur. The central light spot on the droplet is a reflection of the flashlight. No movement or deformation of the droplet was observed in this phase. As the droplet falls at a rate of only about 0.5 mm/ms in the film boiling phase, no falling move-

ment can be observed. Direct interaction between droplet and liquid is not observed in this phase; this phase therefore corresponds to the initial state before the reaction takes place.

(II) Film collapse and direct contact

Time: From the arrival of the trigger pressure pulse to about 50 µs.

Pictures: No. 2 to 5

The collapse of the vapour film takes place so fast that it cannot be observed accurately on the pictures. Within three pictures, i.e. pictures No. 1 to 3, i.e. during a period of about 25 µs, sections of the droplet surface become white and silver-coloured. On Picture 2, this change of colour has occurred in the bottom hemisphere of the droplet. On its top hemisphere, there is a relatively thick vapour space of irregular, i.e. not round, contour which diminishes in size during Pictures 3, 4, and 5. At the same time, there is a progressive change of colour from silvery white to a dull white in the central section of the droplet.

Neither a marked pressure increase nor a significant growth of the reaction zone were noticed in this period. There is no measurable liquid fraction in the reaction zone. The observed change of colour of the boundary layer from dark to silver is assumed to be caused by a decrease in the vapour film thickness or even by local direct contact between droplet and liquid. The film collapse takes place within this period of about 25 µs, i.e. it is too fast to be recorded on the pictures. The dull white belt observed in the central section of the droplet at a later stage reflects the local evaporation caused by direct contact. Changes of this type do not always start in the bottom section of the droplet, where the trigger front impacts first, but often in the central section of the droplet as in our experiments, especially if the trigger pressure is relatively low. This observation will be taken into account in the discussion of the mechanism initiating the reaction.

(III) Sudden evaporation and fragmentation

- Time: 50 - 125 µs
- Pictures: No. 5 - 11

In the early stage of this phase, Pictures 5-7, dull white spots continue to spread on the droplet surface. After 100 µs, on Picture 9, the whole droplet surface has turned to dull white. Small-scale eruptions are observed in the upper section of

the droplet but there is no visible deformation of the droplet itself. The reaction zone expands in all directions.

As seen in Fig. 12, the reaction pressure increases, and the growth of the reaction zone accelerates. Shortly before 100 µs, the peak value of $1.2 \cdot 10^5$ m/s^2 is reached. After a short delay of about 30 µs, the peak of the radial growth rate of the reaction zone follows, i.e. about 8 m/s. At the end of this phase, the reaction pressure drops to system pressure, and negative acceleration values are obtained. The minimum value is at $-4 \cdot 10^4$ m/s^2. The liquid volume does not increase until after a delay of 87.5 µs (Picture 8), reaching a peak value of 56 % within a period of 50 µs. During the period in which the liquid volume increases, the whole droplet surface becomes a dull white (Fig. 11, Pictures 9, 10, and 11). This observation corresponds to the increase of the liquid fraction in the reaction zone as a result of mixing with the liquid. This approximation is the first quantitative proof that mixing of vapour with the surrounding liquid really does take place.

Point B on Fig. 12 indicates the liquid volume that could evaportate if the total thermal energy of the droplet is assumed to contribute to the evaporation of the liquid. For further discussions of this point see Chapter 5.1.5.

Referred to the whole course of the reaction, the reaction pressure and acceleration, the expansion rate of the reaction zone, and the rate of mixing with the liquid all reach peak values in this third phase. It is therefore assumed that during this Phase III, which lasts for about 75 µs, the main reaction processes take place, i.e. evaporation of the heated liquid, fragmentation of the droplet, and mixing with the liquid. For this reason, this phase is referred to as "sudden evaporation and fragmentation".

(IV) Transition phase

- Time: 125 - 200 µs
- Pictures: No. 11 - 15

No visible changes in the structure of the boundary layer of the reaction zone are observed in this period. The reaction zone continues to expand in all directions, and the small-scale eruptions already observed in Phase III get more violent.

The reaction pressure drops to system pressure, with no further pressure pulse occurring. The acceleration of the phase boundary, which assumed negative values at the end of Phase III, returns to the positive range. The second peak of the acceleration is about $4 \cdot 10^4$ m/s^2, i.e. only one third of the peak value measured in

Phase III. It assumes negative values again after 30 µs. At the onset of Phase IV, the growth rate slows down to 5.5 m/s and then increases again. There is a second peak of 6.5 m/s which is clearly smaller than the first peak of Phase III. The liquid fraction in the reaction zone is reduced from 56 % to 40 %. The mixing rate decreases from 6 m/s to 2 m/s.

(V) Slow mixing and expansion

- Time: 200 - 500 µs
- Pictures: No. 15 - 19

The surface of the reaction zone is not as smooth as before; especially at the end of Phase V (Pictures 18, 19), small "projections" protruding into the surrounding liquid are visible on the reaction zone surface. These are estimated to be several tenths of millimeters in diameter; they are visible in the pictures as white spots on the boundary layer of the reaction zone. The contour of the reaction zone gets increasingly blurred, as is clearly seen at the end of Phase V.

The reaction pressure obviously does not exceed the system pressure (Fig. 12), while the growth rate of the reaction zone remains constant at 6 m/s in the period between 200 and 400 µs, i.e. the reaction zone volume keeps increasing. The mixing rate increases again, causing also the liquid volume to increase. The second peak of the mixing rate is at 4 m/s, i.e. less than the first peak of 6.5 m/s in Phase III. It is therefore assumed that the mixing process of Phase V has other causes and mechanisms than in Phase III.

The characteristic feature of Phase V is the further growth of the reaction zone and of the liquid volume in the reaction zone, without any significant reaction pressure being built up. This phase therefore was named "slow mixing and expansion".

(VI) Condensation

- Time: 500 µs to about 1 ms
- Pictures: No. 20 and 21

In the period after a time of 500 µs, the interface between the liquid and the reaction zone becomes increasingly blurred in the high-speed pictures. At the same time, sodium fragments are visible for the first time, whose positions partly correspond to the "projections" on the surface of the reaction zone observed in Phase

V. The fragments are observed as white spots on the pictures, especially on Picture No. 21.

During the first 100 µs of Phase VI the reaction zone volume and the liquid fraction increase only slightly (Fig. 12). Both the growth rate of the reaction zone and the mixing rate decrease to zero, entailing in the following a reduction of the reaction zone volume and of the liquid fraction in the reaction zone. The maximum growth rate (R) remains lower by a factor of 7 to 8 than the maximum growth rate of Phases III or V. As the reduction of the reaction volume is caused by vapour condensation, we refer to Phase VI as "Condensation".

In some cases, a second reaction (not shown in Fig. 13) takes place after the first reaction has terminated or during the shrinking phase of the reaction zone. The pressure build-up during this second reaction is too small to be visible. The high-speed pictures show that a second fragmentation of the still unfragmented part of the droplet takes place.

4.2.3 Summary

The observed processes and characteristic features of a typical reaction of sodium and pentane were described in order to illustrate the reaction process. The reaction process can be summarized as follows:

- A reaction pressure builds up with a certain delay (about 50 µs) after impact of the trigger pulse. The pressure build-up time, i.e. about 80 µs for sodium droplets and about 250 µs for silicone oil droplets, is longer than the trigger pulse (about 20 to 30 µs)

- The impulse ratio is several times higher for the silicone oil/pentane system than for the sodium/pentane system.

- The reaction process for the sodium/pentane system comprises the following stages:

  (I) Film boiling
  (II) Film collapse and direct contact
  (III) Sudden evaporation and fragmentation
  (IV) Transition phase
  (V) Slow mixing
  (VI) Condensation

- As the reaction zone grows, it mixes with the surrounding liquid and therefore contains a certain volume of non-evaporated liquid.

- Fragmentation of the droplet takes place mainly during Phase III.

- Mixing with liquid takes place mainly in Phases III and V. The mixing mechanisms of the two phases have different causes.

4.3 Influence of Experimental Parameters

4.3.1 Time Curves for Different Experimental Parameters

Figs. 15 to 18 present the experimental results for sodium droplets obtained with different experimental parameters. All figures are presented in the same manner as in Fig.12.

Fig. 15 shows the time curves of the main parameters of the reaction process for a lower droplet temperature of 120 °C and an identical trigger pressure of 10 bar. The film shows no film boiling during the first phase; instead, there is a typical transition boiling pattern with large vapour bubbles. Once the external trigger has impacted on the droplet, the reaction pressure first increases with a delay of about 60 µs comparable to that in Fig. 10. However, the reaction pressure is narrower by a factor of 3 and lower by a factor of 2 than the reaction pressure for the higher droplet temperature of 150 °C in Fig. 12. The acceleration of the phase boundary and the growth rate of the reaction zone increase as well. Almost simultaneously, the mixing rate increases, followed by the liquid fraction in the reaction zone. This is clearly a Phase III pattern, but the peak values of acceleration, growth rate and mixing rate are significantly lower than for the high droplet temperature of 150 °C (Fig. 12). After this, the pressure drops to system pressure, paralleled by the other parameters. This pattern corresponds to Phase IV. Phase V shows a constant growth rate of the reaction zone and the recovery of the mixing rate, but the peak value of the mixing rate in Phase V is only half as high as in Fig. 12. In general, we may state that the reaction or fragmentation are milder at the lower droplet temperature (120 °C) than at the higher droplet temperature (150 °C) if the same trigger is applied.

Fig. 16 shows the reaction for a higher droplet temperature (400 °C) and the same trigger of 10 bar. This reaction, too, follows the six phases of Fig. 12 for a droplet temperature of 150 °C. The maximum reaction pressure is 8 bar as compared with

12 bar at 150 °C. The acceleration and the growth rate of the reaction zone are smaller, paralleled by the mixing rate and the liquid volume. Mixing with the liquid at 400 °C during Phase V as in Fig. 16 is more pronounced than at 120 °C, although the reaction in both cases is relatively mild as compared with the violent reaction at the droplet temperature of 150 °C.

Comparisons were also made between experiments with different external trigger pressures. Fig. 17 shows the evaluated reaction process for a trigger pressure P_{Tr} = 4 bar and a droplet temperature T_T = 180 °C and Fig.18 that for P_{Tr} = 8 bar and T_T = 180 °C, i.e. identical droplet temperatures. All maximum values estimated for the higher trigger pressure of 8 bar are higher by a factor of 1.5 to 2 than for the lower trigger pressure, with the exception of the volume ratio V/V_0. The difference was highest for the reaction pressure pulse, the acceleration of the reaction zone growth rate, and the rate of mixing with the liquid, i.e. in Phase III. This suggests that an external trigger influences not only the collapse of the vapour film but also the evaporation and fragmentation phase.

In spite of these differences, the time curves of the growth rate, reaction zone acceleration, liquid mixing rate, and liquid volume were similar in all experiments. The six phases described in Section 4.2.2. are observed in all cases and are therefore considered to be generally valid.

4.3.2 Reaction Pressure and Delay Time

In order to illustrate the effect of the droplet temperature on the reaction, the maximum reaction pressure (Fig. 19) and the maximum rate of mixing with the liquid in Phase III (Fig. 20) are presented for the sodium/pentane system. The two diagrams read as follows:

- At a trigger of 10 bar, reaction pressures and mixing rates are significantly higher (by a factor around 1.5) in the temperature range between T_{HN} and T_{Kr} than outside this temperature range.

- At a trigger of 4 bar, reaction pressures are in the same range (3 to 4 bar). These values are constantly lower than for a trigger of 10 bar at identical droplet temperatures.

- The higher reaction pressure of about 10 bar also results for a higher droplet temperature of 360 °C if a higher trigger of 15 bar is used.

- The mixing rate for a lower trigger of 4 bar is only half as high as the mixing rate at 10 bar. This evaluation was made only for a droplet temperature of 180 °C.

Fig. 21 shows the maximum reaction pressure of the siliconeoil/pentane system for each droplet temperature.The trigger pressure was nearly constant (0.8 to 1.3 bar). The points are derived from a series of experiments not described in Table 4. The droplet temperatures were corrected by the method described in Appendix A. They correspond to the droplet temperature prior to the incidence of the trigger pressure pulse. According to Appendix A, especially the drop of the surface temperature of the silicon oil droplet during film boiling should not be neglected. Here, too, the reaction pressure is shown to increase significantly if the contact temperature T_K is higher than T_{HN} = 145 °C. The reaction pressure has a peak at a contact temperature of 180 °C. This peak value differs from the lower values for lower contact temperatures by about a factor of 2.5. At contact temperatures higher than 180 °C, the measured reaction pressures decreased. It was observed that after the reaction, unfragmented sections of the droplet remain in the film boiling state, owing to the fact that only part of the droplet takes part in the reaction in the first place. This phenomenon is called "partial fragmentation". The resulting reaction pressure therefore is lower than for lower contact temperatures. In the silicon oil experiments, it was impossible to heat the droplet to a temperature, which resulted in a contact temperature higher than the critical temperature of pentane, i.e. 197 °C, so that the range of measurement is limited. Still, there is a trend showing a significant reduction of the reaction pressures in the temperature range near T_{Kr} as referred to the contact temperature. This trend is compatible with the results of the sodium experiments (Fig. 19).

The delay time, i.e. the time between the trigger peak and the reaction pressure peak, is another important parameter. Roughly, it comprises the following physical processes: Vapour film collapse, initial interactions between the hot droplet and the cold liquid caused by heat transfer and evaporation of the superheated liquid, and reaction pressure build-up. The delay time is a characteristic parameter reflecting the effect of an external trigger on the reaction pressure build-up. Its size has decisive influence on the violence of the reaction in its initial phase. Figs. 22, 23 show the delay times as functions of droplet temperature and trigger pressure, respectively, for the sodium/pentane system. Fig. 22 shows that the delay time has a minimum around T_{Kr}. This function is inverse to the reaction pressure function (Fig. 19). Fig. 23 shows this even more clearly. A shorter delay time will result from a more violent interaction between droplet and liquid, e.g. as a

result of higher heat transfer from the hot droplet to the cold liquid. This more violent interaction will cause a higher reaction pressure build-up.

Fig. 24 shows the delay time as a function of the contact temperature for the silicone oil/pentane system. Like in the experiments with sodium, the delay time decreases with the contact temperature up to T_K = 180 °C. Compared with the results for sodium/pentane, the delay times of silicone oil/pentane appear to be shorter (average delay 40 µs). As already mentioned, experiments with a contact temperature above 180 °C were impossible for the silicone oil/pentane system, so it remains unclear whether there is an increasing trend in the delay time above T_{Kr}.

4.3.3 Summary

The influence of the different experimental parameters is summarized as follows:

- Reactions are the most violent in the temperature range $T_{HN} < T_K < T_{Kr}$, with high reaction pressures and mixing rates with the liquid as referred to a given trigger pressure. This range therefore has the highest energy yield. It is more or less identical with the well-known "Thermal interaction zone" (TIZ).

- Apart from initiating the reaction, the external trigger also determines the whole reaction process up to the build-up of the reaction pressure as a result of evaporation of superheated liquid and droplet fragmentation.

- For a full-scale droplet reaction at an extremely high droplet temperature, i.e. far beyond T_{Kr} of the liquid as referred to the contact temperature, a higher external trigger pressure is required.

- A violent reaction accompanied by a high reaction pressure results in a short delay time.

4.4 Energetic Aspects of the Trigger and the Reaction

For the sodium droplet experiments evaluated in the pictures, the thermodynamic work of the reaction can be estimated by integrating PdV. This procedure can also be used for estimating the whole thermodynamic work of the trigger released during the wire explosion. However, only a small fraction of this trigger work is available to the reaction between the hot droplet and the cold liquid. Table 5 compares thermal energies (not considering the solidification enthalpy) and reaction works for some typical experiments with sodium droplets.

These examples show that higher droplet temperatures and triggers will increase the reaction work. The total trigger work itself is higher than the corresponding reaction work. However, the effective fraction of the trigger work, which can be estimated by multiplication with the cross section factor, is much smaller than the reaction work, amounting to only one tenth to one fifth of the reaction work. This means that the trigger work alone is too small to initiate a full-scale reaction. Thermal energy has a dominant effect, although the conversion factor of thermal into thermodynamic work is quite small, i.e. around 0.3 %.

4.5 Analysis of Sodium Droplet Fragments

The sodium fragments solidify after the reaction and can be analyzed. The fragments tend to be fine and spherical although some large fragments with diameters larger than 1 mm were found. This clearly indicates that fragmentation took place prior to solidification of the sodium.

Figs. 25 and 26 show the results of the fragment analysis. The external trigger pressure in all cases was around 10 bar; droplet temperatures were 120 °C, 150 °C, 200 °C, and 400 °C. Fig. 25 shows the fragment mass fractions for each group of fragments. At droplet temperatures of 120 °C and 400 °C, there is a 50 % fraction of fragments with diameters larger than 1mm. This is twice as much as at 150 °C and 200 °C. Further, the fraction of smaller fragments, i.e. 0.2 to 0.5 mm, is several times larger at 150 °C and 200 °C than at 120 °C and 400 °C. This is illustrated even more clearly by assuming an average diameter D, which is shown to be clearly smaller for 150 °C and 200 °C (about 1.2 mm) than for 120 °C and 400 °C (about 1.5 mm). Fig. 26 additionally shows the fractions of different groups of fragments. The fraction of fragments up to 0.5 mm in diameter is larger for 150 °C and 200 °C than for all other droplet temperatures.

These results of the fragment analysis suggest that a violent fragmentation reaction resulting in fine fragments really took place in the temperature range between 150 °C and 200 °C. This temperature range is related to the "thermal interaction zone" (TIZ), in which violent reactions with high reaction pressures and mixing rates with liquid were observed.

5. Discussion of the Experimental Findings

5.1 Physical Explanation of the Reaction Processes

Experimental findings concerning the reaction process and its dependence on the experimental parameters were described in the last chapter. Apart from the qualitative description, also a quantitative statement was possible within certain limits, i.e. a relatively high measuring error ($\approx$ 30%) and under the assumption of spherical symmetry. The following chapters will give a plausible physical explanation for each phase of the reaction process. In some cases, plausible hypotheses were introduced for an explanation.

The film boiling and condensation phases (Phases I and IV) are excepted as film boiling requires no explanation and the condensation processes have hardly any direct relation to droplet fragmentation and mixing with the liquid.

5.1.1 Trigger Pressure Front Propagation and Kinetics of Vapour Film Collapse (Phase II)

The vapour film collapse during film boiling was found to be induced by the trigger pressure. This chapter attempts to find out the mechanism dominating this process. This is very important for developing a theory on the first interaction between the droplet and the surrounding liquid at a later stage, as this interaction may be a function of the contact mode.

The shock front of a wire explosion propagates in the liquid at approximately sonic speed. This shock front is referred to as "trigger pressure front". The pressure ratio P_{Tr}/P_{sys} has maximum values of 1.7 and 9.6 for sodium and silicone oil, respectively, i.e. the shock front is small. It is assumed that the collapse of the vapour film is caused by the motion of the liquid and/or by the elevated system pressure behind the shock front.

The motion of the liquid (cf. Fig. 27), whose velocity is determined to be

$$u = \frac{P_1 - P_0}{C\,\rho_0} = \frac{P_{Tr}}{C\,\rho_0} \qquad (15)$$

causes a motion of the interface between the liquid and the vapour film. The real film collapse is influenced by various additional factors, e.g. local variations of vapour film thickness, interface waves caused by liquid acceleration, etc. These microscopic effects are an obstacle to the development of precise models of vapour film collapse. This chapter therefore will present and discuss only macroscopic models of vapour film collapse on the basis of the two mechanisms observed.

As Fig.27 shows, the droplet is enveloped in a vapour film prior to the arrival of the trigger pressure front. As soon as the trigger pressure front arrives at the boundary between the vapour and the surrounding liquid, this interface begins to move (first mechanism). Instead of eq. (15), which applies to single-phase conditions, this velocity is determined by the following equation:

$$u_G = \frac{2\,(P_2 - P_1)}{C^{(1)(1)}\rho_0^{(1)(1)} + C^{(2)(2)}\rho_0^{(2)(2)}} = \frac{2\,P_{Tr}}{C^{(1)(1)}\rho_0^{(1)(1)} + C^{(2)(2)}\rho_0^{(2)(2)}} \qquad (16)$$

Fig. 28 shows the calculated phase boundary velocity as a function of the trigger pressure. A trigger pressure of 10 bar corresponds to a phase boundary velocity of 2.7 m/s.

With a vapour film thickness of 0.2 mm, as found in the silicone oil experiment, the time until contact between the droplet and the liquid would be at least 75 µs. This calculated interval is much longer than that of the observed process of vapour film collapse (Chapter 4.2.2., Phase II). Observations showed that the droplet changed colour from dark to white or silver (Fig.13) within 25 µs, i.e. the first model is not compatible with the experimental findings. It is concluded that the first mechanism is negligible in the process of vapour film collapse.

At sonic speed the trigger front passes through the vicinity of the droplet in about 7 µs. As long as the trigger pulse lasts, high pressure is maintained in the vicinity of the droplet. This high pressure may induce spherically symmetric film collapse (second mechanism). A model of spherically symmetric collapse was presented by Drumheller /47/. His model is based on the following assumptions: Spherical symmetry, incompressible liquid, non-viscous liquid, no consideration of finite geometry around the droplet. An attempt at assessing the kinetics of the vapour film collapse was made by a simplified recalculation. In addition, a further simplification was introduced, i.e. no temperature increase from heat transfer at

the liquid boundary layer. Fig. 29 shows a schematic representation of the calculation geometry. The equations applied are

Rayleigh Equation:

$$R_V \ddot{R}_V + 3/2\, \dot{R}_V = (P_V - P_{sys})/\rho_F \tag{17}$$

Mass transfer due to evaporation and condensation:

$$\frac{d}{dt}\left[\frac{4\pi}{3}(R_V^3 - R_T^3)\,\rho_V\right] = 4\pi R_V^2 \alpha \sqrt{\frac{M}{2\pi \bar{R} T}}\,(P_{sat}(T_F) - P_V) \tag{18}$$

Equation of state:

$$P_V = \rho_V \frac{\bar{R}}{M} T_V \tag{19}$$

With $R_V = R_T + S$ and substituting ρ_V in equation 18 using equation 19, one obtains:

$$(S + R_T)\ddot{S} + \frac{3}{2}\dot{S}^2 = (P_V - P_{sys})/\rho_V \tag{20}$$

$$\frac{d}{dt}(R_V \cdot S) = \alpha \sqrt{\frac{T_V \bar{R}}{2\pi M}}\,(P_{sat}(T_F) - P_V) \tag{21}$$

where $V_V \approx 4\,\pi R^2{}_V \cdot S$, as $S \ll RT$.

The increased system pressure P_{sys} of the trigger front is modelled by the measured trigger pressure, which lasts for about 30 µs, with a step approximation of the real pressure curve for greater simplicity. The evaporation or condensation coefficient α is assumed to have the value 0.1.

Fig.30 presents an example for molten iron oxide in water calculated with the above simplified model as compared with the results of Drumheller. The two results are comparable in spite of a slight difference especially at the end of the ob-

servation period, possibly due to the effect of heat transfer, which was not considered in the simplified model. In view of the fact that the temperature difference between sodium or silicone oil droplets and pentane is several times smaller than the temperature difference between molten iron oxide and water, the simplified model is applicable for describing the process of vapour film collapse in the experiment with sodium or silicone oil droplets.

Fig. 31 presents a calculated example for the sodium/pentane system. The vapour film, which is assumed to be 0.2 mm thick, collapses within less than 25 µs. This is well compatible, e.g., with the experimental result of Chapter 4.2.2., i.e. a change of colour of the droplet within 25 µs after impact of the trigger pressure front. The mean shock velocity of the surrounding liquid at the droplet is about 7.5 m/s, i.e. more than twice as high as the velocity of the interface at the front stagnation point of the droplet resulting from liquid motion behind the shock front (2.7 m/s, see above). This comparison shows that the spherically symmetric motion of the surrounding liquid towards the droplet is dominant. For a smaller trigger pressure, e.g. 4 bar, the collapse time is calculated to be about 30 µs. The observed change of colour of the droplet in test V.19 at a trigger pressure of 4 bar took place after the impact of the trigger pressure front. This difference remains within the error of time correlation, (Chapter 3.5). In general, the observed vapour film collapse times tend to be smaller than the calculated values, possibly due to the fact that the real vapour film thickness was less than the assumed value of 0.2mm.

These considerations suggest that a macroscopic explanation of the vapour film collapse process is possible using the spherically symmetrical model applied to the conditions of increased system pressure behind the shock front.

The modelling of the real vapour film collapse must be structured more finely, with greater emphasis on the local differences in vapour film thickness and boundary surface waves (Rayleigh-Taylor instability) resulting from slowing of the liquid motion. Fig. 31 shows the rapid pressure increase in the vapour film before impact on the droplet, Fig. 32 shows the vapour pressure immediately before impact as a function of the trigger pressure. In a real system, this higher pressure must have a slowing-down effect on the liquid which will initiate the Rayleigh-Taylor instability. These two effects first permit only local direct contacts between the droplet and the liquid, or even formation of a vapour jet may be formed due to the Rayleigh-Taylor instability. The vapour film collapse time remains un-

changed, however, as the Rayleigh-Taylor instability will not become effective until the final stage of vapour film collapse.

After film collapse, direct contact takes place between droplet and liquid, accompanied by contact heat transfer. The heat flux is

$$q = \frac{1}{\sqrt{\pi}} \left(\frac{1}{\beta_T} + \frac{1}{\beta_F} \right)^{-1} \frac{\Delta T}{\sqrt{t}} \tag{22}$$

By time integration and consideration of the total contact surface, the total heat Q transferred from the droplet to the liquid is shown to be

$$Q = \frac{2}{\sqrt{\pi}} A_K \left(\frac{1}{\beta_T} + \frac{1}{\beta_F} \right)^{-1} \Delta T \sqrt{t} \tag{23}$$

i.e. heat transfer increases with the size of the contact surface A_K and the contact time t_K. This heat transfer is the first interaction between droplet and liquid; the heat transferred to the liquid is an important source of energy for the subsequent reaction. For example, a larger amount of heat will initiate a more violent reaction with higher reaction pressure build-up and faster growth of the reaction zone. Considering that at identical temperature conditions a higher trigger pressure, e.g. 8 bar, will initiate a more violent reaction with higher reaction pressure and a higher reaction zone growth rate than a lower trigger of 4 bar (Figs. 17 and 18), it is clear that the external trigger has an important function in this type of heat transfer. These arguments suggest that a higher trigger pressure will also enlarge the contact surface and/or prolong the contact time.

5.1.2 Boundary Surface Instabilities (Phase III)

The vapour film collapse is followed by local direct contact between droplet and liquid. The liquid in the point of contact is superheated by direct contact heat transfer and evaporated. Especially if the contact temperature is higher than the spontaneous nucleation temperature, spontaneous nucleation will result in a sudden evaporation. Evaporation of the superheated liquid causes pressure build-up to saturation pressure corresponding to the contact temperature in the point of direct contact. This local high vapour pressure has a recoil effect on the two liquids, i.e. the droplet and the surrounding liquid, and at the same time drives vapour flows along the boundary surface. This may result in two kinds of boundary surface instability as shown schematically in Fig. 33. One of these, the Rayleigh-Taylor instability (R-T), may be caused by the high acceleration induced by the vapour (light phase) in the two liquids (heavy phase). The other, i.e. the Kelvin-Helmholtz instability (K-H), results from the local relative velocity between the

vapour and the boundary surface of the liquid. Both the R-T and the K-H instability refer to the vapour pressure resp. the vapour velocity. Fig. 33 also gives a plausible representation of vapour pressure distribution and vapour velocity. The vapour pressure reaches a peak in the center of the local point of contact and decreases towards the vicinity of the point of contact. The distribution of the vapour flow velocity is in the opposite direction. The R-T instability is effective in the center of the point of contact and the K-H instability in its vicinity. The boundary surface waves resulting from these two instabilities, whose growth is faster than the decrease in vapour pressure, enable fragmentation of the droplet and mixing with the liquid.

According to Kelvin, as cited in /33/, there is the following equation for the growth rate of boundary surface waves with the direction of a_T as shown in Fig. 33:

$$\gamma^2 = -\omega^2 = \frac{\rho_T \rho_V K^2}{(\rho_T + \rho_V)^2} U_V^2 - \frac{\rho_T - \rho_V}{\rho_T + \rho_V} a_T K - \frac{\sigma_T K^3}{\rho_T + \rho_V} \qquad (24)$$

If $\gamma^2 > 0$, the amplitudes of the waves may grow exponentially. The first element on the rhs of this equation refers to the K-H instability, the second to the R-T instability. From this equation, the following characteristic values are derived for boundary surface waves:

Critical wavelength	Rayleigh-Taylor	Kelvin-Helmholtz	
$\lambda_{Kr} =$	$2\pi\sqrt{\frac{\sigma_T}{a_T(\rho_T - \rho_V)}}$	$2\pi\frac{\sigma_T(\rho_T + \rho_V)}{\rho_T \rho_V V_V^2}$	(25)

The wavelength with the fastest growth is

$\lambda_m =$	$\sqrt{3}\,\lambda_{kr}$	$\frac{3}{2}\,\lambda_{kr}$	(26)

The growth rate for λ_m is

$$\gamma = \left(\frac{2}{3\sqrt{3}}\right)^{\frac{1}{2}} \frac{[a_T(\rho_T - \rho_V)]^{\frac{3}{4}}}{\sigma_T^{\frac{1}{4}}(\rho_T + \rho_V)^{\frac{1}{2}}} \qquad \left(\frac{4}{27}\right)^{\frac{1}{2}} \frac{(\rho_T \cdot \rho_V)^{\frac{3}{2}} v_V^3}{\sigma_T(\rho_T + \rho_V)^2} \tag{27}$$

"Critical wavelength" refers to the shortest possible wavelength, "wavelength of fastest growth" to the wavelength with the maximum growth rate.

The acceleration of the droplet interface resulting from the high vapour pressure is

$$a_T = \frac{P_V}{\rho_T L} \tag{28}$$

where L is that thickness of a layer within the droplet, $0 < L < R$, which later participates in fragmentation.

Fig. 34 (A) shows the most unstable wavelength for each vapour pressure or L and the growth time constant calculated for this wavelength using eqs. (27) and (28). If the vapour pressure is near the critical pressure of pentane, the most unstable waves occur at $\lambda = 50$ to 100 µm. The corresponding growth time constants (Fig. 34 (B)) being between 1 and 10 µs are short enough to permit droplet fragmentation.

The vapour flow can be calculated assuming a steady isentropic change of phase.

$$\rho_V U_V^2 = 2 \varphi P_V \frac{\kappa}{\kappa - 1} \left[1 - \left(\frac{P_{sys}}{P_V}\right)^{\frac{\kappa-1}{\kappa}}\right] \tag{29}$$

where φ is the friction coefficient, with values between 0 and 1.

Fig. 35 presents calculated results for the Kelvin-Helmholtz instability based on eqs. (25) , (26), (27), and (29). For example, with $\varphi = 0.1$ the most unstable waves are at 5 to 10 µm. The growth rate constant is 0.1 - 0.5 µs. These figures suggest that the K-H instability may cause droplet fragmentation.

The calculated examples apply to instabilities at the droplet boundary surface. The described mechanism of boundary layer instability was also applied to the

surface of the cold liquid. As the surface tension of pentane is lower by a factor of 10 than the surface tension of sodium, the surface of pentane must be much more unstable. This boundary surface instability, in turn, is a precondition for mixing of the cold liquid in the reaction zone. It is apparent that the two phenomena, i.e. fragmentation and mixing, should be linked closely. The fast evaporation of the superheated liquid, the resulting acceleration of both liquid surfaces, and the local vapour flows cause fragmentation of the droplet and mixing with the liquid.

The calculations show on the other hand that the two instabilities have different effects and are effective at different times, see Table 6:

- The K-H instabilities propagates rather quickly parallel to the boundary layer.
- The fragments resulting from the K-H instability should be several times smaller than those resulting from the R-T instability.
- The R-T instability acts rather more slowly, and the fragments are coarse as compared with the K-H instability, but the growth time constant is small enough to induce fragmentation.
- For these reasons, no vapour flow and no K-H instability will occur once the reaction field covers the whole surface area of the droplet. This is reflected in Pictures 9 and 10 and Fig. 13, in which the whole surface of the droplet has become a dull white.

The conclusions are:

- The K-H instability is important only during fast expansion of the reaction field, with very fine fragmentation and mixing.
- The R-T instability causes fragmentation and mixing after the reaction field has spread across the whole droplet surface.

As the K-H instability spreads very rapidly, it was impossible, by means of the high-speed pictures taken, to identify the events proceeding at the small droplet. Its effect on the real fragmentation and mixing process appears to be rather low. In a system comprising a large volume of hot liquid, the K-H instability should have an important effect as the fast growth of the reaction field may at the same time induce high vapour pressure build-up.

On the other hand, in the small-scale droplet experiments, fragmentation and mixing are based mainly on the R-T instability as far as optical observations were possible.

The acceleration of the two-phase boundary derived from film observations can be used for calculating a mixing rate of the surrounding cold liquid due to R-T instability:

$$\dot{V}_F = A \cdot 4\pi R_V^2 \sqrt{a_F \lambda_{kr}} \tag{30}$$

As λ_{Kr} is the critical wavelength,

$$\lambda_{kr} = 2\pi \sqrt{\frac{\sigma_F}{a_F(\rho_F - \rho_V)}} \tag{31}$$

The mixing rate per unit area of the droplet surface therefore is

$$\dot{V}_F / 4\pi R_V^2 = A \sqrt[4]{4\pi^2 \frac{a_F \sigma_F}{(\rho_F - \rho_V)}} \tag{32}$$

in which A $\approx$ 4·Ac in accordance with Corradini. Ac is the total surface area of direct contact; its value here is 0.5.

Fig. 36 compares the theoretical mixing rates with the experimental findings based on the peak value of the mixing rate in Phase III (Fig. 12). In spite of a slight deviation of the experimental results, trends are similar and in good agreement for A = 2. This suggests that the optically observable processes of mixing with the liquid and droplet fragmentation can be explained by the R-T instability.

This is supported by the fragment analysis. Most fragments are in the range of 0.05 to 0.5 mm in diameter, i.e. the fragment diameters expected for the R-T instability. The presence of smaller fragments suggests that a K-H instability effect cannot be excluded.

Droplet fragmentation enlarges the whole droplet surface as well as the area of direct contact between the droplet and the liquid. This leads to further interactions between droplet and liquid in the form of heat transfer, evaporation of the superheated liquid, and pressure build-up in the vapour space. Pressure build-up continues until the pressure build-up from liquid evaporation and the pressure decrease from the expansion of the reaction zone are in equilibrium. The possibility of repeated direct contact between droplet and liquid decreases as the reaction zone grows, and the pressure drops again after reaching a peak.

5.1.3 Transition Phase and Slow Mixing (Phases IV, V)

After reaching peak values in Phase III, the vapour pressure and the acceleration of the two-phase boundary decrease. Transition to Phase IV takes place (Fig.12). Interactions may still occur but with the growth of the vapour space the number of direct contact events between the droplet, fragments, and liquid continues to decrease, strongly reducing the evaporation rate and the reaction zone growth rate. At the same time, the boundary layer between the liquid and the reaction zone returns to the stable state as the direction of liquid acceleration is reversed. This slowing-down of the boundary layer motion causes an increasing relative velocity between the boundary layer and the fragments which, due to inertia, maintain a higher velocity in the direction towards the boundary layer. Droplet fragments thus impact on the boundary layer and may submerge in the liquid, causing higher heat transfer between the fragments and the liquid and thus, eventually, additional evaporation. The developing multiphase region makes the reaction zone expand, and a new boundary is formed. This, of course, means further mixing with the liquid.

This process was clearly observable on the high-speed films although no quantitative data are available. "Projections" on the reaction zone surface in the direction of the liquid (described in Chapter 4.2.2., Phases IV,V) are interpreted as fragment immersion events.

The preceding discussions have proved that immersion of fragments in the surrounding liquid must be viewed as the main mechanism of reaction zone growth in Phase V. It is maintained until the fragments cool down.

Fig. 37 gives a schematic representation of the processes of Phases I to VI as described in the preceding chapters. The fragmentation mechanism of Phase III is based on hydrodynamic processes, i.e. the formation of boundary layer waves,

but these are not caused by external shock waves or by a relative velocity but by a thermodynamic effect of pressure build-up as a result of local evaporation. The model assumption discussed here therefore refers to a thermal fragmentation process.

5.1.4 Estimation of Minimum Mixing Energies

The preceding chapters have shown that mixing of surrounding cold liquid in the reaction zone takes place in Phases III and V and have presented a plausible explanation. This chapter will discuss the mixing process from the energetic view, i.e. if and in what conditions mixing with the liquid may occur.

Cho et al. /48/ presented a method for assessing the energy required for a simplified hypothetic fragmentation process. This method was applied without modification for estimating the energy required for mixing of the liquid. The following assumptions were made: All liquid particles are identical in size, spherical shape, and velocity. No interactions take place between the particles. As Fig. 38 shows, the mixing process comprises the following phases:

1) Fragmentation phase

   The energy required for the formation of a number of N small liquid particles is

$$E_\sigma = N\,(4\pi R_F^2)\,\sigma_F \tag{33}$$

2) Motion phase

   Finely dispersed liquid expands and moves through the vapour space. This requires kinetic energy and produces friction work. These are calculated by

$$E_{ki} = N\,(4\pi R_F^3/3)\,\rho_F\,U_F^2/2 \tag{34}$$

$$E_R = N\,c_D\pi R_F^2\,(\rho_V U_F^2/2)\,L_0 \tag{35}$$

   in which L_0 is the average the mixing distance.

By introducing the liquid volume V_F as the sum of the volumes of the N liquid particles we obtain

$$E_\sigma = 3 V_F \sigma_F / R_F$$
$$E_{ki} = V_F \rho_F U_F^2 / 2 \qquad (36)$$
$$E_R = V_F c_D (3/8) \rho_V U_F^2 L_0 / R_F$$

In the calculations, U_F is replaced by the mixing rate per unit of area $\dot{V}_F/4\pi R^2_F$ and L_0 by the thickness S of the reaction zone. For R_F, the value estimated regarding the R-T instability is assumed. The following values are obtained:

$E_\sigma = 1.5 \cdot 10^{-4}$ J

$E_{Ki} = 5.4 \cdot 10^{-3}$ J

$E_R = 2.6 \cdot 10^{-3}$ J

The thermal energy of the droplet without the heat of fusion is

$$E_T = \rho_T V_T c_{p,T} \Delta T = 28 \text{ J} \qquad (37)$$

for sodium and $T_T = 150$ °C.

This suggests that the estimated mixing energy is very small not only as compared with the available thermal energy but also with the thermodynamic energy of the reaction (see Table 5). From the energetic view, this proves that mixing of the liquids is easily reached in this geometrical set-up.

5.1.5 Internal Energy Balance of the Reaction Zone

The finely dispersed liquid particles in the reaction zone act as a heat sink for the hot droplet or its fragments. To evaporate these particles a certain heat is required. To understand the energy balance, it is useful to determine the part of the mixed liquid that can be evaporated with the thermal energy of the droplet. This is done by approximation.

The thermal energy of the droplet available for heating and evaporation of the liquid is

$$E_T = \rho_T V_T [\, c_{PT} (T_T - T_{satF}) + W_m \,] \qquad (38)$$

For T_T = 150 °C, E_T is in the range of 64 J.

The liquid volume that can be evaporated with E_T is

$$V_{FV} = \frac{E_T}{\rho_F [\, c_{PF} (T_{satF} - T_F) + W_V \,]} \tag{39}$$

With the available data, a value of about 0.27 cm^3 is obtained.

Fig.12 shows this liquid volume in the reaction zone in Point B. If the total thermal energy contained in the droplet is available for evaporation of the liquid, no further liquid can be evaporated in the reaction zone beyond Point B. In other words, the amount of liquid in the reaction zone beyond Point B acts as a heat sink for vapour in the heat balance. This liquid, which in all probability consists of small droplets, has a large total surface and may therefore be the main contributing factor to heat transfer between vapour and liquid. The conclusion is that in a real reaction, due to the internal heat sink the reaction zone should collapse earlier than in a predicted reaction in which mixing with the surrounding liquid is not taken into account. Further, in case of mixing with liquid the reaction zone will not grow as much as in a model without mixing.

5.2 Influence of the Homogeneous Nucleation Temperature (T_{HN} Criterion)

The findings of the sodium droplet experiments have shown the reaction to be more violent if the droplet is heated beyond T_{HN} of pentane. The results with silicone oil confirm that the reaction pressure will increase significantly at a contact temperature beyond T_{HN}. As the high reaction pressure is accompanied by fine fragmentation of the droplet and intensive mixing with the cold liquid, it is clear that T_{HN} has an important part in boiling fragmentation.

These findings and their interpretation are compatible with the results of earlier publications. In the silicone oil droplet experiments of the present study, the following reaction processes were observed in detail using high-speed films (Figs. 39 and 40):

- Case 1 $T_K < T_{HN}$ Fig. 39

After vapour film collapse, a small local mixing region started to form which grew until the whole surface area of the droplet was covered. At the same time, the mixing region expanded during a period of about 300 µs.

- Case 2 $T_K > T_{HN}$ Fig. 40

After the incidence of the trigger pressure wave, the whole surface was initially covered by a white layer corresponding to the reaction zone. This lasted for about 50 µs, after which the reaction zone started to grow quickly.

The following simple mechanism is assumed: If $T_K > T_{HN}$, the superheated liquid evaporates without delay, i.e. fast vapour pressure build-up takes place in several local points of direct contact. The results are a high reaction pressure and violent instabilities, causing droplet fragmentation and intensive mixing with the liquid.

The experimental findings, i.e. high-speed films and reaction pressure measurements (Figs. 19 and 21) show that Fauske's criterion is an important thermal precondition for a violent vapour explosion. However, a reaction with droplet fragmentation in the temperature range below T_{HN} cannot be completely excluded (Fig. 19). Reactions less violent than those at higher droplet temperatures did indeed take place, i.e. the T_{HN} criterion is not a necessary but only a sufficient thermal condition for a violent thermal reaction.

5.3 Influence of the External Trigger Pressure

The experimental findings show that the trigger pressure required for initiating the reaction between the droplet and the surrounding liquid is a function of the droplet temperature (Figs. 7 and 8). In the temperature range above T_{HN} as referred to the droplet temperature (sodium droplet) or contact temperature (silicone oil droplet), the trigger pressure required increases with the droplet temperature. This is explained as follows:

- Publications in this field have shown that the stability of film boiling is determined by the temperature difference between the reacting materials. Yao /6/ observed that the number of spontaneous local intermittent direct contact events between the two materials during film boiling decreased as the temperature of the hot material increased. This applies in particular to temperatures above the critical temperature T_{Kr} of the cold liquid.

- Conditions should be similar with an external disturbance as, in our case, the trigger wave. Due to the higher temperature, more liquid is evaporated prior to direct contact, which will delay or even prevent the film collapse and subsequent direct contact which initiate the reaction.

At temperatures below T_{HN}, the required trigger size increases with the decreasing droplet temperature, suggesting compensation of the lower thermal energy of the droplet by the external trigger.

On the other hand, experimental findings show (Figs. 7 and 8) that the sodium droplet requires an external trigger of at least 3 bar while 1 bar is sufficient for the silicone oil droplet. Further, at a contact temperature near T_{HN} the temperature of silicone oil droplets is higher than the temperature of sodium droplets. Assuming that the external trigger induces only the collapse of the vapour film, a reaction should take place in both systems, i.e. Na/pentane and silicone oil/pentane, at identical minimum triggers. This is not the case.

Further, also the reaction curves for two different trigger pressures and identical droplet temperatures (Figs. 17, 18 in Chapter 4.3) indicate that an external trigger pressure not only induces the reaction but dominates the whole reaction process.

These facts suggest that the external trigger not only serves to establish direct contact between the two liquids, i.e. the droplet and the surrounding liquid, but that important dynamic and/or thermal interactions take place as well. These may be explained as follows:

Explanation 1

As described in Chapter 5.1.1, the mechanism of vapour film collapse is as follows:

The system pressure increases after the shock wave has passed the droplet in the film boiling state, causing a spherically symmetric collapse of the vapour film. The following events are conceivable:

- In addition to its spherically symmetrical movement, the surrounding liquid moves also in the direction of the trigger.

- As the liquid collides with the droplet, the relative velocity reaches a peak near the droplet equator vertical to the direction of motion of the trigger wave.

- This relative velocity causes the two liquids, i.e. the droplet and the surrounding liquid, to mix as a result of hydrodynamic effects, e.g. boundary layer stripping.

The high-speed films show that the reaction field originates at the droplet equator at the onset of the reaction, especially if the trigger is small. It must therefore be assumed that the first mixing at the droplet equator is due to hydrodynamic effects. This assumption will be investigated in the following.

Shortly after contact between the droplet and liquid, the velocity development in the two boundary layers with different initial velocities (see sketch) is given by the momentum equations:

$$\frac{\partial U_F}{\partial t} = \nu_F \frac{\partial^2 U_F}{\partial y^2} \qquad (40)$$

$$\frac{\partial U_T}{\partial t} = \nu_T \frac{\partial^2 U_T}{\partial y^2}$$

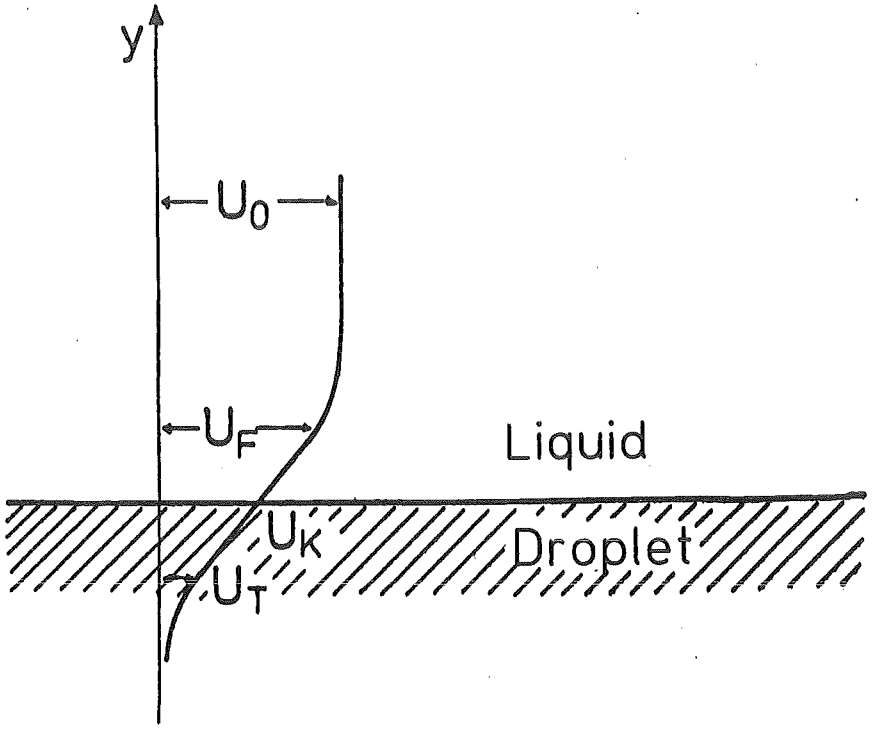

From eq. (40), the boundary surface velocity U_K can be derived:

$$U_K = \frac{\xi U_0}{1+\xi} \quad , \quad \xi = \sqrt{\frac{\mu_F \rho_F}{\mu_T \rho_T}} \tag{41}$$

The result is the shearing stress acting on the boundary layer:

$$\tau = \frac{\mu_F \rho_F U_0}{(1+\xi)\sqrt{\pi t}} \tag{42}$$

The initial relative velocity U_0 at the droplet equator results from eq. (16):

$$U_0 = 3/2\, U_G \tag{43}$$

For an external trigger of 10 bar acting on a sodium droplet and t = 10 µs we obtain $\tau = 160$ N/m^2. This value is higher than the surface tension $2\sigma_T/R_T$, which is calculated as 50 N/m^2, i.e. boundary layer stripping should occur. This may possibly cause enlargement of the contact surface, i.e. higher heat transfer between the two liquids.

Explanation 2:

In his experiments on a non-melting, heated metal wire in water, Inoue /49/ found that the characteristics of heat transfer will change at a trigger pressure threshold value as soon as the film boiling collapses after trigger impact. If the external trigger pressure is above this threshold level, heat transfer from the hot to the cold material is several times higher than below this threshold level. The heat transfer has a peak at a certain trigger pressure if the contact temperature is near the critical temperature of water.

The results of this study with regard to the delay between the trigger pressure peak and the reaction pressure (Figs. 22, 23, 24) show:

- The higher the trigger, the shorter will be the delay time and the higher the reaction pressure.

- At a certain trigger pressure and T_{Kr}, the delay time reaches a minimum value while the reaction pressure has a peak.

This is qualitatively well compatible with Inoue`s findings and indicates that the external trigger has the same function in both series of experiments.

Fig. 41 is a simple representation of the mechanism of an external trigger. Both cases, i.e. premixing as a result of boundary layer stripping or enhanced heat transfer by direct contact, cause the mean temperature of the cold liquid in the superheated boundary layer to rise. The higher temperature of the liquid induces a higher vapour pressure, which causes a more violent reaction.

5.4 Influence of the Main Material Properties on the Fragmentation Process

The preceding chapter attempted to explain the mechanism of droplet (i.e. hot liquid) fragmentation and mixing with the surrounding cold liquid. This chapter will discuss the effects of the reaction system material properties on the fragmentation process and attempt a prediction of the fragmentation behaviour of the material systems used in nuclear reactors.

As shown in the preceding chapter, a thermal reaction involving droplet fragmentation and mixing with the surrounding liquid comprises several phases, of which the third phase (Phase III) is the most important. This phase is dominated by the two instabilities of the boundary layer (see Chapter 5.2.2.). The growth rates of these two instabilities, i.e. the Rayleigh-Taylor and the Kelvin-Helmholtz instability are determined using eq. 27:

$$\gamma_{RT} = (2/3\sqrt{3})^{\frac{1}{2}} \frac{[a_T(\rho_T - \rho_V)]^{3/4}}{\sigma_T^{1/4}(\rho_T + \rho_V)^{1/2}}$$

$$\gamma_{KH} = (4/27)^{\frac{1}{2}} \frac{(\rho_T \rho_V)^{3/2} u_V^3}{\sigma_T(\rho_T + \rho_V)^2}$$

The higher these two growth rates, the more violent will be the fragmentation of the hot droplet, causing a violent vapour explosion. With local direct contact between the hot and cold liquids, the vapour pressure will increase as a result of sudden evaporation of the cold liquid. In theory, the pressure may continue to

rise to the saturation pressure of the contact temperature; in reality, however, the rise is slowed down by the fast expansion process. The average pressure therefore is assumed to be proportional to the saturation pressure. According to Corradini /39/, $P_{eff} = 1/4\, P_{sat}(T_K)$, i.e. in this case

$$\bar{P}_V \propto P_{sat}(T_K) \tag{44}$$

The acceleration of the droplet surface a_T and of the vapour flow $\rho_V U_V^2$ is determined by P_V. Eqs. 28 and 29 result in

$$a_T \propto \frac{\bar{P}_V}{\rho_T} \tag{45}$$

$$\rho_V U_V^2 \propto \bar{P}_V \tag{46}$$

Eqs. (27), (44), (45), and (46) and the assumption $\rho_V \ll \rho_T$ result in the following equations:

$$\gamma_{RT} \propto \frac{P_{sat}(T_K)^{3/4}}{\sigma_T^{1/4}\,\rho_T^{1/2}} = \left(\frac{P_{sat}}{\sigma_T^{1/3}\,\rho_T^{2/3}}\right)^{3/4} \tag{47}$$

$$\gamma_{KH} \propto \frac{P_{sat}(T_K)^{3/2}}{\sigma_T\,\rho_T^{1/2}} = \left(\frac{P_{sat}}{\sigma_T^{2/3}\,\rho_T^{1/3}}\right)^{3/2} \tag{48}$$

The expressions $\dfrac{P_{sat}}{\sigma_T^{1/3}\,\rho_T^{2/3}}$ and $\dfrac{P_{sat}}{\sigma_T^{2/3}\,\rho_T^{1/3}}$ may be viewed as characteristic values of the violence of boiling fragmentation to be expected. These characteristic values are higher if

1) the saturation pressure (M.P.1) increases with the contact temperature, and

2) the surface tension and density (M.P.2) of the hot liquid decrease.

These material properties, M.P.1 and M.P.2, can thus be directly related to the violence of the boiling fragmentation.

Table 7 lists the characteristic values for different systems of materials. This table shows relatively higher figures for those systems in which violent explosive reactions were observed under certain conditions. There is a simple explanation of the different results of fragmentation experiments with different material systems.

- In molten metal/water, violent fragmentation takes place, /19/, /290/, /21/, /22/ due to M.P.1.

- In water/freon, mineral oil/freon, or silicone oil/pentane, violent fragmentation takes place in spite of the lower saturation pressure of the cold liquid /23/, /26/ due to M.P.2.

- In copper/water, fragmentation due to M.P.2 is initiated more easily if the copper surface is oxydated /50/.

- In silicone oil/pentane, the impulse ratio between the reaction pressure and the trigger pressure is higher than in sodium/pentane, due to M.P.2.

This shows a relationship between the main material properties, P_{sat} and σ_T, and the violence of the boiling fragmentation.

The calculated characteristic values for the UO_2/pentane system are small as well, which is assumed to be due to the low contact temperature resp. the lower saturation pressure of Na and the rather high density of UO_2. It is therefore assumed that the reaction between molten UO_2 and Na should be mild, with coarse fragmentation of UO_2. On certain conditions, the Na may be heated to near its critical temperature. If small Na volumes penetrate into large UO_2 volumes, the contact temperature may increase with the Na temperature and may reach the critical temperature, as the temperature of molten UO_2 is far above the critical temperature of Na. In this case the reaction may be violent but incoherent due to its contact mode, as no coarse mixing can be expected in the initial phase.

In the UO_2/water system, on the other hand, violent boiling fragmentation may take place if the external trigger is high enough to overcome stable film boiling as a result of the high temperature difference.

The violence of fragmentation is related to the fineness of the fragments. The fine fragments result from the more violent fragmentation. To verify this statement, Fig. 42 compares the analyses of fragments of different material systems. The mass fractions of the fine fragments of Na/pentane and UO_2/sodium /51/ are comparable, while systems of Cu (oxydized)/water /42/ or UO_2/water /28/ yield very fine fragments. This comparison is well compatible with the predictions of eqs. 47 and 48 and with the experimental findings.

6. Summary and Conclusions

In this study, experiments on boiling fragmentation in a thermal reaction were carried out, and the results were presented, analyzed, and discussed. Single droplets heated up dropped into a liquid where they were made to react in these experiments. The reaction was found to be a thermal interaction between the hot droplet and the cold, volatile liquid. If a large number of hot droplets is present in a cold liquid, violent vapour explosions with high pressure build-up may occur under certain boundary conditions. The experiments are characterized as follows: The use of a high-speed camera with a taking speed up to 10^5 frames per second enabled more detailed observations of the processes than in earlier investigations. In order to reduce the hydrodynamic effects between the hot droplet and the cold liquid, suitable experminental systems were chosen, i.e. sodium or silicone oil droplets and pentane as the cold liquid. The density ratio of these systems is around 1. One of the experimental parameters was the trigger pressure wave required for initiating the reaction. The experiments yielded new findings on the reaction process with boiling fragmentation of the hot droplet, and the following conclusions can be drawn:

In both systems, i.e. sodium/pentane and silicone oil/pentane, a reaction with fragmentation occurs only if the external trigger pressure exceeds a given threshold. This required trigger pressure has a minumum value if the contact temperature between the hot droplet and pentane is in the range of the homogeneous nucleation temperature of pentane. After detailed visual evaluation of the high-speed films in consideration of the measured, highly transient pressure curves, the triggered reaction can be divided into the following phases, in which different physical processes are dominant:

(I) Film boiling

(II) Film collapse and direct contact

(III) Sudden evaporation and fragmentation

(IV) Transition

(V) Slow mixing

(VI) Condensation

A reaction pressure resulting directly from the thermal interaction and an accelerated growth of the reaction zone were measured only during Phase III (sudden evaporation and fragmentation); it accounts for only one tenth of the whole re-

action time, that is about 1 ms. It is assumed that also the droplet fragmentation takes place in this phase. Visual observations of the high-speed films show that fragmentation is initiated by evaporation of the superheated liquid in the points of direct contact. The boundary layer instabilities in the region of fast pressure build-up, i.e. the Rayleigh-Taylor and Kelvin-Helmholtz instability, determine the further fragmentation process of the droplet.

Further, the evaluation of the high-speed films showed intensive mixing with the surrounding liquid in Phase III (Sudden evaporation and fragmentation). This was measured quantitatively for the first time by recording the motion of the liquid surrounding the reaction zone. It is assumed that the initiating mechanism is identical with the mechanism causing droplet fragmentation. At the end of Phase IV (Transition) and in Phase V (Slow mixing), a further diffusion of liquid into the reaction zone was observed, although at a mixing rate several times lower than in Phase III. The finely dispersed liquid confined in the reaction zone causes further evaporation and thus further growth of the reaction zone in Phase III. In the later Phases V and VI (Slow mixing and Condensation), however, the mixed liquid not only enhances vapour condensation in the reaction zone, but also acts as internal heat sink for the droplet and its fragments. The heat balance clearly indicates that the thermal energy of the droplet is not sufficient for evaporating the total volume of mixed liquid, which may account for up to 60% of the total reaction zone volume. A quantitative statement on the effects of the mixed liquid on the reaction process was not possible, but it was shown qualitatively that the effects of liquid mixed into the reaction zone must not be neglected in future models of vapour explosion.

The high-speed films show further details of the reaction process, the intensity of fragmentation, and the pressure build-up: If the contact temperature was above the homogeneous nucleation temperature, T_{HN}, the reaction area spread across the whole droplet surface prior to the expansion of the reaction zone. This is assumed to be the cause of the higher reaction pressure measured. If the contact temperature was below T_{HN}, there was no fast expansion of the reaction area but only local growth of the reaction zone, e.g. slightly above the central area of the droplet. The latter was accompanied by lower pressure build-up. The two different results show the important function of homogeneous nucleation in the development of the reaction zone resp. in reaction pressure build-up. With an increasing temperature difference between droplet and liquid, i.e. at a contact temperature far above the critical temperature T_{Kr} of the liquid, stable film boiling can be interrupted only by a significant increase of the trigger pressure. In this case, a

full scale thermal reaction or fine boiling fragmentation can be initiated only with the aid of a high external trigger. If these arguments are applied to the material systems encountered after a serious hypothetical accident (HCDA), i.e. molten UO_2 and sodium or molten UO_2 and water, the following results are to be expected:

- UO_2/sodium

As the contact temperature will always be lower than the T_{HN} of sodium, only local growth of the reaction zone and only mild pressure build-up are to be expected after direct contact.

- UO_2/water

In a system of UO_2 heated high above its melting point and water, a contact temperature far beyond T_{Kr} may result, i.e. fast expansion of the reaction zone across the droplet surface is possible, accompanied by high pressure build-up, but only if a high external trigger causes the stable vapour film to collapse.

Further, the experimental findings suggest that the trigger required for initiating a reaction is a function of the material system. If the trigger exceeds this given threshold, it will cause the vapour film around the droplet to collapse and will also have an important influence on the further interactions between the reacting liquids. This study gives two reasons for this: Due to the relative velocity between the droplet and the surrounding liquid in Phase II (Film collapse and direct contact), boundary layer stripping occurs in the points of contact. Also, the heat transfer in the points of contact changes considerably, favouring sudden evaporation with high local vapour pressure build-up. For a quantitative modelling, however, a more precise description of vapour film collapse and of the interaction between the two liquids behind the trigger front will be required.

Based on the new findings obtained in this study on boiling fragmentation processes and on the analysis of the most important boundary layer instabilities, an attempt was made to determine two characteristic values for the expected reaction patterns of different material systems. These characteristic values are a simple representation of the main physical properties, i.e. density, surface tension and saturation pressure referred to the contact temperature:

$$\frac{P_{sat}}{\sigma_T^{1/3}\,\rho_T^{2/3}} \qquad , \qquad \frac{P_{sat}}{\sigma_T^{2/3}\,\rho_T^{1/3}}$$

The higher these characteristic values the more violent will be the boiling fragmentation. As expected, the characteristic values of the sodium/pentane system, whose rather mild reaction is accompanied only by coarse fragmentation, are lower by a factor of 2 than those of, e.g., the Al/water system in which a violent reaction with fine fragmentation was observed. The following statements were derived from applying these characteristic figures to the UO_2/sodium and UO_2/water systems:

- UO_2/sodium

As the characteristic values of the UO_2/sodium system are in the same range as those of the sodium/pentane system, only a rather mild boiling fragmentation is expected.

- UO_2/water

In the UO_2/water system, on the other hand, the higher characteristic values (i.e. a factor of 1.5 as compared to sodium/pentane), a more violent boiling fragmentation must be expected. The characteristic figures are comparable with those of Cu/water and Sn/water, which cause violent reactions with fine fragmentation. However, the repeatedly stated condition, i.e. collapse of the stable film boiling of the UO_2/water system induced by a high external trigger, must be met additionally.

7. Appendix A

Droplet temperature curves during film boiling

- Silicone oil -

While the hot droplet is immersed in the cold liquid, its surface temperature decreases due to heat transfer during film boiling. To determine of the contact temperature between the two liquids, as accurate as possible, this temperature drop was assessed by the following integral method:

Fig. A-1 shows the assumed temperature distribution. Initially, the temperature distribution is flat (T_{T0}). After a certain delay, the surface temperature of the droplet decreases (T_{TS}) as heat is transferred through the vapour film. The temperature distribution within the thermal boundary layer of the droplet is assumed to have a parabolic function, i.e.

$$\frac{T_{T0} - T(r)}{T_{T0} - T_{TS}} = \frac{(r - R_{TB})^2}{(R_T - R_{TB})^2} \qquad \text{(A-1)}$$

The energy balance in the thermal boundary layer is:

$$\int_{R_{TB}}^{R_T} \left[\frac{\partial T(t,r)}{\partial t} - \frac{\theta}{r^2} \frac{\partial}{\partial r} \left(r^2 \frac{\partial T(t,r)}{\partial r} \right) \right] 4\pi r^2 dr = 0 \qquad \text{(A-2)}$$

where $\theta = k/\rho c_p$ = thermal diffusivity

The energy balance at the droplet surface is

$$-k_T \left. \frac{\partial T}{\partial r} \right|_{r=R_T} = h_{FB} (T_{TS} - T_F) \qquad \text{(A-3)}$$

h_{FB} = heat transfer coefficient

From eqs. (A-1) and (A-2), the following dimensionless quantities are obtained:

$$\tilde{T} = \frac{T_{T0} - T_{TS}}{T_{T0} - T_F} \qquad \tilde{R} = \frac{R_{TB}}{R_T} \qquad \widetilde{Nu}_T = h_{FB}\frac{2R_T}{k_T} \qquad \tilde{t} = \frac{\theta}{R_T^2}t \tag{A-4}$$

Differentiation of T with respect to time t gives:

$$\frac{d\tilde{T}}{d\tilde{t}} = \frac{60\,\tilde{T}}{(1-\tilde{R})[(1-\tilde{R})(\tilde{R}^2+3\tilde{R}+6)+\frac{\tilde{T}(1-2\tilde{T})}{\widetilde{Nu}_T(1-\tilde{T})^2}(3\tilde{R}^2+4\tilde{R}+3)]} \tag{A-5}$$

Introducing

$$\tilde{R} = 1 - \frac{4\tilde{T}}{\widetilde{Nu}_T(1-\tilde{T})} \tag{A-6}$$

and considering that $1-R \ll 1$ and T^4 resp. $T^5 \ll 1$, one obtains:

$$\frac{d\tilde{T}}{d\tilde{t}} = \frac{15\,\widetilde{Nu}_T^3}{50\,\widetilde{Nu}_T\tilde{T} + (90\,\widetilde{Nu}_T - 56)\tilde{T}^2} \tag{A-7}$$

i.e.

$$25\,\widetilde{Nu}_T\tilde{T}^2 + (30\,\widetilde{Nu}_T - 56/3)\tilde{T}^3 = 15\,\widetilde{Nu}_T^3\tilde{t} \tag{A-8}$$

According to Frederking /53/ the Nusselt number for film boiling in case of spherical symmetry is

$$Nu = \frac{2}{3}(Ra^*)^{1/4} = h_{FB}\frac{2R_V}{k_V} \tag{A-9}$$

in which Ra* is the modified Rayleigh number; the result is

$$Ra^{*} = Gr_{\bar{V}} \cdot Pr_{\bar{V}} \frac{(W_V + 0{,}5\, c_{p,V} \Delta T_V)}{c_{p,V} \Delta T_V} \qquad \text{(A-10)}$$

where Gr and Pr are the Grashof number and Prandtl number, respectively. $\widetilde{Nu}_T$ can be calculated on this basis.

$$\widetilde{Nu}_T = h_{FB} \frac{2R_T}{k_T} = Nu \frac{k_V}{2R_V} \frac{2R_T}{k_T} = Nu \frac{k_V}{k_T} = \frac{2}{3} \frac{k_V}{k_T} (Ra^{*})^{\frac{1}{4}} \qquad \text{(A-11)}$$

After entering the material data, the result for silicone oil is

$$\widetilde{Nu}_T = 4.4 \,. \qquad \text{(A-12)}$$

Fig. A-2 shows the temperature drop and the growth of the thermal boundary layer as a function of time. As film boiling on average lasts about 50 ms until the impact of the trigger pressure wave, the temperature drop is found to be 15% of the temperature difference $T_{TO} - T_F$, with the thermal boundary layer in the droplet growing by up to 16% of the droplet radius.

- Sodium -

The above method of estimating the droplet temperature drop during film boiling is not applicable to sodium droplets. There is a simpler method, i.e. the "point approximation" as the thermal conductivity of sodium is high enough to assume a flat temperature distribution in the droplet.

The temperature drop is characterized as follows:

$$T_{TO} - T_{TS} = \frac{4\pi R_T^2 h_{FB} (T_{TS} - T_F) \cdot t_{FB}}{\rho_T V_T c_{PT}} = \frac{3\, t_{FB} h_{FB}}{R_T \rho_T c_{PT}} (T_{TS} - T_F) \qquad \text{(A-13)}$$

or

$$\frac{T_{TO} - T_{TS}}{T_{TO} - T_F} = \widetilde{T} = \frac{(3\, t_{FB} h_{FB}) / (R_T \rho_T c_{PT})}{[1 + (3\, t_{FB} h_{FB}) / (R_T \rho_T c_{PT})]} \qquad \text{(A-14)}$$

If t_{FB} = 50 ms and $h_{FB} = Nu\ k_V/2R_V$ = 220 W/m^{2}K are applied, the temperature drop is only 0.7%, i.e. the temperature drop during film boiling is negligible in the case of sodium.

The temperature drop resulting from radiative heat transfer and from the heat required for generating the vapour film at the onset of film boiling is negligible as well.

8. Appendix B

Approximation of the pressure in the reaction site

In order to estimate the difference between the pressure in the measuring point and the pressure in the reaction site, a calculation was made using the three-dimensional code "SING" /54/. This code, which assumes the liquid to be incompressible, models the spatial pressure distribution by a point source along the potential flux.

Fig. B-1 presents the result of a pressure distribution calculation as referred to the cross section of the experimental vessel at which two pressure transducers are mounted. The horizontal axis is the distance from the center of the vessel, while the vertical axis is the corresponding relative pressure. One of the pressure transducers is installed at 7.5 mm from the center, while the other is mounted flush with the wall at a distance of 15 mm (see Fig. 3). According to the calculation, the two measured values ought to differ by a factor of 1.28.

The factor derived from the measurements has an average value of 1.21 (see Figs. 9-11). The two factors are well compatible. Further, the reaction pressures in the reaction site according to Fig. B-1 should be higher by a factor of 1.2 than the pressures measured by transducer A, i.e. the measured values are a good practical representation of the reaction pressures on the droplet. The reaction pressures are assumed to be evenly distributed across the whole reaction zone. They cannot be compared with the very high vapour pressures resulting in local points of contact.

9. Nomenclature

Symbol	*Definition*	*Unit*
A	Factor of the direct contact surface	-
A_C	Fictitious fraction of the direct contact surface	-
A_K	Total direct contact surface	m^2
C	Sound velocity	m/s
c_D	Friction coefficient	-
c_p	Specific heat at constant pressure	J/kg K
D	Diameter	m
E	Energy	J
e	Energy density	J/m^3
F_F	Volume fraction of mixed liquid in the reaction zone	-
δf	Error	
g	Acceleration due to gravity	m/s^2
h	Heat transfer coefficient	$W/ m^2 K$
J	Nucleation rate	1/s
K	$= 2 \pi/\lambda$, circular wave number	1/m
$\bar{k}$	Boltzmann constant	J/K
k	Thermal conductivity	W/mK
L	Length	m
M	Molar weight	kg/mol
N	Number	-
Nu	Nusselt number	-
P	Pressure	N/m^2
Q	Energy	
q	Heat flux	W/m^2
R	Gas constant	J/mol K
R	Radius	m

R_F	Radius of the liquid particle	m
Ra, Ra*	Rayleigh number	-
S	Vapour film thickness	m
SF	Probable error	
T	Temperature	°C
T_{HN}	Homogeneous nucleation temperature	°C
t	Time	s
u, U	Velocity	m/s
V	Volume	m^3
W	Bubble formation energy	J
W_m	Heat of melting	J/kg
W_V	Latent heat of evaporation	J/kg
x	Length	m
X	Motion of the surrounding liquid	m

Greek symbols

Symbol	*Definition*	*Unit*
α	Evaporation and condensation coefficient	-
β	Thermal effusivity	$J/m^2Ks^{1/2}$
γ	Growth rate of boundary surface wave	-
δ, Δ	Difference	m^2/s
Θ	Temperature diffusibility	-
κ	$= c_p/c_v$, ratio of specific heats capacities	m
λ	Wavelength	
λ_{Kr}	Critical wavelength of boundary layer instability	m
λ_m	Fastest growing wavelength of boundary layer instability	m
μ	Dynamic viscosity	kg/ms
ν	Kinematic viscosity	m^2/s

π	Circular constant	-
ρ	Density	kg/m^3
σ	Surface tension	N/m
τ	Shearing force	N/m^2
φ	Friction coefficient	-
ω	Circular frequency	1/s

Subscripts

eff	effective
F	cold liquid
FB	film boiling
G	boundary layer
K	contact
Ki	kinetic
Kr	critical
L	immediate environment of hot droplet
min	minimum
R	friction
sat	saturation
sys	system
t	total
T	hot droplet
TB	thermal boundary layer
RS	droplet surface
RT	Rayleigh-Taylor
KH	Kelvin-Helmholtz
Tr	Trigger
V	vapour
σ	surface energy

0	initial
1, 2, i	time curve

Superscripts

$^{(1)}$, $^{(2)}$	medium 1, 2
$\sim$	dimensionless
$\dot{}$	first derivation with respect to time
$\ddot{}$	second derivation with respect to time

10. Bibliography

/1/ Smidt, D:
Reaktortechnik, Bd. 2: Anwendungen, G. Braun, Karlsruhe 1977

/2/ Schumann, U:
"Dampfexplosion - Physikalische Grundlagen und Bezug zur Reaktorsicherheit", KfK 3388, 1982

/3/ Bankoff, S.G.:
"Vapour Explosions", Reactor Safety Heat Transfer,
Hemisphere Pub. Co., 1981

/4/ Cronenberg, A.W. and Benz, R.:
"Vapour Explosions Phenomena with Respect to Nuclear Reactor Safety Assessment", Adv. Nucl. Science and Technology,Vol. 12, 247-334, 1978

/5/ Bradfield, W.S.:
"Liquid-Solid Contact in Stable Film Boiling",
Industrial and Engineering Chemistry Fundamentals, Vol. 5, 200-204, 1966

/6/ Yao, S. and Henry, R.:
"An Investigation of the Minimum Film Boiling Temperature on Horizontal Surfaces", Int. Heat Transfer, Vol. 400, 260-267, 1978

/7/ Hicks, E.P. and Menzies:
"Theoretical Studies on the Fast Reactor Maximum Accident",
ANL-7120, 654-670, 1965

/8/ Anderson, R.P. and Armstrong, D.R.:
"Comparison between Vapor Explosion Models and Recent Experimental Results",AIChE Symposium Series, No. 138, Vol. 70, 31-47, 1974

/9/ Caldarola, L:
"A theoretical Model with Variable Masses for the Molten Fuel-Sodium Thermal Interaction in a Nuclear Fast Reactor", Nucl. Engrg. and Design, Vol. 34, 181-201, 1975

/10/ Board, S.J. et. al.:
"Detonation of Fuel Coolant Explosions", Nature, Vol. 254, 319-321, 1975

/11/ Fishlock, T.P.:
"Calculations on Propagating Vapor Explosions for the Aluminium/Water and UO_2/Sodium Systems",
Fourth CSNI Spec. Meetg. on Fuel-Coolant Interaction in Nucl. Reactor Safety, Bournemouth, CSNI Report No. 37, Vol. 1, 54-80, 1979

/12/ Jacobs, H.:
"Computational Analysis of Fuel-Sodium Interactions with an Improved Method", Proc. Int. Meetg. Fast Reactor Safety and Related Physics, Chicago, CONF-761001, Vol. 3, 926-935, 1976

/13/ Fauske, H.K.:
"The Role of Nucleation in Vapor Explosions",
Trans. ANS, Vol. 15, 813-814, 1972

/14/ Fauske, H.K.:
"On the Mechanism of Uranium Dioxide-Sodium Explosive Interactions",
Nucl. Sci. and Engrg., Vol. 51, 95-101, 1973

/15/ Fauske, H.K.:
"Some Aspects of Liquid-Liquid Heat Transfer and Explosive Boiling",
Proc. of the Fast Reactor Safety Meetg., Beverly Hills, CONF-740401, 992-1005, 1974

/16/ Ochiai, M. and Bankoff, S.G.:
"Liquid-Liquid Contact in Vapour Explosions",
Proc. Int. Meeting. Fast Reactor Safety and Related Physics, Chicago, CONF-761001, Vol. 4, 1843-1851, 1976

/17/ Anderson, R.P. and Armstrong, D.R.:
"R-22 Vapor Explosions", Nucl. Reactor Safety Heat Transfer,
Proc. Winter Annual Meetg. ASME, Atlanta, 31-45, 1977

/18/ Briggs, A.J.:
"Experimental Studies of Thermal Interactions at AEE Winfrith", Third Specialist Meetg. on Sodium Fuel Interactions, Tokyo, PNC N251, 75-96, 1976

/19/ Board, S.G. and Hall, R.W.:
"Propagation of Thermal Explosions, Part 1: Tin/Water Experiments",
CEGB Report RD/B/N2850, 1974

/20/ Reynolds, J.A. et.al.:
"Fuel-Coolant Interactions - Some Basic Studies at the UKAEA Culham Laboratory", Third Spec. Meetg. on Sodium Fuel Interactions, Tokyo, PNC N251, 1976

/21/ Sharon, A. and Bankoff, S.G.:
"Fuel-Coolant Interaction in a Shock Tube with Initially-Established Film Boiling", Chemical Eng. Dep. Northwestern Univ., Evanson, IL 60201, COO-2512-16, 1979

/22/ Fry, C.J. and Robinson, C.H.:
"Experimental Observations of Propagating Thermal Interactions in Metal/Water Systems", Fourth CSNI Spec. Meetg. on Fuel-Coolant Interaction in Nucl. Reactor Safety, Bournemouth, CSNI Report No. 37, Vol. 2, 329-362, 1979

/23/ Henry, R.E. et.al.:
"Large Scale Vapor Explosion",
Fast Reactor Safety Meetg., Beverly Hills, CONF-740401, 922-934, 1974

/24/ Board, S.J., et. al.:
"The Role of Spontaneous Nucleation in Thermal Explosions - Freon /Water Experiments", Fast Reactor Saf. Meetg., Beverly Hills, CONF-740401, 935-936, 1974

/25/ Armstrong, D.R.:
"Reactor Development Program Progress Report", ANL-RDP-2, 1972

/26/ Amblard, M. and Berthoud, G.:
"UO_2-Na Interactions - The CORECT-II Experiment",
Fourth CSNI Spec. Meetg. on Fuel-Coolant Interaction in Nucl. Reactor Safety, Bournemouth, CSNI Report No. 37, Vol. 2, p. 508, 1979

/27/ El-Genk, M.S. and Hobbins, R.R.:
"Analysis of Molten Fuel-Coolant Interaction during a Reactivity Initiated Accident Experiment", Winter Annual Meetg. of ASME Washington, D.C., HTD-Vol. 19, 1-16, 1981

/28/ Schmidt, T.R.:
"LMFBR Prompt Burst Excursion (PBE) Experiments in the Annular Core Pulse Reactor (ACPR)", ANS/ENS Meetg., Chicago, Oct. 1976, SAND-76-5386

/29/ Wrigth, R.W. et.al.:
"Summary of Autoclave Treat Tests on Molten Fuel Coolant Interactions", Fast Reactor Safety Meetg., Beverly Hills, CONF-740401, 254-267, 1974

/30/ Patel, P.D. and Theofanous, T.G.:
"Hydrodynamic Fragmentation of Drops", J. Fluid Mech., Vol. 103, 207-223, 1981

/31/ Theofanous, T.G. et.al.:
"The Role of Hydrodynamic Fragmentation in Fuel Coolant Interactions", Fourth CSNI Spec. Meetg. on Fuel-Coolant Interaction in Nucl. Reactor Safety, Bournemouth, CSNI Report No. 37, Vol. 1, p. 112, 1979

/32/ Bains, M. et.al.:
"The Hydrodynamics of Large-Scale Fuel-Coolant Interactions", Nuclear Techn., Vol. 49, 27-39, 1980

/33/ Schriewer, J.:
Zur Theorie der hydrodynamischen Fragmentation von Flüssigkeitstropfen in flüssigen Medien durch Stoßwellen mit Anwendung auf die Systeme Hg/H_2O, FeH_2O, Stahl/Na, UO_2/Na", Dissertation, Institut für Kernenergetik und Energiesysteme, Univ. Stuttgart 1979

/34/ Swift, D. and Baker, L.:
"Reactor Development Program Report", ANL-7152, 87-96, 1965

/35/ Witte, L.C. et.al.:
"Heat Transfer and Fragmentation During Molten-Metal/Water Interactions", J. of Heat Transfer, Trans. ASME, Ser. C, Vol. 95, 521-527, 1973

/36/ Katz, D.L. and Sliepcevich, C.M.:
"LNG/Water explosions: cause &effect", Hydrocarbon, Processing, 240-244, Nov. 1971

/37/ Wey, B.O. et.al.:
"Boiling Fragmentation Studies and their Relevance to the Initiation and Propagation of FCI's, ICHMT Seminar, International Centre for Heat and Mass Transfer, Dubrovnik, Sept. 1980

/38/ Colgate, S.A. and Sigurgeirsson, T.:
"Dynamic Mixing of Water and Lava", Nature, Vol. 244, 552-555, 1973

/39/ Corradini, M.:
"Analysis and Modelling of Steam Explosion Experiments", SAND 80-2131

/40/ Buchanan, D.J.:
"A Model for Fuel-Coolant Interactions", Journal of Physics, D-7, 1441-1457, 1974

/41/ Caldarola, L. and Kastenberg, W.E.:
"On the Mechanism of Fragmentation during Molten Fuel/Coolant Thermal Interaction", Proc. of the Fast Reactor Safety Meetg., Beverly Hills, CONF-740104, 937-954, 1974

/42/ Ando, M. and Caldarola, L.:
"Triggered Fragmentation Experiments at Karlsruhe",
Proc. Information Exchange Meetg. on Post Accident Debris Cooling, Karlsruhe, July, Braun, 13-21, 1982

/43/ Beirak, E.:
Docteur These, "Etude de la Recondensation d'une Bulle Diphasique Chaude se Detendant dans son Liquide Froid en Presence ou Non de Gaz Incondensables", Universite de Grenoble, 1981

/44/ Lienhard, J.H. and Karimi, A.:
"Homogeneous Nucleation and the Spinodal Line",
J. Heat Transfer, Trans. ASME, Vol. 103, 61-64, 1981

/45/ Hütte des Ingenieurs Taschenbuch: Maschinenbau Teil A,
Verlag von Wilhelm Ernst & Sohn, Berlin, 1954

/46/ Spiegler, P. et al.:
"Onset of Stable Film Boiling and the Foam Limit",
Int. Journal of Heat & Mass Transfer, Vol. 6, 987-994, 1963

/47/ Drumheller, D.:
"The Initiation of Melt Fragmentation in Fuel Coolant Interactions", Nucl. Sci. Engrg., Vol. 72, 347-350, 1979

/48/ Cho, D. et al.:
"Some Aspects of Mixing in Large-Mass, Energetic Fuel Coolant Interactions", Proc. Int. Meeting Fast Reactor Safety and Related Physics, Chicago, CONF-761001, Vol. 4, 1852-1861, 1976

/49/ Inoue, A. et al.:
"Study on Transient Heat Transfer of Film Boiling due to Arrival of Pressure Shock", Proc. the Seventh Int. Heat Transfer Conf., München, Vol. 4, 403-408, 1982

/50/ Zyskowski, W.:
"Results of Measurements of Thermal Interaction between Molten Metal and Water", KfK 2193, 1975

/51/ Mizuta, H.:
"Fragmentation of Uranium Dioxide after Molten Uranium Dioxide Sodium Interaction", Journal of Nucl. Sci. Techn., Vol. 11, 480-487, 1974

/52/ McClure, J.A.:
"Particle Size Distributions from Fuel Rod Fragmented during Power Burst Test in the Capsule Driver Core", IN-1428, 1970

/53/ Frederking, T.H.K.:
"Laminar Two-Phase Boundary Layers in Natural Convection Film Boiling of Subcooled Liquids", Journal of Applied Math. and Phys., Vol. 15, 388-399, 1964

/54/ Hoang, Y.S.:
(Personal communication)

List of Tables

Table 1	Properties of experimental materials
Table 2	Characteristic values of a typical trigger pressure pulse
Table 3	Results of experiments for different experimental conditions in the sodium/pentane system
Table 4	Results of experiments for different experimental conditions in the silicone oil/pentane system
Table 5	Comparison between thermal energy and reaction work in the sodium/pentane system
Table 6	Comparison of the two instabilities
Table 7	Characteristic values for different material systems

List of Figures

Fig. 1	Sequences of events leading to a vapour explosion with high potential damage
Fig. 2	Schematic representation of the experimental set-up
Fig. 3	Schematic illustration of the geometry of the reaction zone and instrumentation in the sodium/pentane system
Fig. 4	Vaccum and gas supply system and the sodium distillation facility, schematically
Fig. 5	Schematic measuring principle of the motion of the surrounding liquid
Fig. 6	Flow chart of the sequence of events
Fig. 7	Experimental results for sodium droplets in pentane
Fig. 8	Experimental results for silicone oil droplets in pentane
Fig. 9	Trigger pressure curve (without reaction)

Fig. 10 Reaction pressure curve and trigger pressure curve in sodium/pentane

Fig. 11 Reaction pressure curve and trigger pressure curve in silicone oil/pentane

Fig. 12 Reaction process in the sodium/pentane system (1)

Fig. 13 High-speed pictures

Fig. 14 Reaction zone growth and liquid volume growth

Fig. 15 Reaction process in the sodium/pentane system (2)

Fig. 16 Reaction process in the sodium/pentane system (3)

Fig. 17 Reaction process in the sodium/pentane system (4)

Fig. 18 Reaction process in the sodium/pentane system (5)

Fig. 19 Maximum reaction pressure as a function of droplet temperature for sodium droplets

Fig. 20 Maximum mixing rate as a function of droplet temperature for sodium droplets

Fig. 21 Maximum reaction pressure as a function of droplet temperature (silicone oil)

Fig. 22 Delay time as a function of droplet temperature (sodium)

Fig. 23 Delay time as a function of trigger pressure (sodium droplets)

Fig. 24 Delay time as a function of droplet temperature (silicone oil)

Fig. 25 Particle size distribution of sodium fragments (mass fraction)

Fig. 26 Particle size distribution of sodium fragments (frequency)

Fig. 27 Shock wave propagation and vapour film collapse (first mechanism)

Fig. 28	Velocity of reaction zone boundary induced by the shock wave
Fig. 29	Schematic representation of symmetric vapour film collapse
Fig. 30	Calculated example of the vapour film collapse process for iron and water as compared with calculations presented by Drumheller /47/
Fig. 31	Calculated vapour film collapse process in the sodium/pentane system
Fig. 32	Flow velocity of the liquid and vapour pressure before impact on the sodium droplet
Fig. 33	Schematic representation of the two kinds of instability in a local point of contact
Fig. 34	Fastest growing wavelength and growth time constant for Rayleigh-Taylor instability
Fig. 35	Fastest growing wavelength and growth time constant for Kelvin-Helmholtz instability
Fig. 36	Maximum mixing rate of liquid in the experiments as compared with calculations
Fig. 37	Schematic fragmentation model
Fig. 38	Scheme for assessment of the mixing energy
Fig. 39	High-speed pictures recorded for the silicone oil/pentane system (1)
Fig. 40	High-speed pictures recorded for the silicone oil/pentane system (2)
Fig. 41	Schematic representation of the mechanism of the external trigger
Fig. 42	Particle size distribution of fragments for different systems of materials
Fig. A-1	Schematic temperature distribution prior to fragmentation

Fig. A-2 Time curve of the temperature and the thermal boundary layer of the droplet

Fig. B-1 Radial pressure distribution in the measuring plane calculated with the SING code /54/

Tab. 1: Properties of experimental materials

	Silicone oil	Sodium	Pentane
Boiling temperature at standard atmosphere (°C)	-	880	36
Critical temperature (°C)	-	2235	197
Critical pressure (bar)	-	256 - 400	34
Homogeneous nucleation temperature (°C)	-	1600 - 1900	145
Thermal conductivity (W/Km)	0.14	62	0.12
Specific heat (J/kg K)	1560	1250	2250
Density (kg/m^3)	850 - 900	880	630
Thermal effusivity (J/m^2 s $^{1/2}$ K)	450	7800	375
Heat of evaporation (J/kg)	-	$3.6 \cdot 10^6$	$3.6 \cdot 10^5$
Surface tension (N/m)	0.02	0.14	0.01
Dynamic viscosity (m/s)	0.27	$0.2 \cdot 10^{-3}$	$0.23 \cdot 10^{-3}$
Sound velocity (m/s)	~900	2500	1170

Table 2: Characteristic values of a typical trigger pressure pulse

Number	Electrical Energy (J)	Pressure (bar)	Impulse (Pa.s)	∫PdV (J)
1	0.4	1.6	-	-
2	0.49	2.4	1.3	$1.5\ 10^{-2}$
3	0.64	4.0	20	$3.6\ 10^{-2}$
4	0.81	5.0	24	$5.0\ 10^{-2}$
5	1.0	6.4	30	- -
6	1.4	8.0	40	$1.2\ 10^{-2}$
7	2.0	11.0	52	2.2 -
8	2.5	15.0	62	$2.2\ 10^{-2}$

Table 3: Results of the experiments for different test conditions in the sodium/pentane system

Test No	Temp.	Trigger Pressure	Reaction Pressure	Delay	Impulse Ratio	Fragmen-tation	Film	
	°C	P_{TR}(bar)	P_V(bar)	µs			taken	analysed
V1	120	2	-	-	-	-	-	-
V2	120	4	-	-	-	-	o	-
V3	120	5	2.8	60	0.56	partly	o	-
V4	120	5	2	70	0.4	partly	o	-
V5	120	10	6.2	60	0.744	yes	o	Fig.15
V6	120	10	6.0	60	0.55	yes	o	o
V7	135	2	-	-	-	-	o	-
V8	130	4.5	3	60	1.0	yes	o	-
V9	130	7.5	5	50	0.9	yes	o	-
V10	140	1.5	-	-	-	-	o	-
V11	140	3	2	50	1.6	yes	o	-
V12	142	8	7.5	50	1.25	yes	o	-
V13	155	2	-	-	-	-	o	-
V14	150	4	2.5	50	1.1	yes	o	-
V15	150	10	11.0	50	1.5	yes	o	Fig. 12
V16	150	10	10	40	1.5	yes	o	-
V17	160	2	-	-	-	-	o	-
V18	175	2	-	-	-	-	o	-
V19	180	4	3	60	0.75	partly	o	Fig. 17
V20	180	8	6	45	1.0	yes	o	Fig. 18
V21	295	3.5	-	-	-	-	-	
V22	200	3.0	-	-	-	-	-	
V23	200	10	12	20	1.6	yes	o	-
V24	200	10	10	30	1.3	yes	o	o
V25	220	3	-	-	-	-	o	
V26	220	4	4.2	50	1.7	partly	o	
V27	220	8	8	35	1.4	yes	o	
V28	250	4	-	-	-	-	o	
V29	260	9	6	40	1.0	-	o	
V30	290	5.5	4	60	0.7	yes	o	
V31	305	5	4	65	0.8	partly	o	
V32	300	9	6	50	0.9	Yes	o	o
V33	340	4.5	-	-	-	-	o	
V34	360	7	4	70	0.6	partly	o	
V35	360	10	6	60	0.8	yes	o	o
V36	360	15	10	55	0.7	yes	o	
V37	370	5.5	2.2	60	0.4	partly	o	
V38	400	6	-	-	-	-		
V39	400	8	5.5	65	0.7	yes	o	
V40	400	10	7	55	0.93	yes	o	Fig. 16
V41	400	10	7	60	0.7	yes	o	o

Table 4: Results of the experiments for different test conditions in the silicone oil / pentane system

Test No	Temp.	T_K	Trigger Pressure	Reaction Pressure	Delay	Impulse Ratio	Fragmen-tation	Film
	°C	°C	(bar)	(bar)	µs			
VS1	190	(115)	2.0	2	-	1.0	yes	Fig. 39
VS2	180	(115)	1.0	-	-	-	-	-
VS3	200	(127)	51.0	-	-	-	-	o
VS4	210	(133)	0.5	-	-	-	-	o
VS5	210	(133)	1.0	-	-	-	-	o
VS6	210	(133)	1.5	1.2	30	4	yes	o
VS7	220	(138)	0.5	--	-	-	-	o
VS8	220	(138)	7.5	1.2	25	3	yes	o
VS9	220	(138)	2.5	2.2	25	-	-	-
VS10	235	(145)	2	2.5	25	5.6	yes	o
VS11	240	(150)	0.5	0.4	30	3	-	-
VS12	245	(150)	1.5	1.2	20	5.4	yes	Fig. 40
VS13	247	(155)	1.2	1.4	20	7.3	-	-
VS14	260	(160)	1.0	0.8	40	2.6	yes	o
VS15	260	(160)	1.6	2.0	20	5.3	yes	o
VS16	270	(165)	0.5	-	-	-	-	-
VS17	275	(108)	1.2	2.3	10	9.6	yes	-
VS18	275	(168)	2.2	2.5	10	5.7	yes	o
VS19	290	(176)	2.0	2.2	10	8.8	yes	o
VS20	310	(185)	1.0	-	-	-	-	-
VS21	310	(185)	1.5	-	-	-	-	-
VS22	310	(185)	3.0	3.2	20	6.7	yes	o

Table 5: Comparison between thermal energy and reaction work for the sodium/pentane system

	V.19	V.20	V.36
Droplet temperature T_T (°C)	180	180	360
Trigger pressure P_{Tr} (bar)	4	8	15
Thermal energy E_{th} (J)	11	27	32
Trigger work (J)	$3.6 \cdot 10^{-2}$	$1.2 \cdot 10^{-1}$	$2.2 \cdot 10^{-1}$
Reaction work (J)	$5.6 \cdot 10^{-3}$	$5.1 \cdot 10^{-2}$	$8.6 \cdot 10^{-2}$
Droplet-to-vessel cross section factor	$3.3 \cdot 10^{-2}$	$6.0 \cdot 10^{-2}$	$3.1 \cdot 10^{-2}$

Table 6: Comparison of the two instabilities

Characteristic feature	Rayleigh-Taylor	Kelvin-Helmholz
Driving mechanism	Acceleration of the boundary surface	Impulse of the vapour flow
Expected wave length for P_{sat}	50 ~ 100 µm	1 ~ 10 µm
Expected growth rate	smaller	larger
Expected growth time constant	1 ~ 10 µm	0.1 ~ 1 µm
Direction with respect to boundary surface	normal	parallel

Table 7: Characteristic values (eqs. 47 and 48) for different material systems, with P in N/m^2, σ in N/m, and ρ in kg/m^3

Combination hot / cold		$\frac{P_{sat}(T_K)}{\sigma^{1/3}\rho^{2/3}} \times 10^5$	$\frac{P_{sat}(T_K)}{\sigma^{2/3}\rho^{1/3}} \times 10^5$
Silicone oil / Pentane	($T_{HN} \approx T_{Kr}$)	0.7 - 1.4	2.3 - 4.9
Water / Freon-22	($T_{HN} \approx T_{Kr}$)	0.8 - 1.3	2.0 - 3.3
Aluminium / Water	(T_{Kr})	1.3	1.7
Tin / Water	(T_{Kr})	0.72	1.6
Copper / Water (Cu oxydized)	(T_{Kr})	0.85	1.6
Copper / Water		0.56	1.0
Sodium / Pentane	($T_{HN} \approx T_{Kr}$)	0.35 - 0.71	0.61 - 1.2
UO_2 / Water	(T_{Kr})	0.77	1.6
UO_2 / Sodium	(T_{Kr})	0.25	0.33
	T_{HN} = 1900° C	0.8	1.6

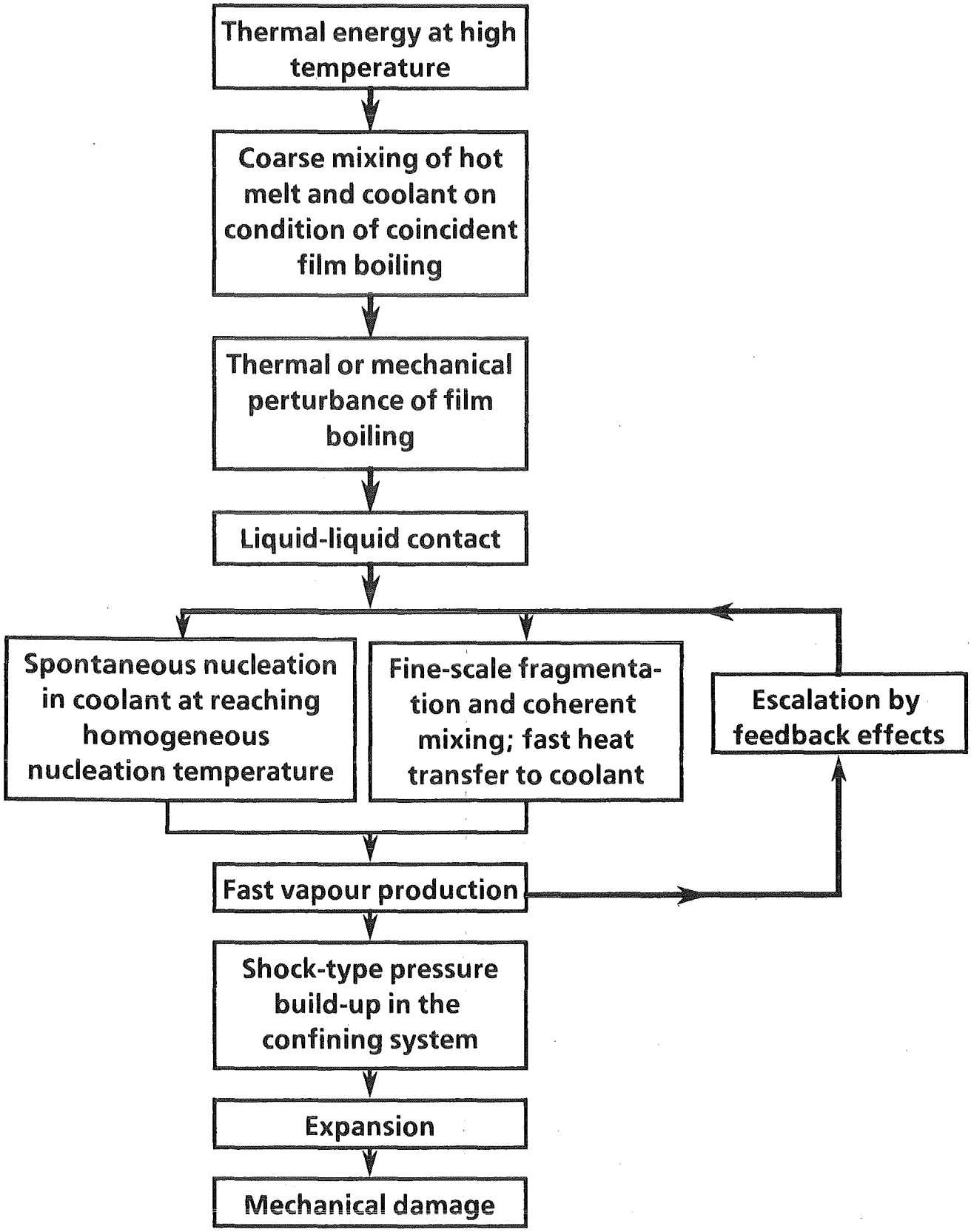

Fig. 1 Sequences of Events Leading to a Vapour Explosion with High Potential Damage

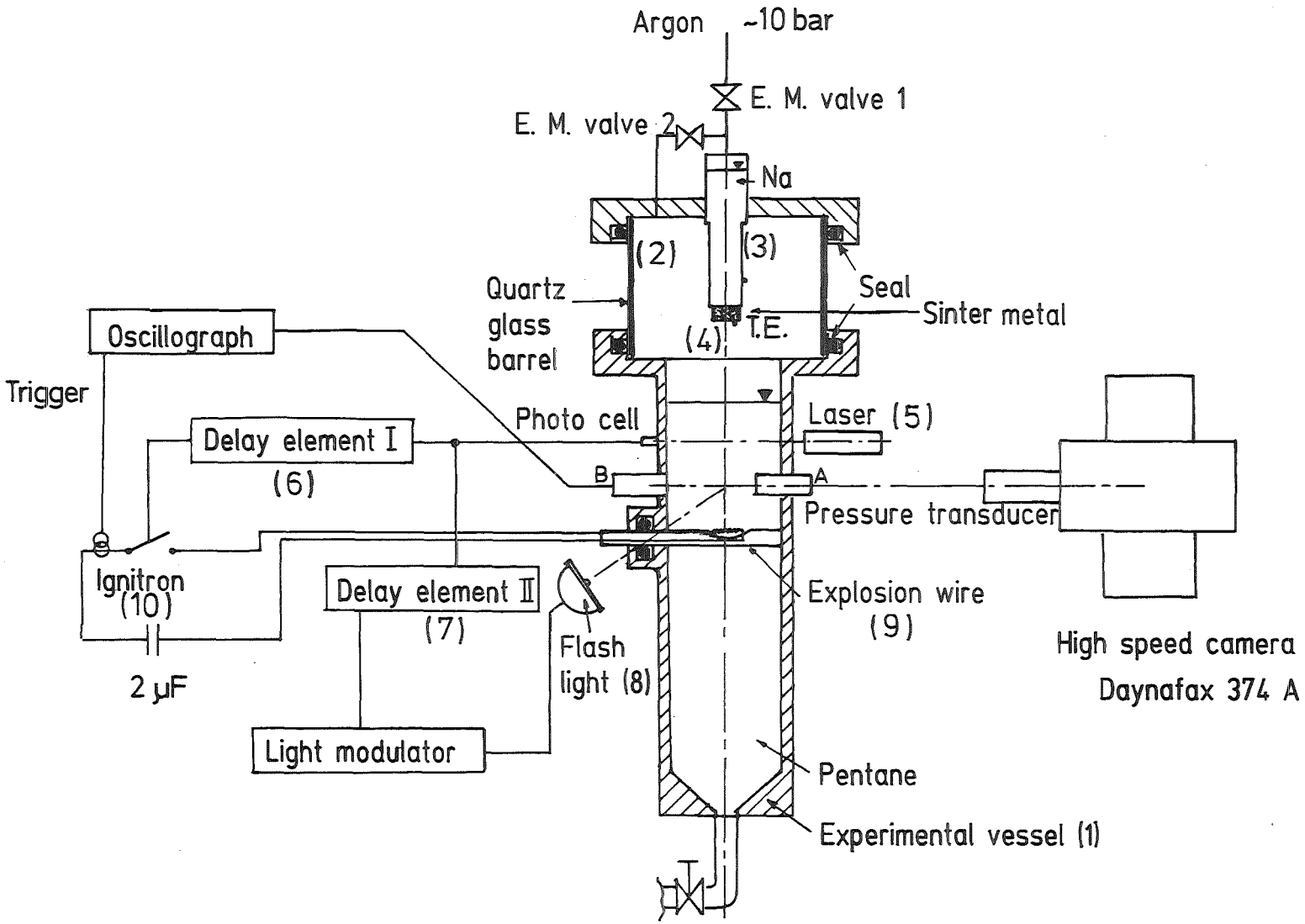

Fig. 2 Schematic Representation of the Experimental Set-up

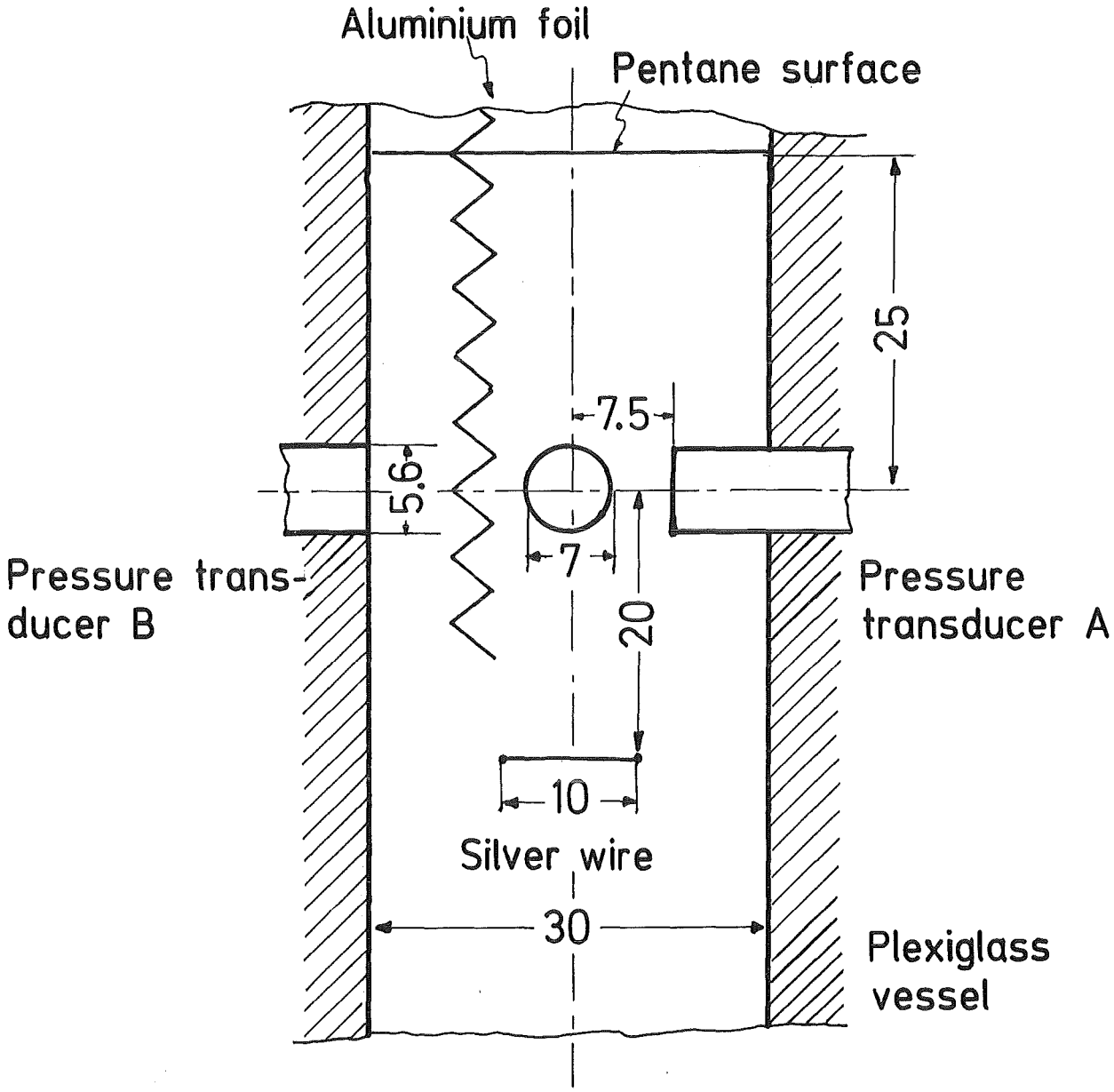

Fig. 3 Schematic Illustration of the Geometry of the Reaction Zone and Instrumentation in the Sodium/Pentane System

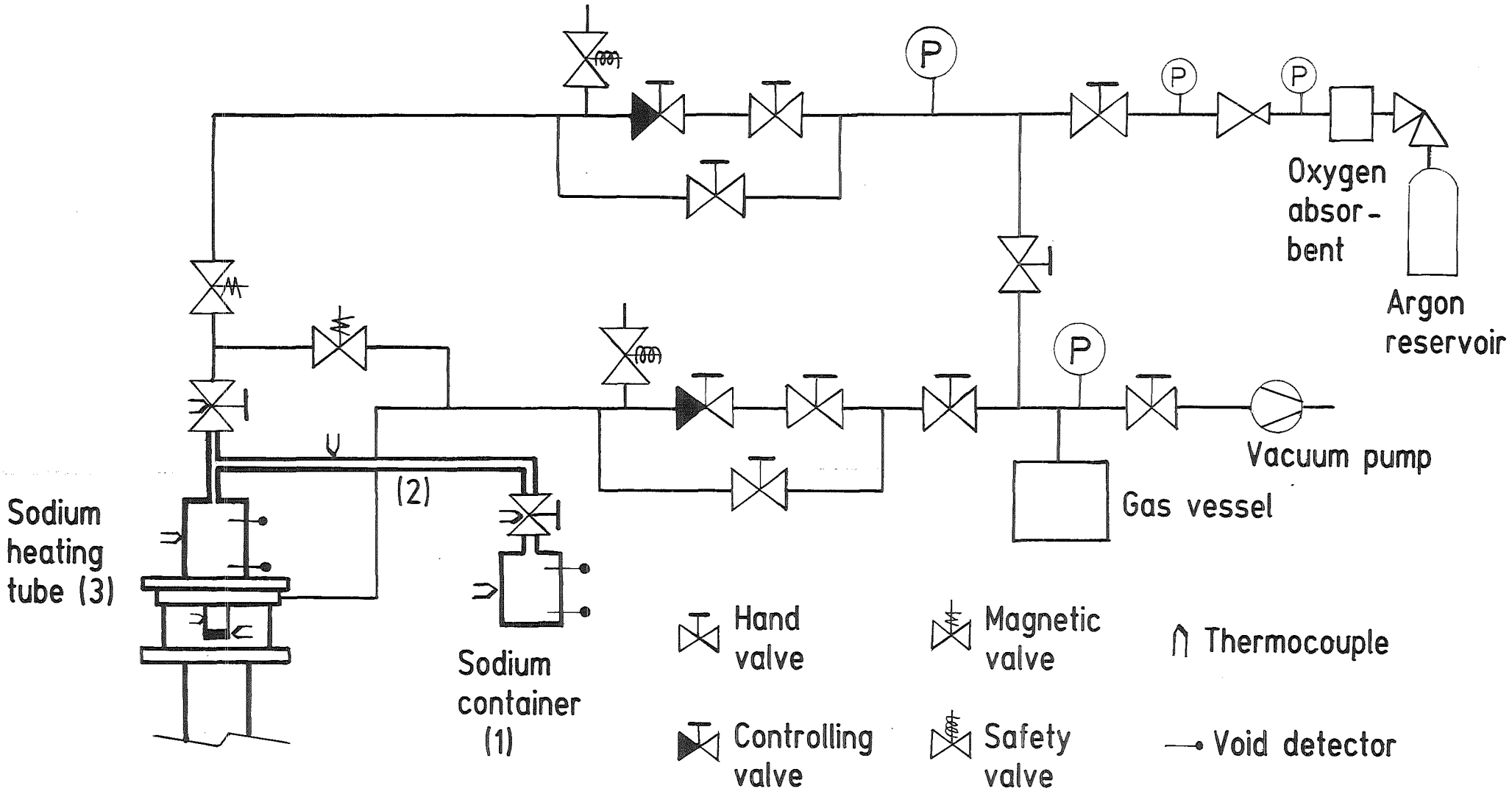

Fig. 4 Vacuum and Gas Supply System and the Sodium Distillation Facility, Schematically

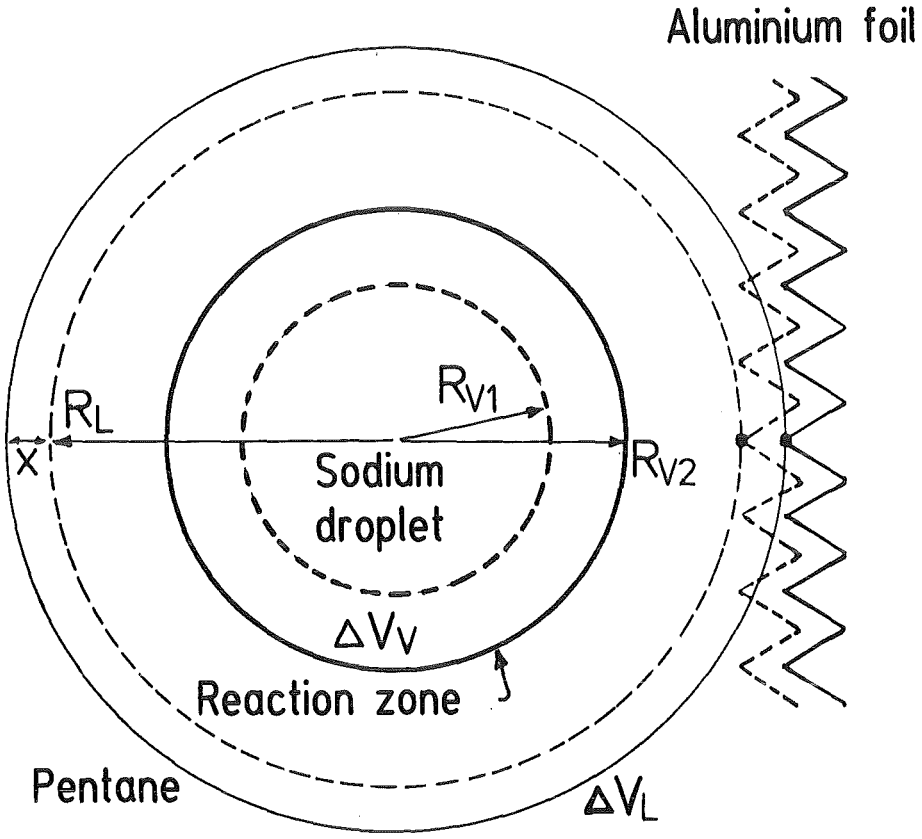

Fig. 5 Schematic Measuring Principle of the Motion of the Surrounding Liquid

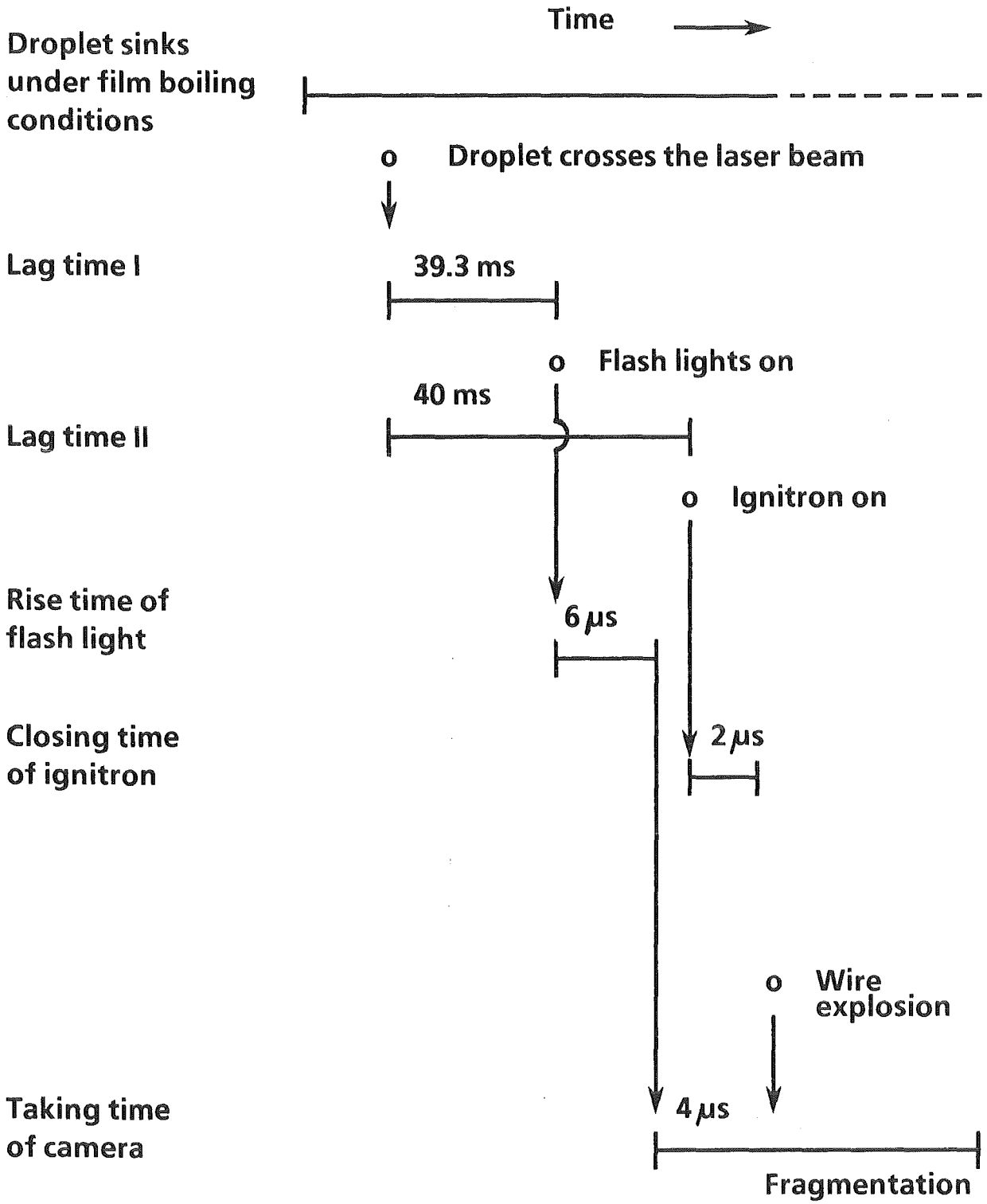

Fig. 6 Flow Chart of the Sequence of Events

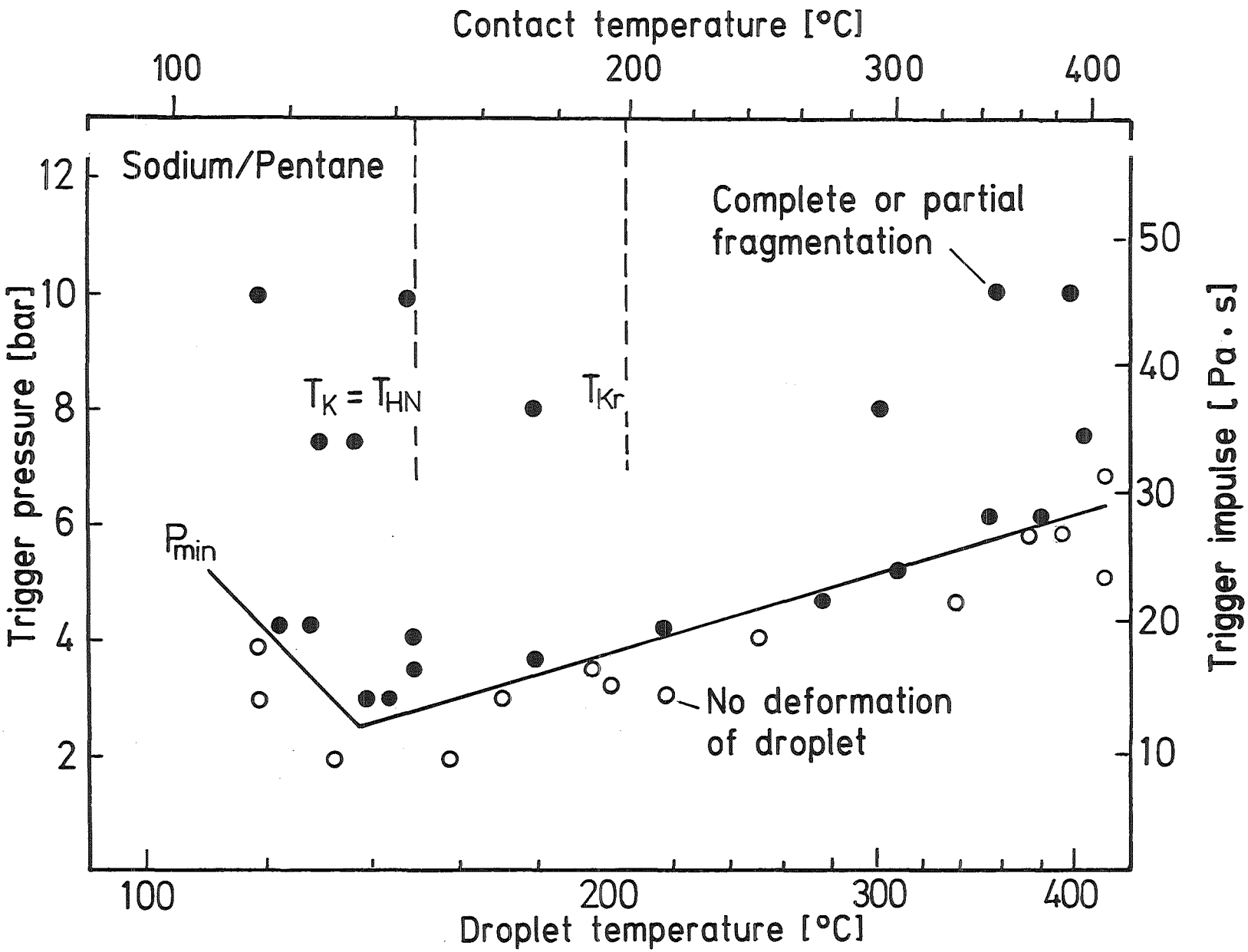

Fig. 7 Experimental Results for Sodium Droplets in Pentane

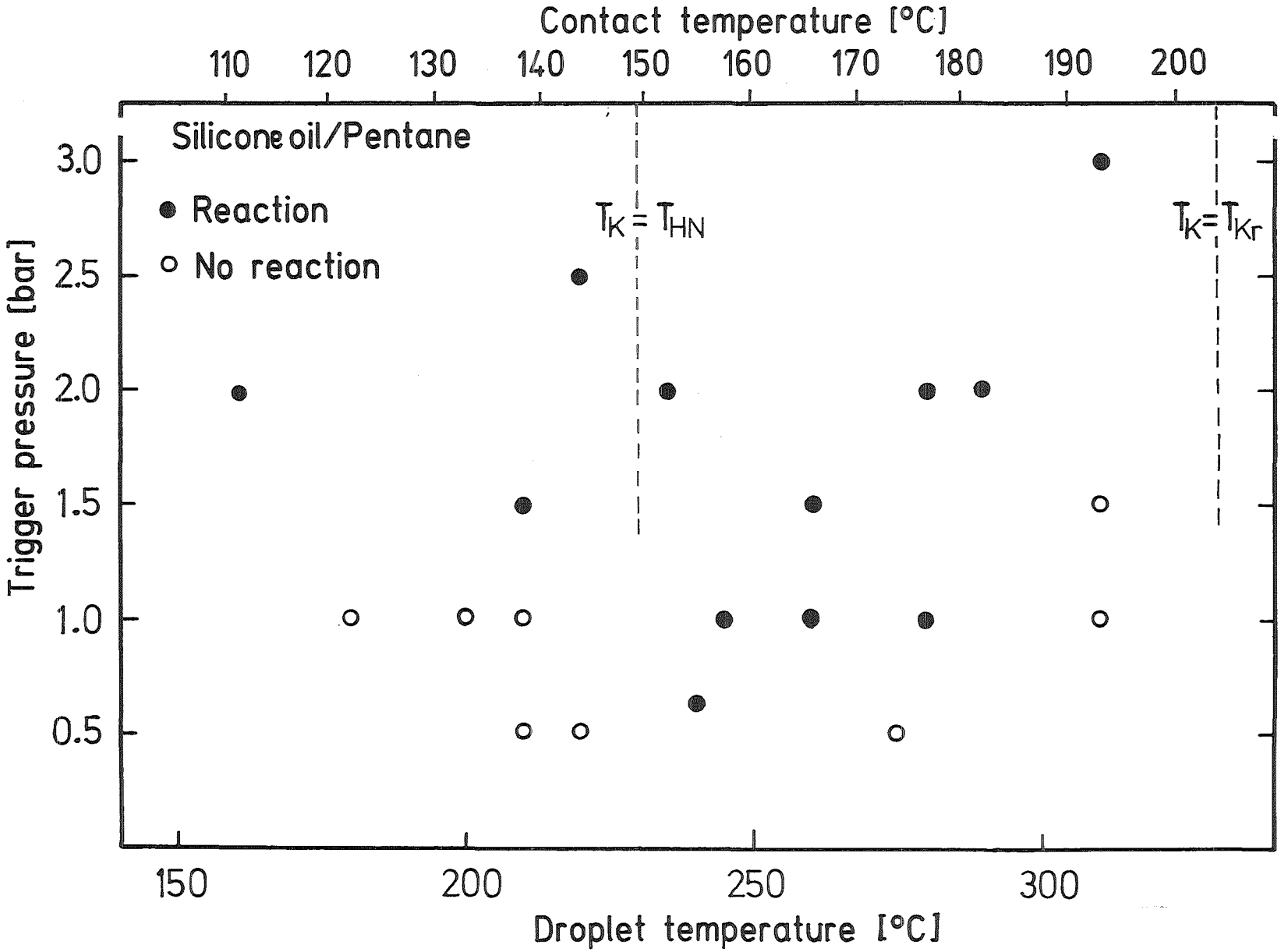

Fig. 8 Experimental Results for Silicon Oil Droplets in Pentane

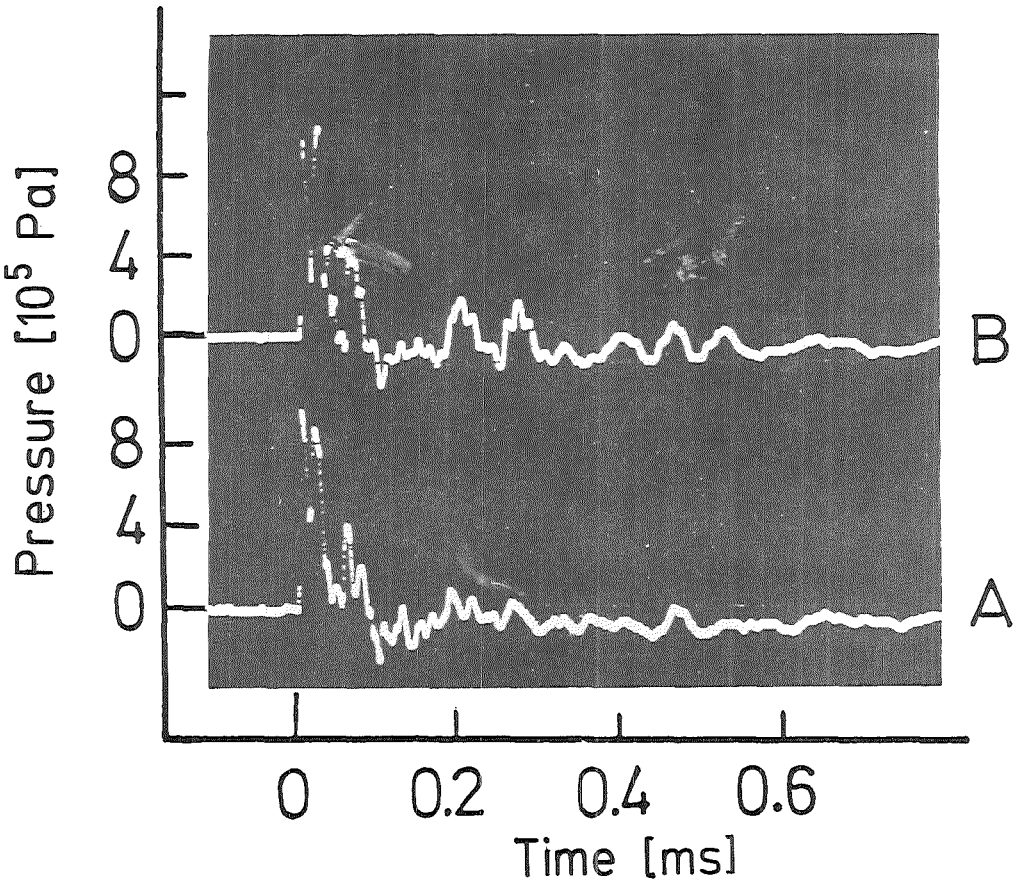

Trigger pressure: 10 bar

Fig. 9 Trigger Pressure Curve (without Reaction)

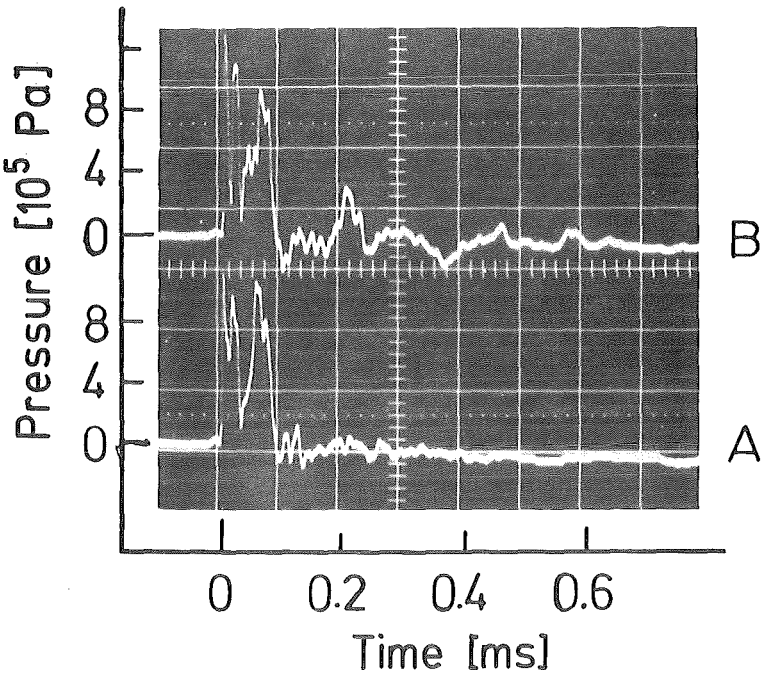

a) Pressure curve of reaction

Droplet temperature 150°C (sodium)

Trigger pressure: 10 bar

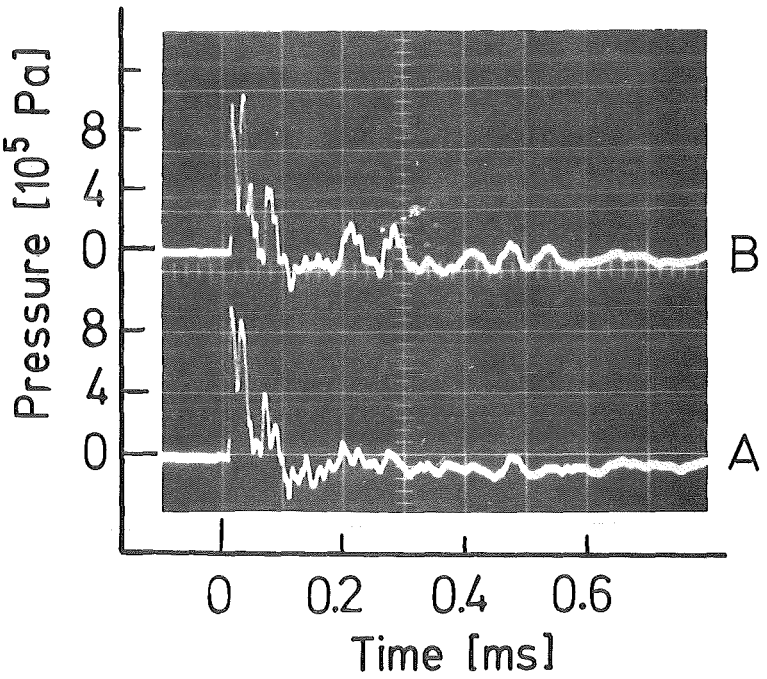

b) Pressure curve of trigger

Trigger pressure: 10 bar

Fig. 10 Reaction Pressure Curve and Trigger Pressure Curve in Sodium/Pentane

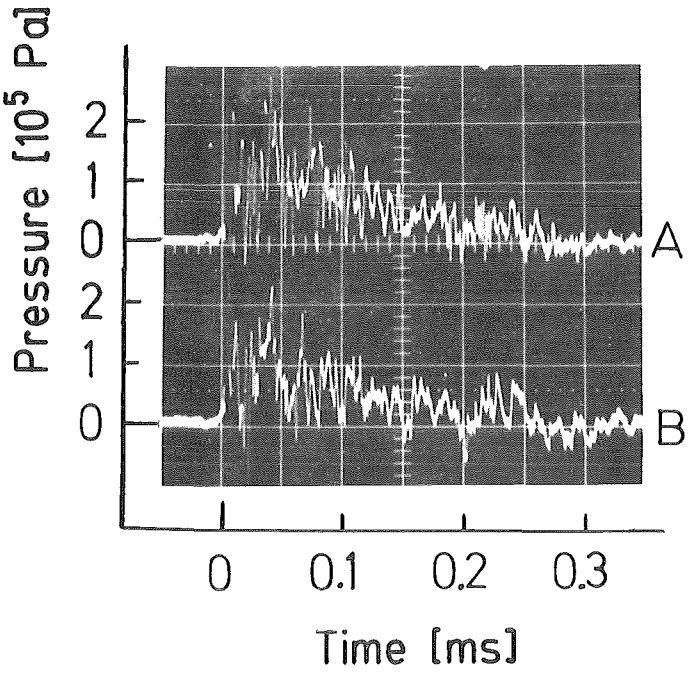

a) Pressure curve of reaction

Droplet temperature: 260°C (Siliconeoil)

Trigger pressure: 1.8 bar

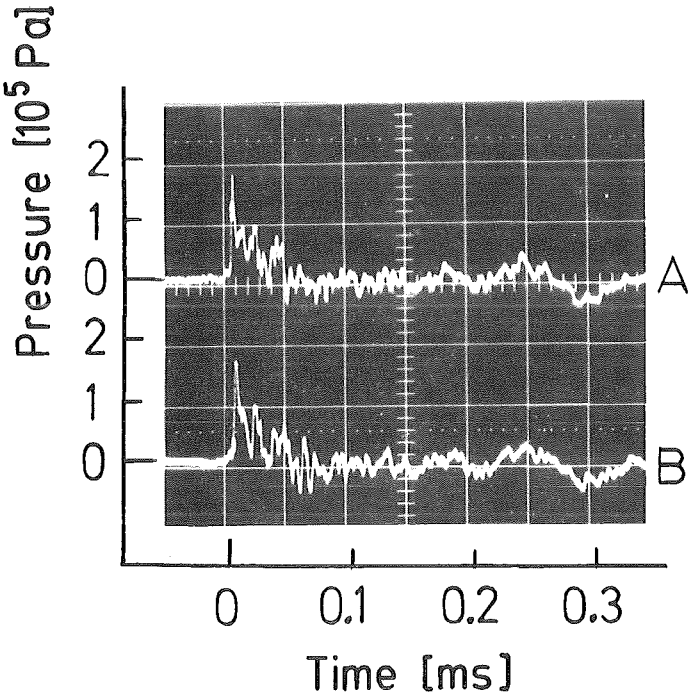

b) Pressure curve of trigger

Trigger pressure: 1.6 bar

Fig. 11 Reaction Pressure Curve and Trigger Pressure Curve in Silicone Oil/Pentane

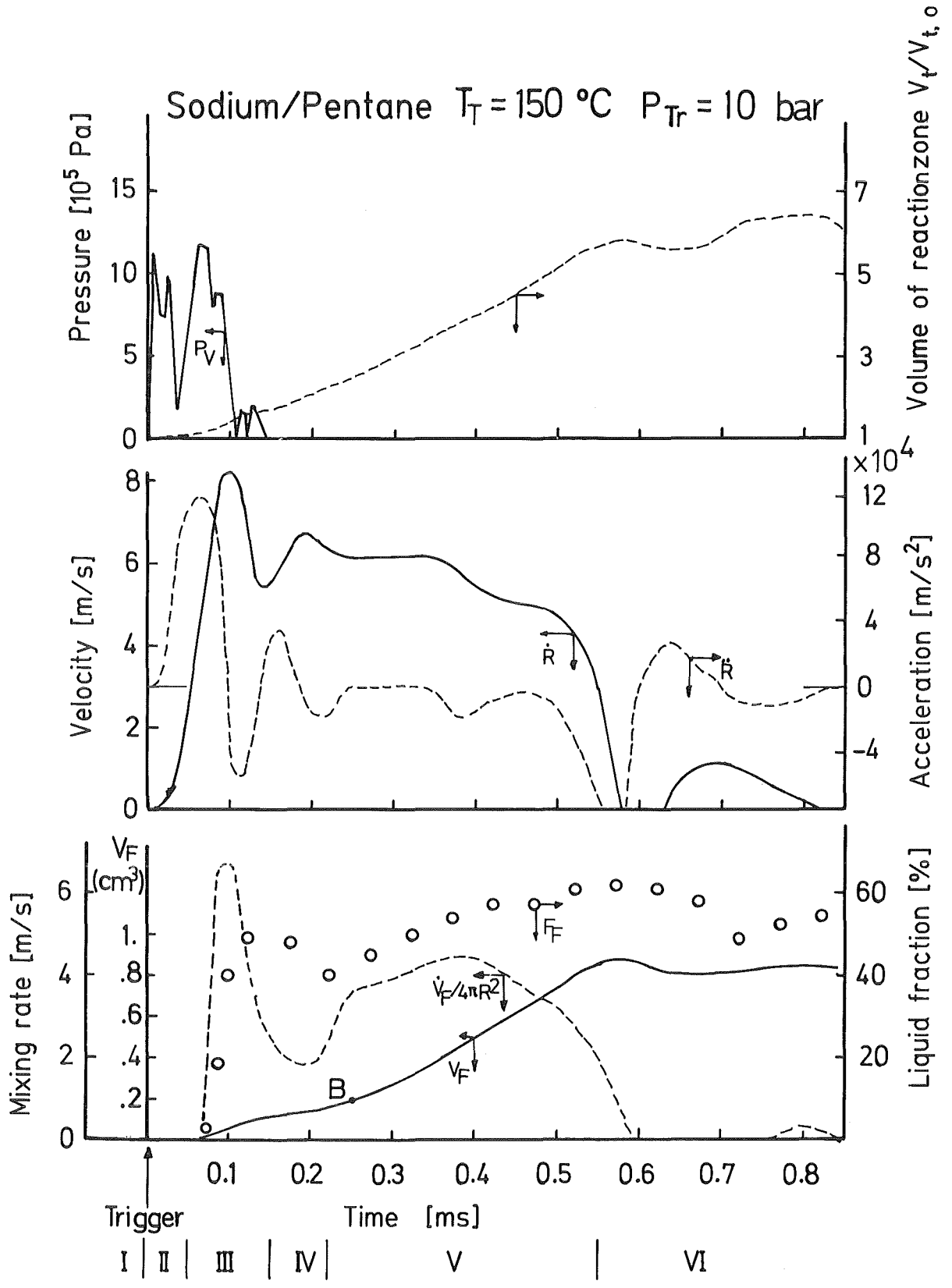

Fig. 12 Reaction Process in the Sodium/Pentane System (1)

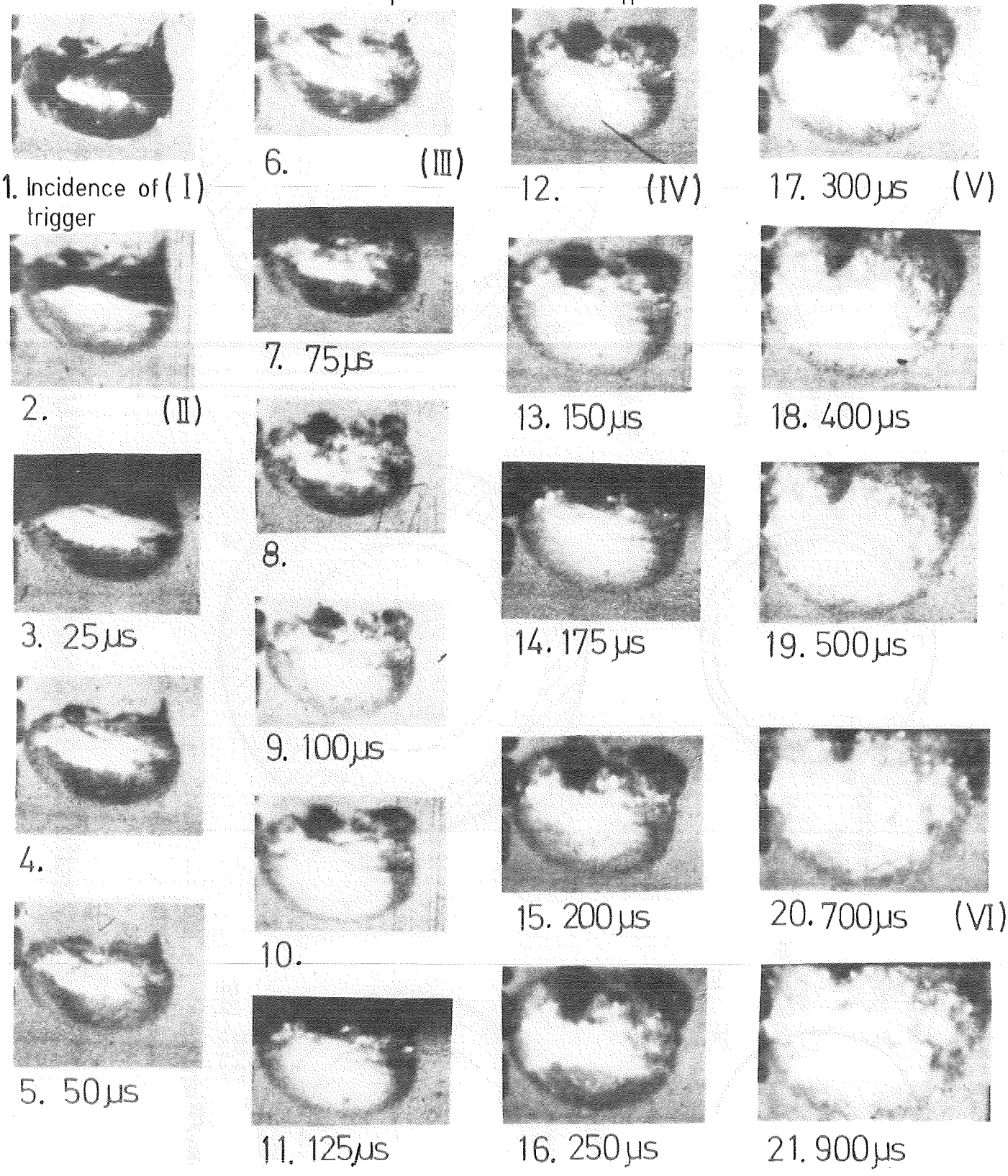

Fig. 13 High-speed Pictures

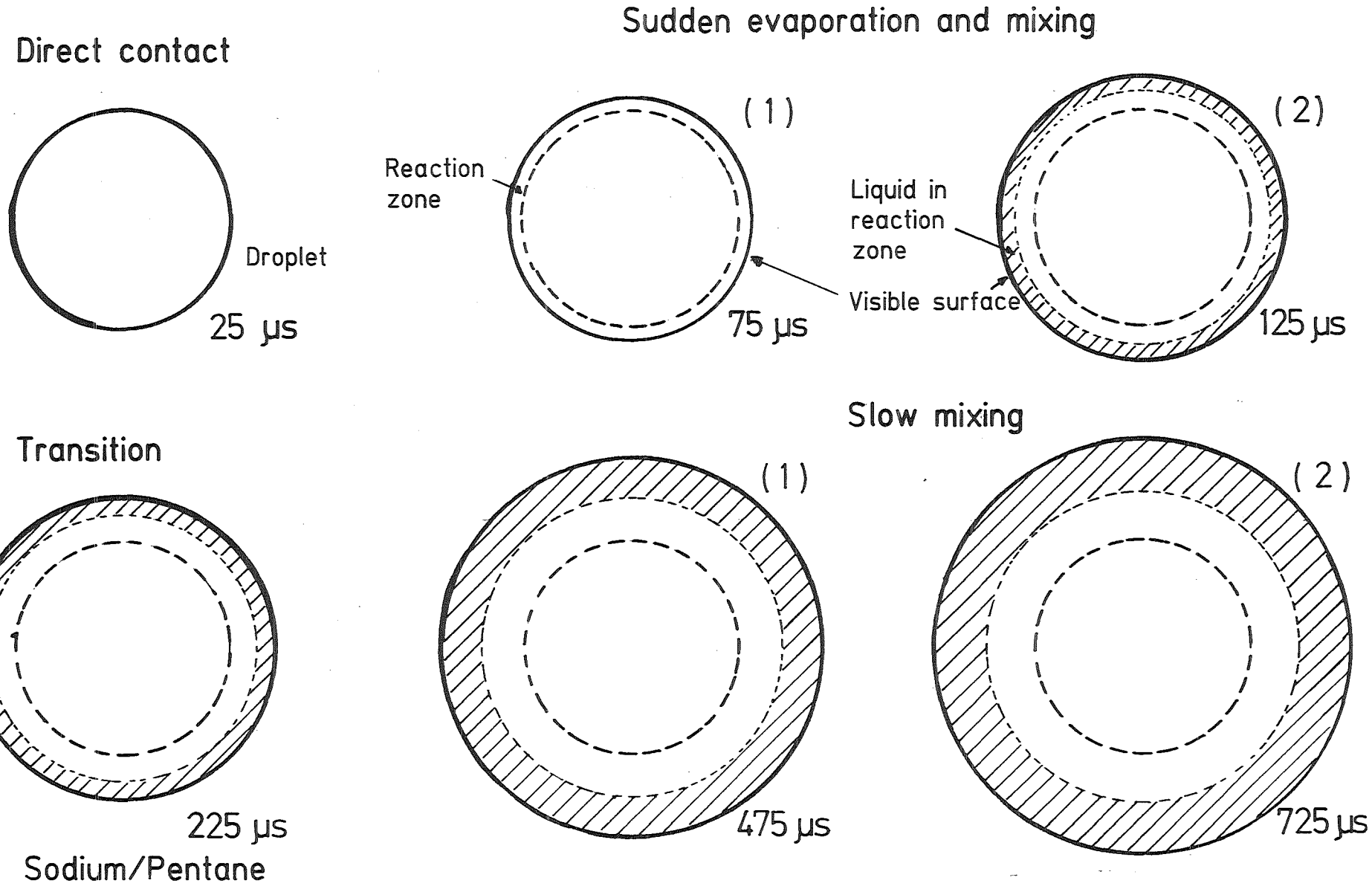

Fig. 14 Reaction Zone Growth and Liquid Volume Growth

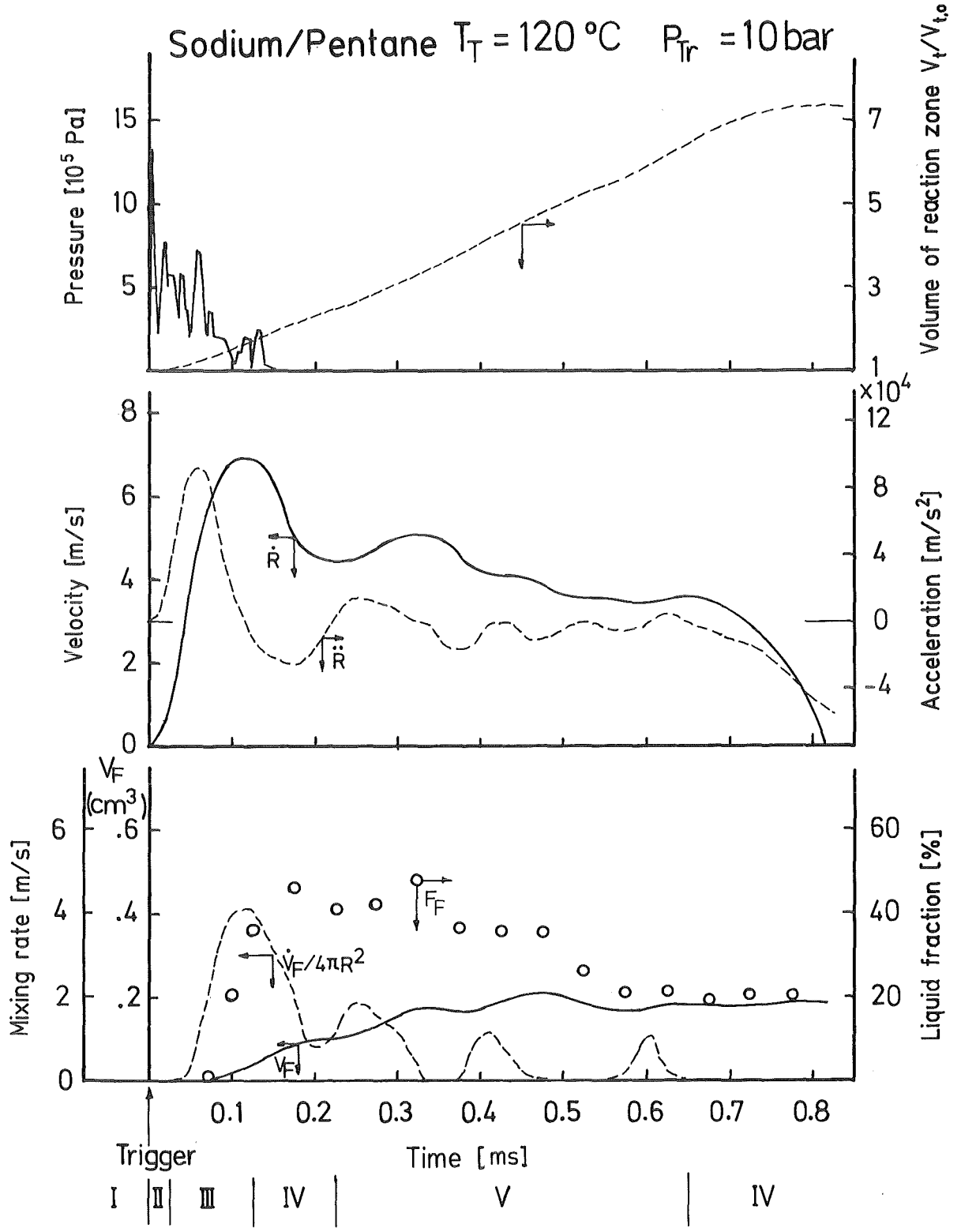

Fig. 15 Reaction Process in the Sodium/Pentane System (2)

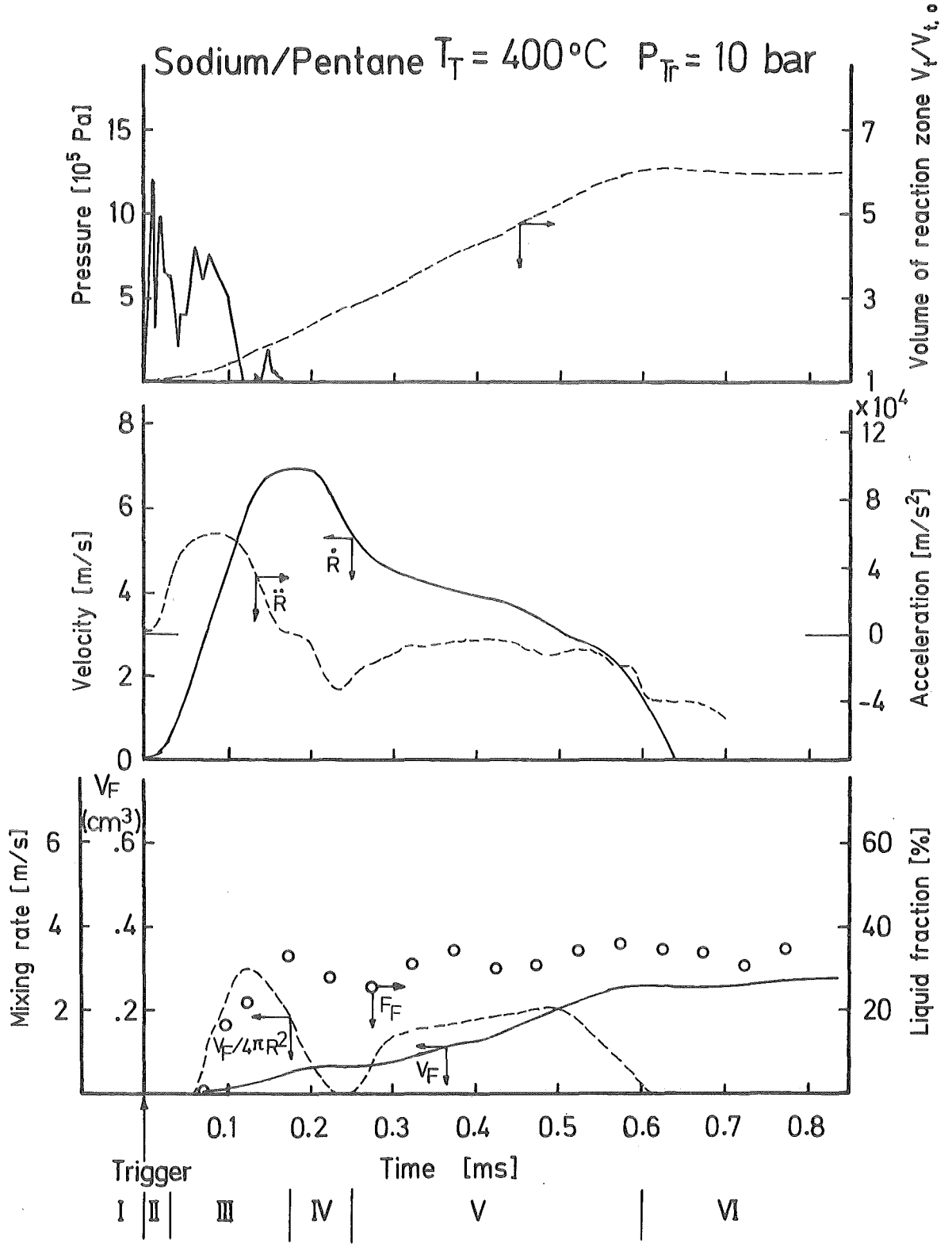

Fig. 16 Reaction Process in the Sodium/Pentane System (3)

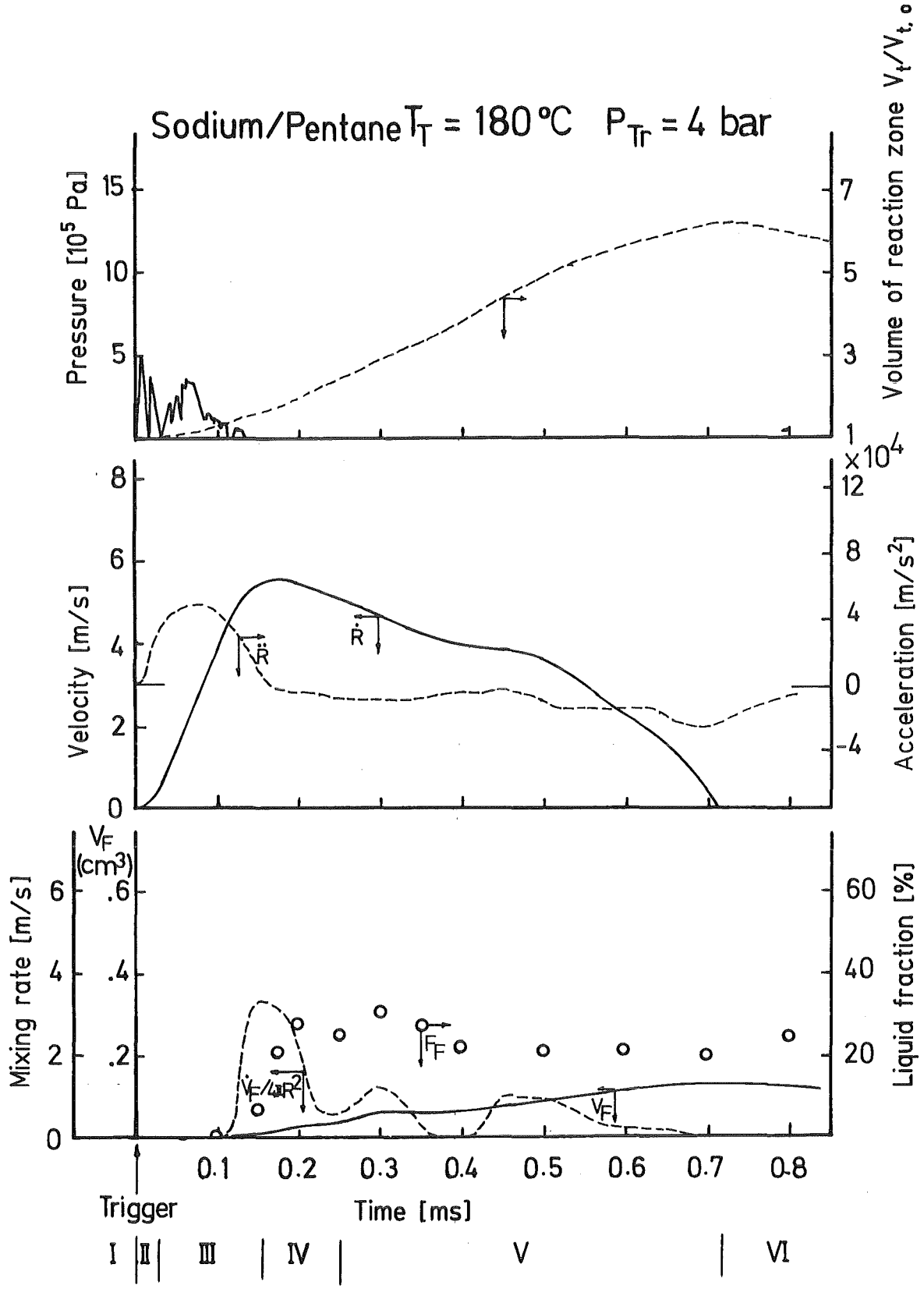

Fig. 17 Reaction Process in the Sodium/Pentane System (4)

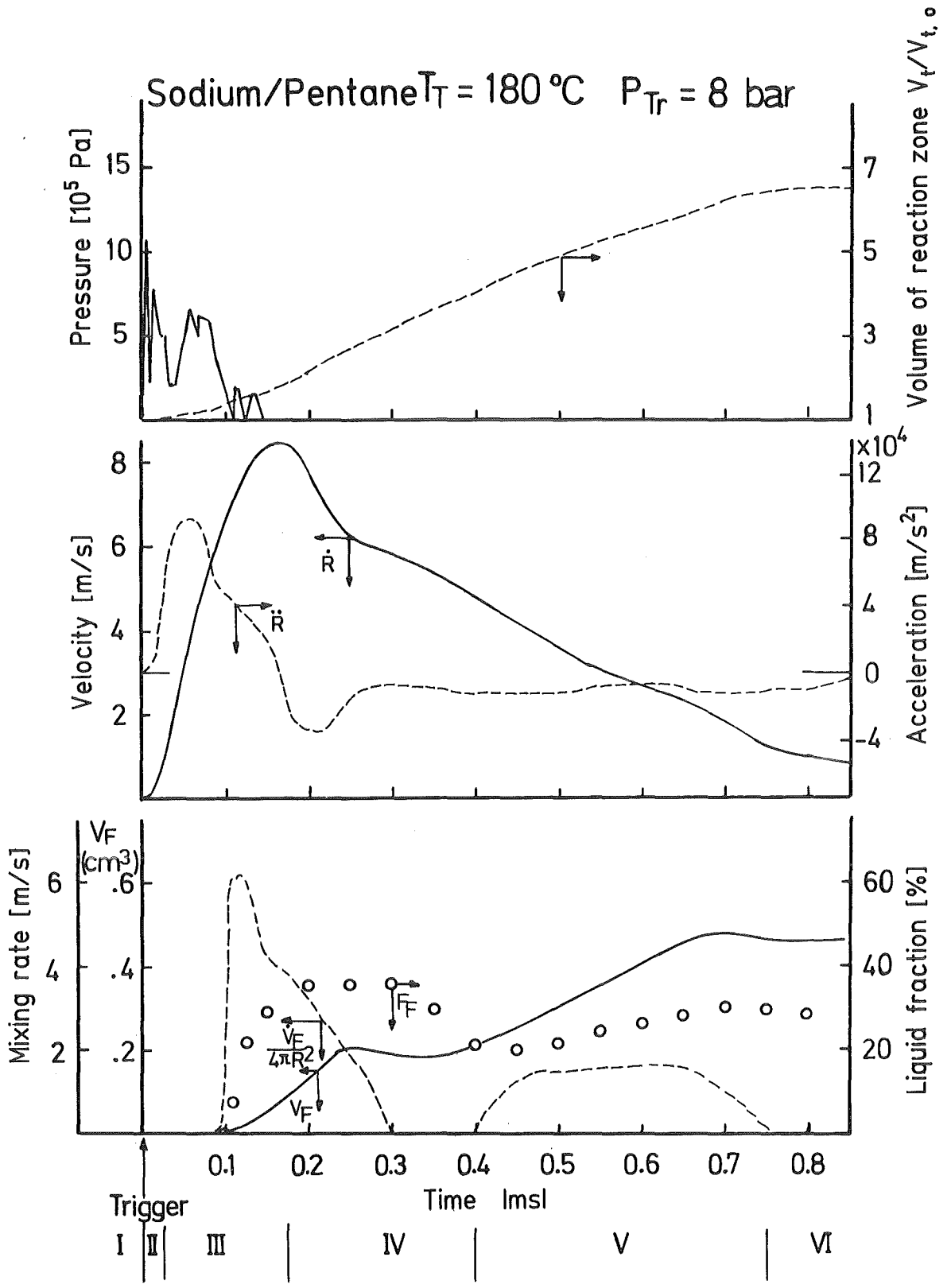

Fig. 18 Reaction Process in the Sodium/Pentane System (5)

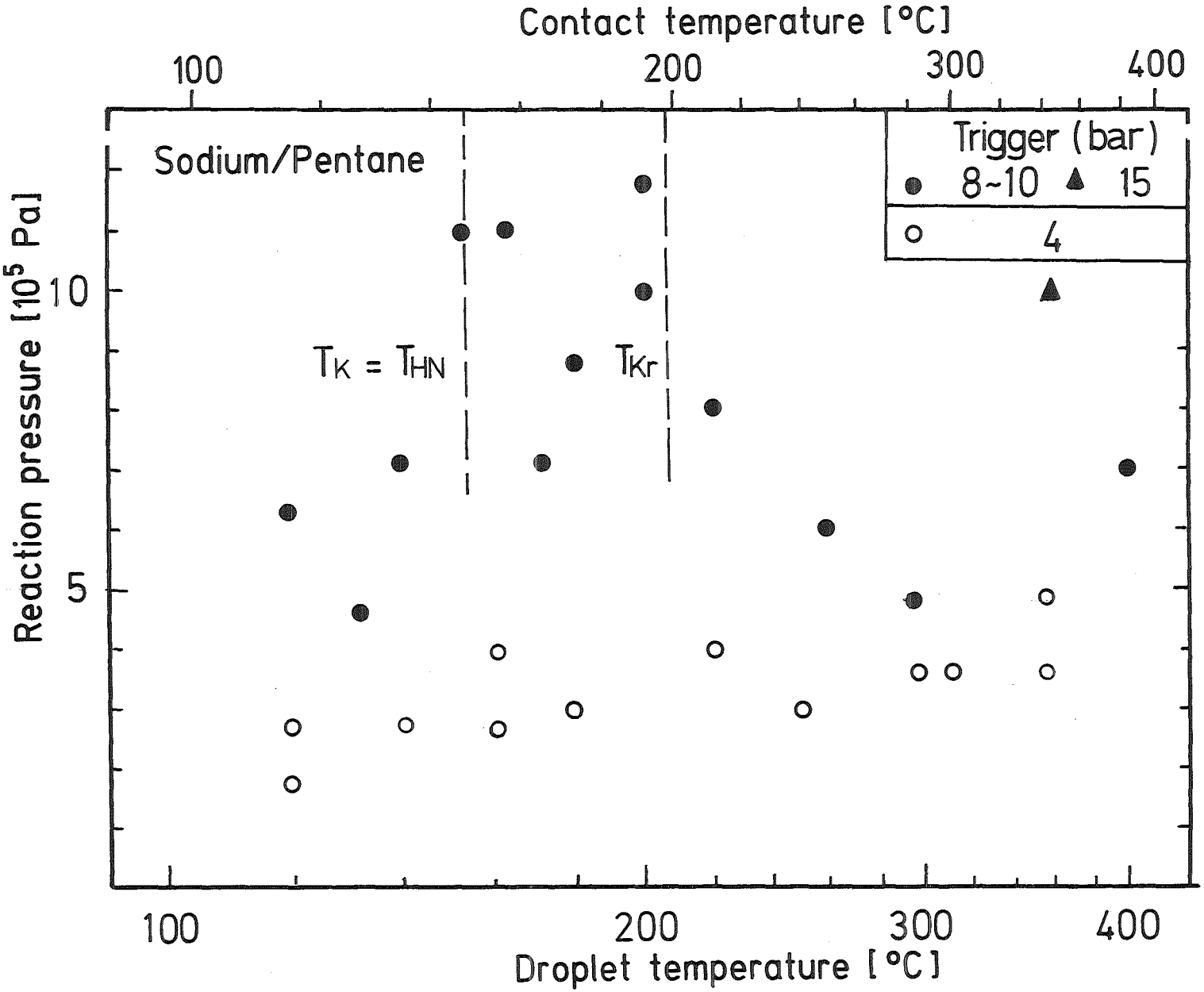

Fig. 19 Maximum Reaction Pressure as a Function of Droplet Temperature for Sodium Droplets

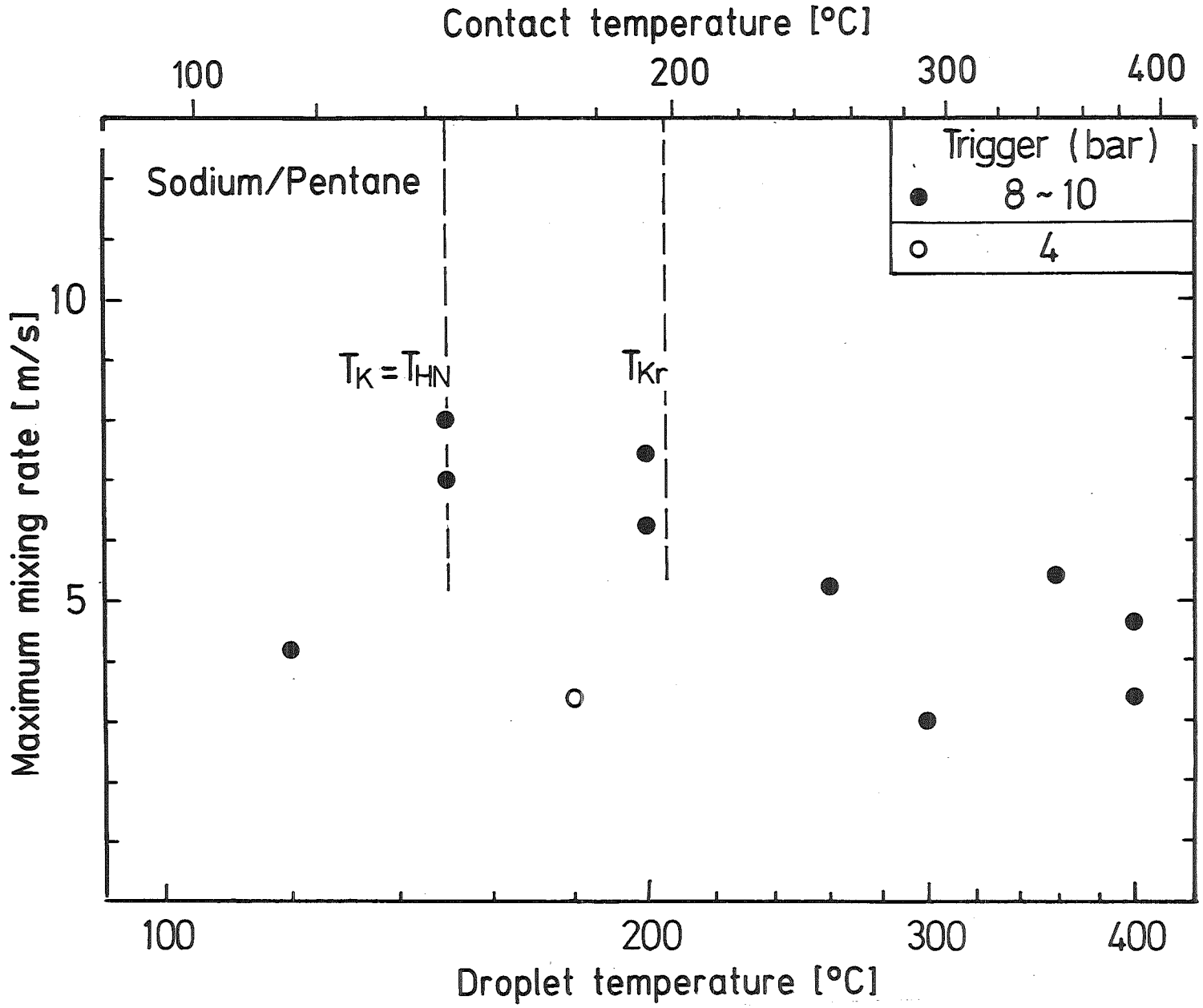

Fig.20 Maximum Mixing Rate as a Function of Droplet Temperature for Sodium Droplets

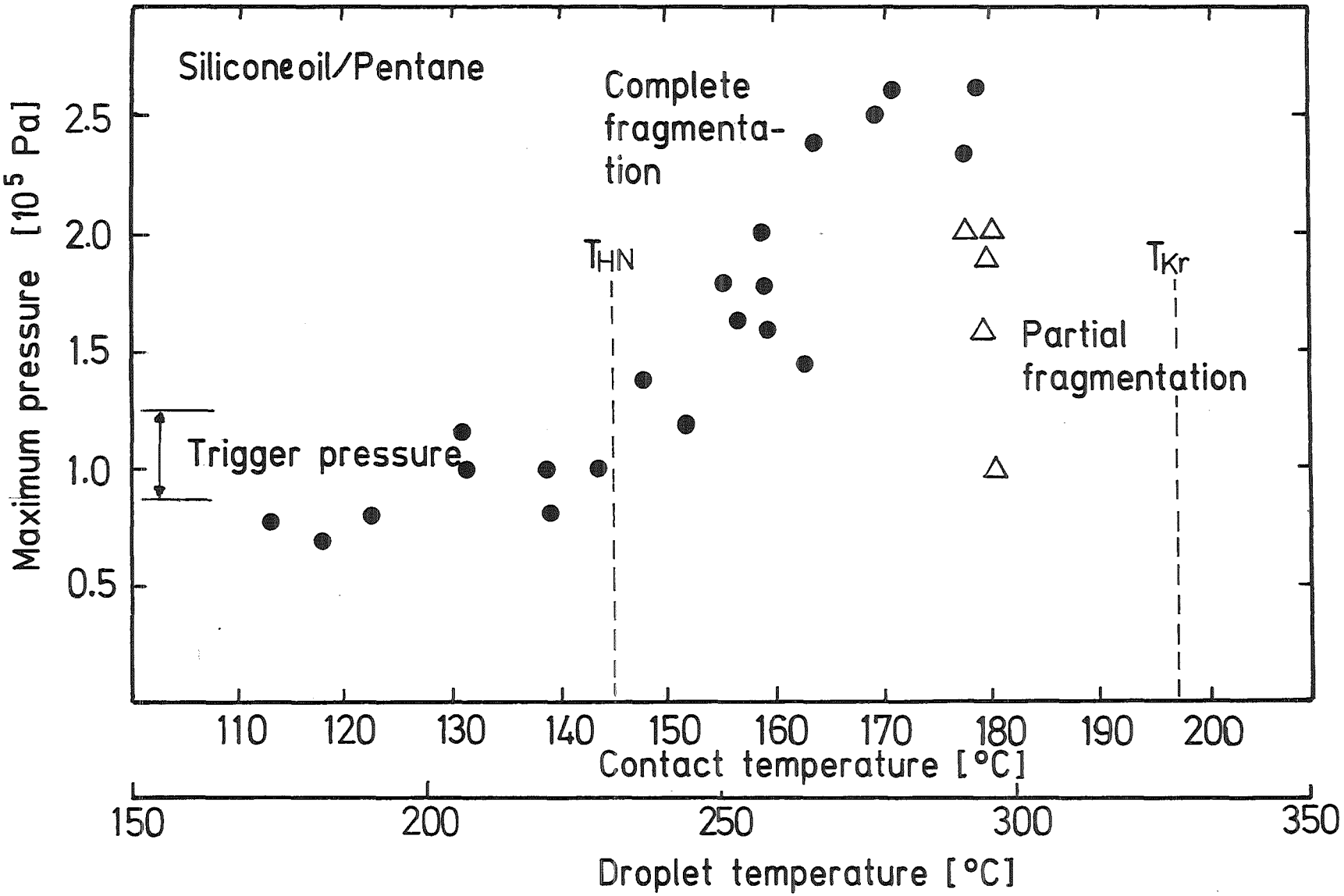

Fig. 21 Maximum Reaction Pressure as a Function of Droplet Temperature (Silicone Oil)

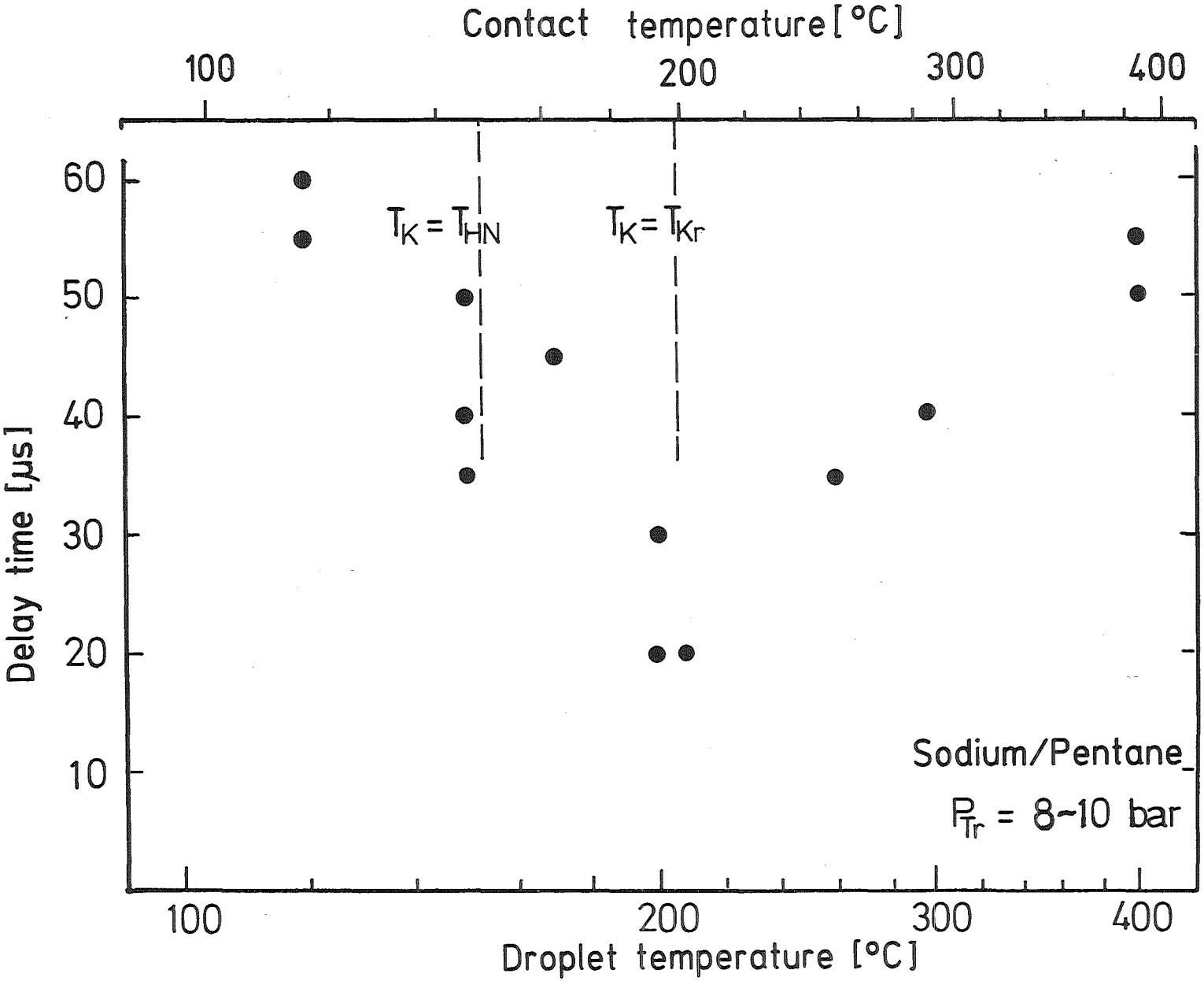

Fig.22 Delay Time as a Function of Droplet Temperature (Sodium)

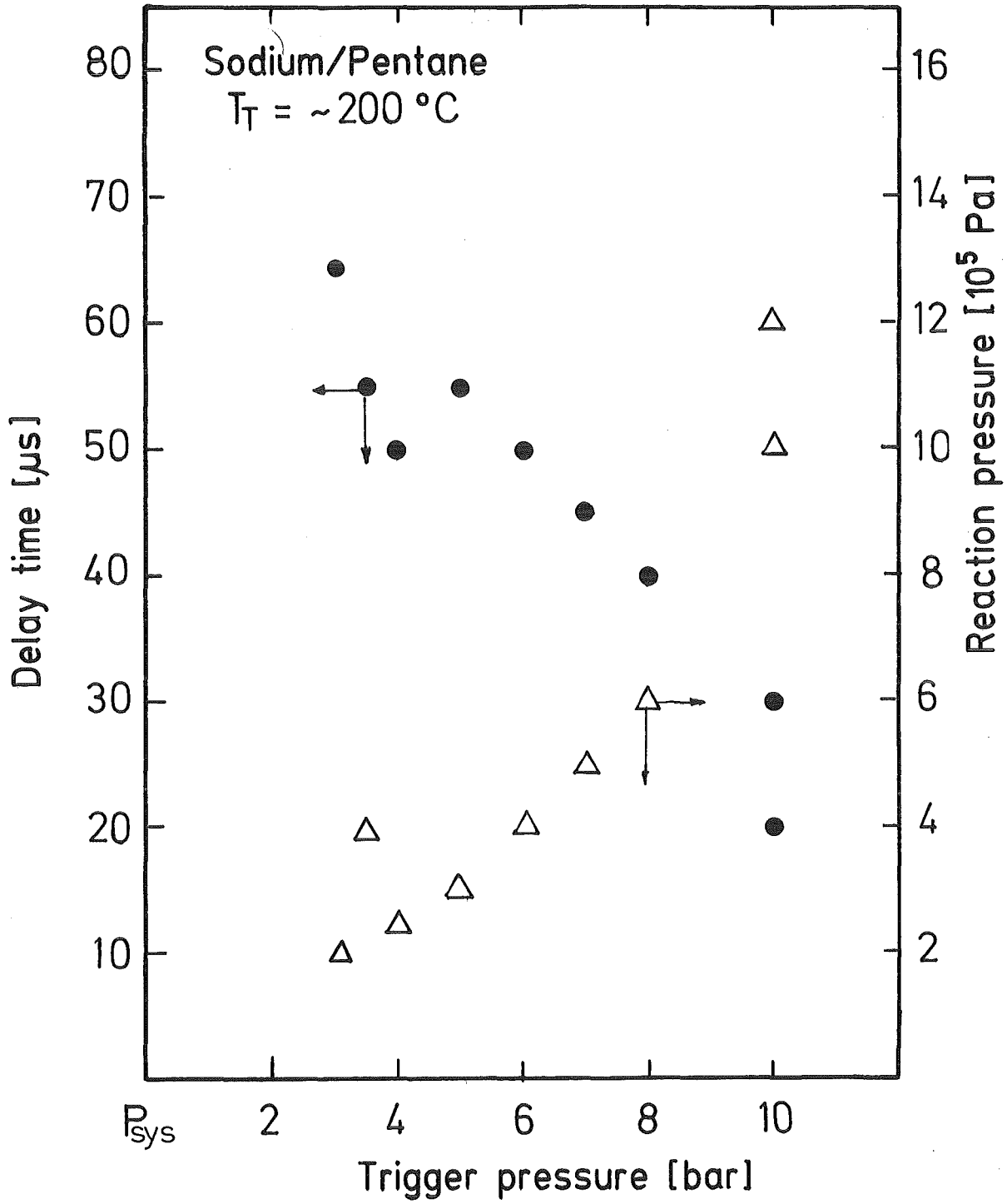

Fig. 23 Delay Time as a Function of Trigger Pressure (Sodium Droplets)

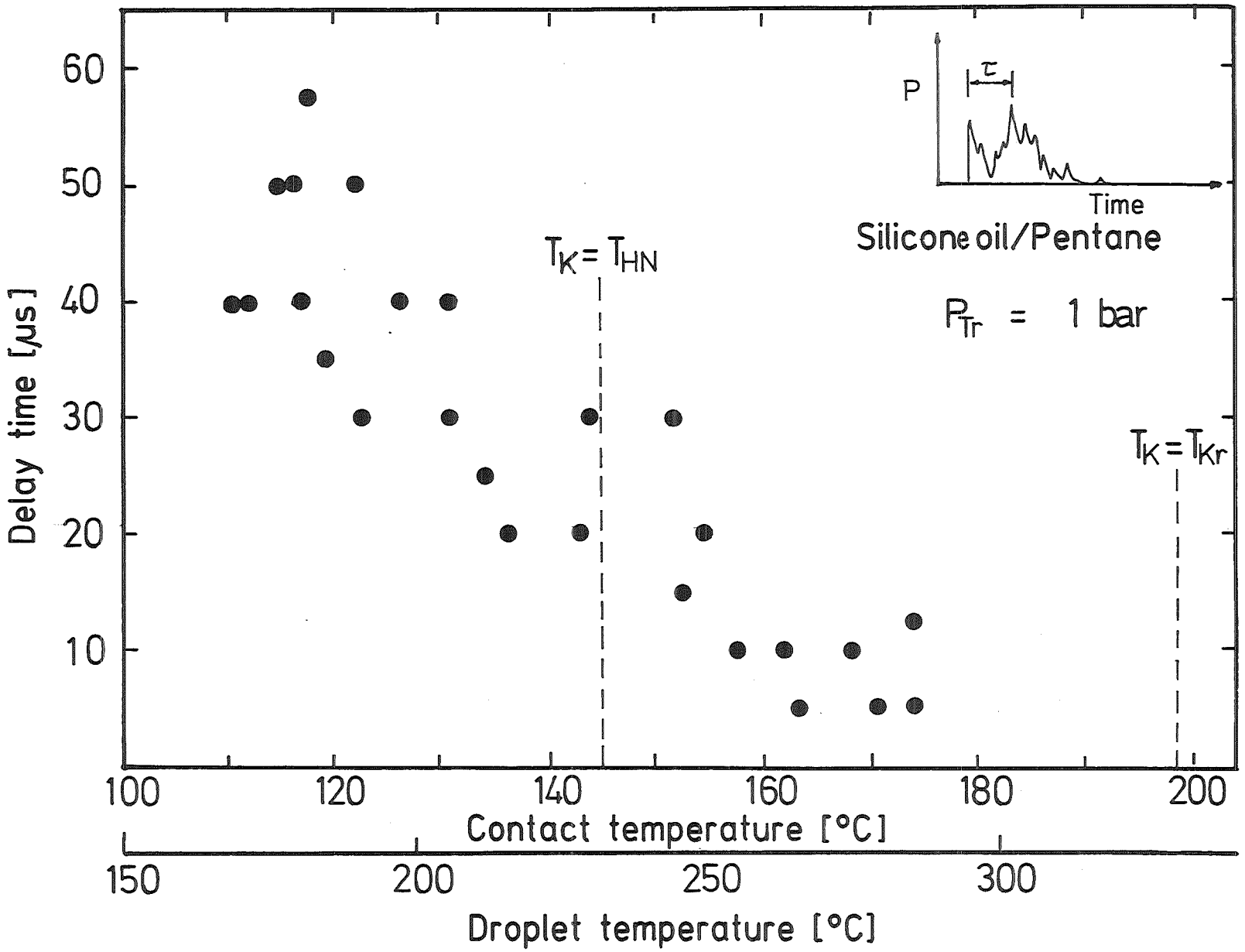

Fig. 24 Delay Time as a Function of Droplet Temperature (Silicone Oil)

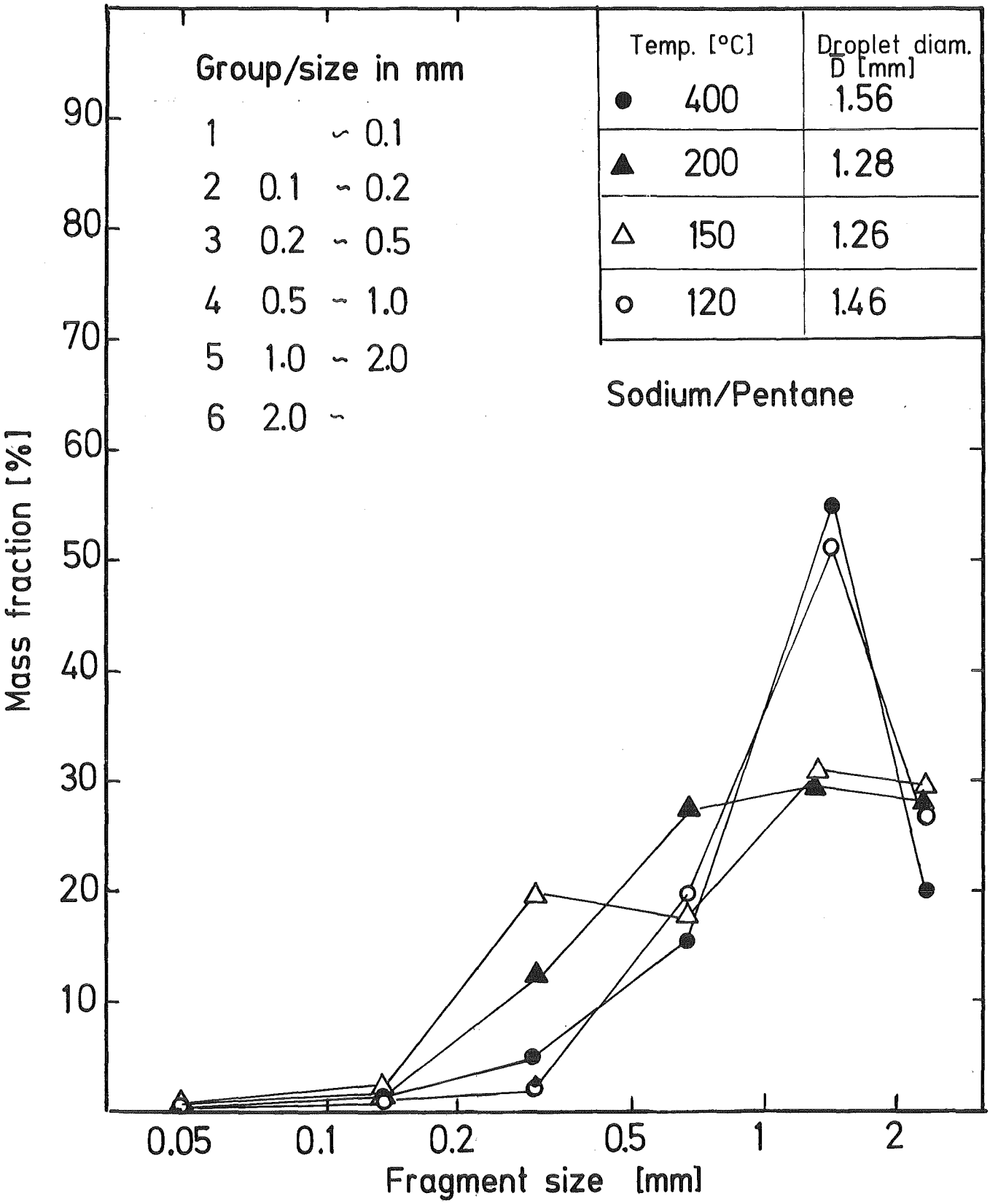

Fig. 25 Particle Size Distribution of Sodium Fragments (Mass Fraction)

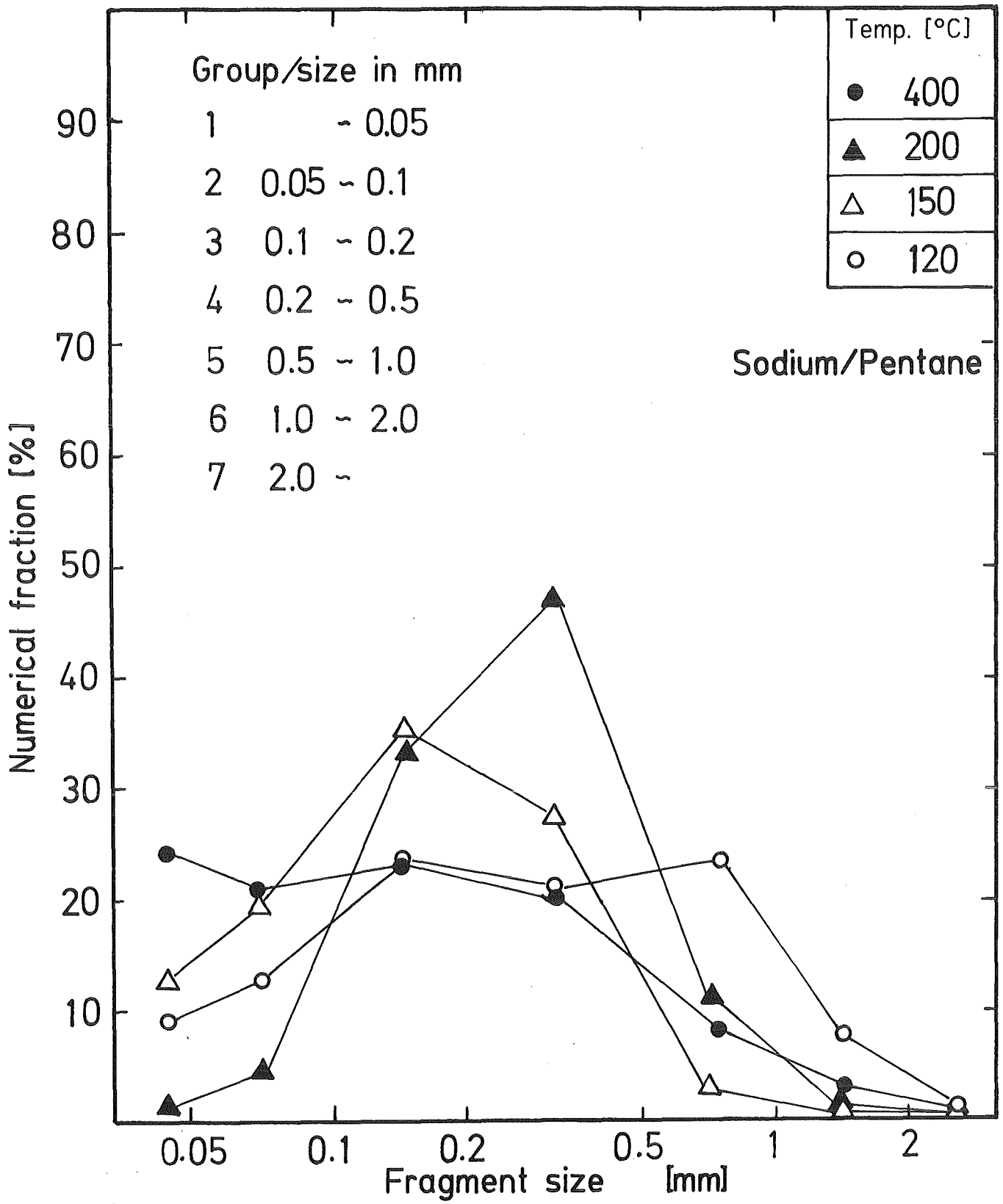

Fig. 26 Particle Size Distribution of Sodium Fragments (Frequency)

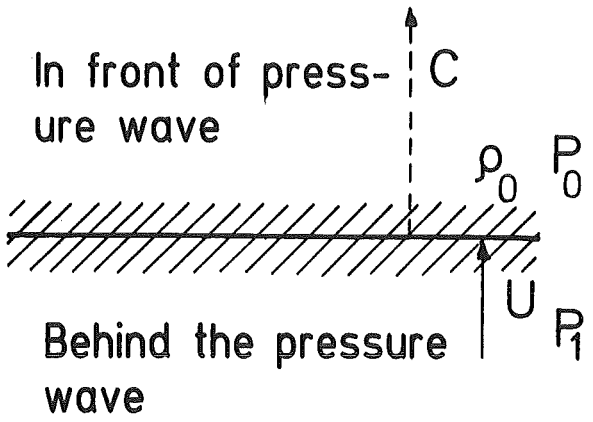

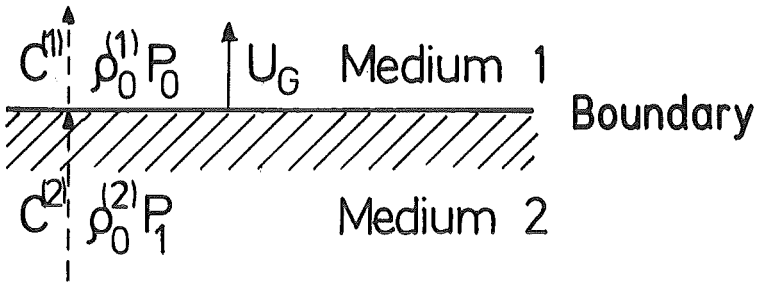

Movement of the boundary
due to pressure wave

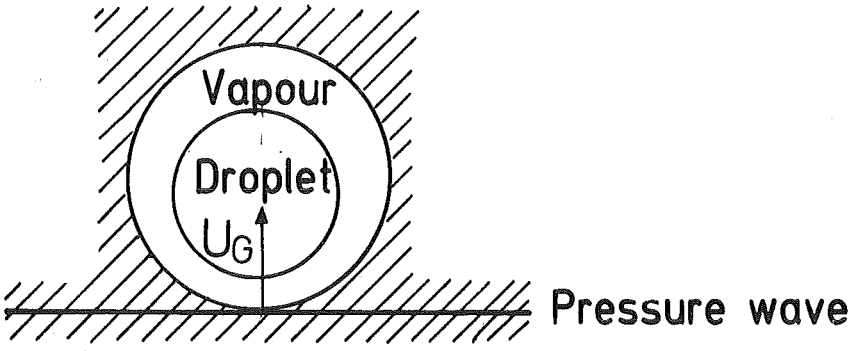

Reaction zone at the start of
collapse due to pressure wave

Fig. 27 Shock Wave Propagation and Vapour Film Collapse (First Mechanism)

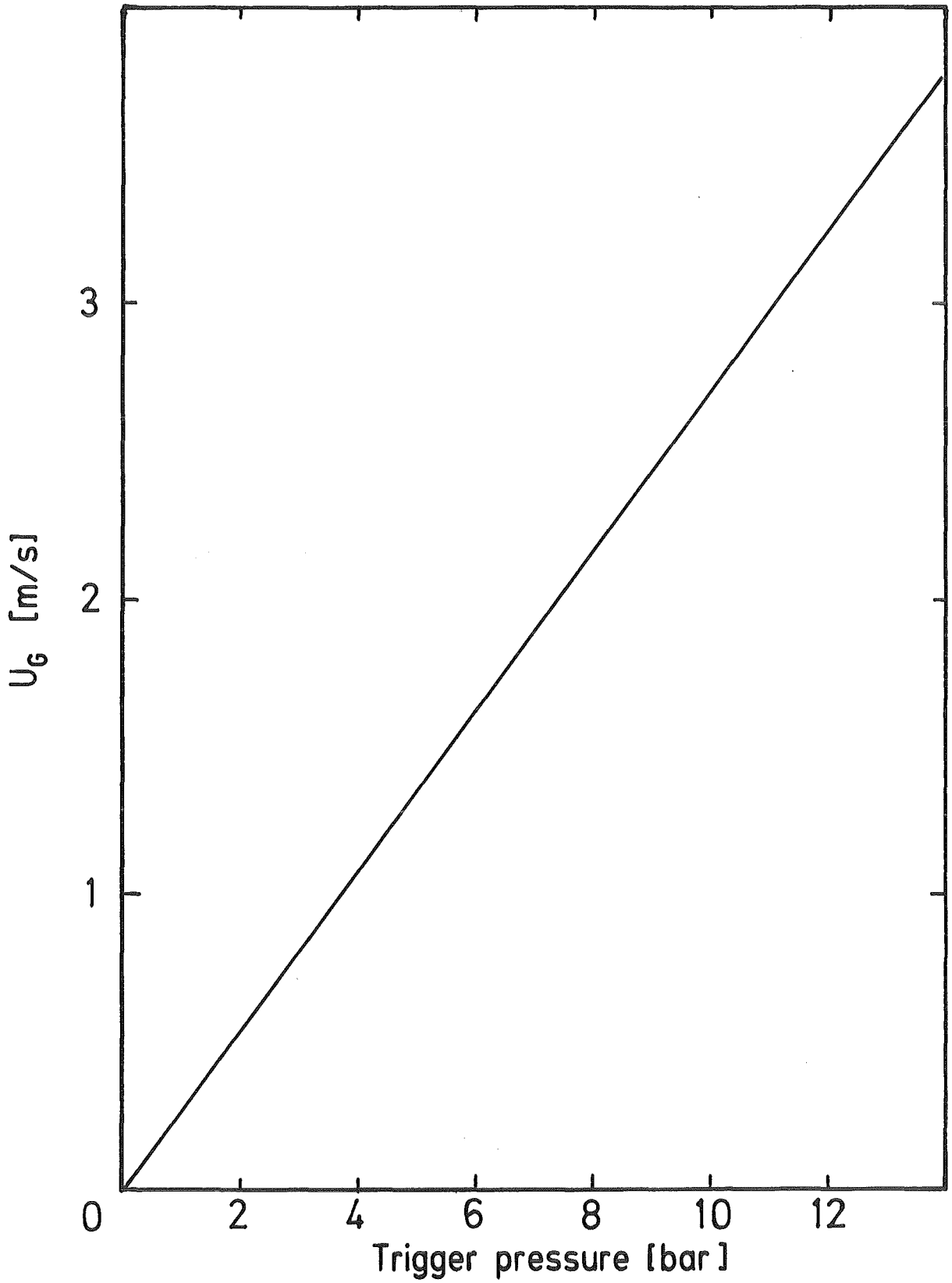

Fig. 28 Velocity of Reaction Zone Boundary Induced by the Shock Wave

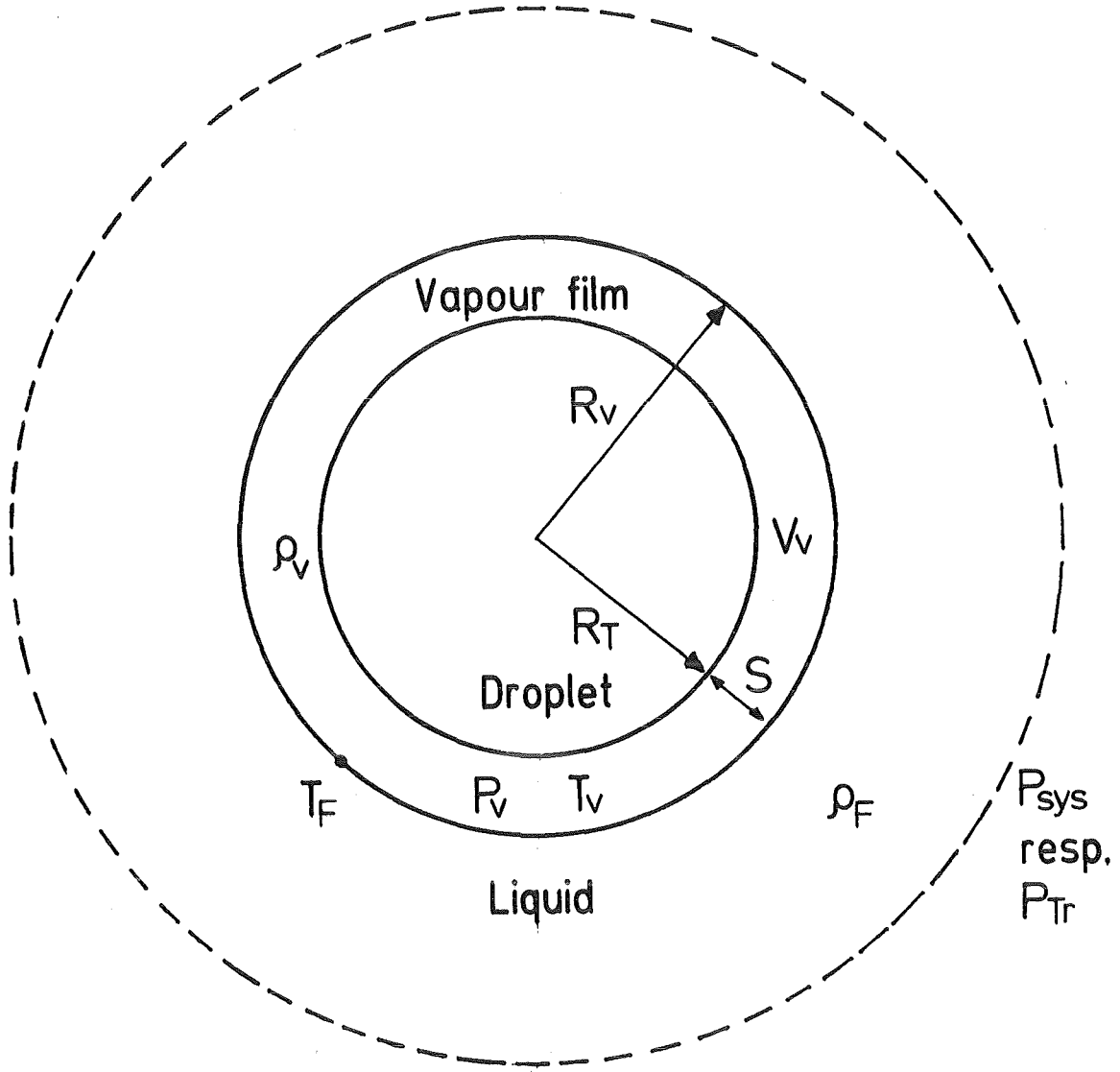

Fig. 29 Schematic Representation of Symmetric Vapour Film Collapse

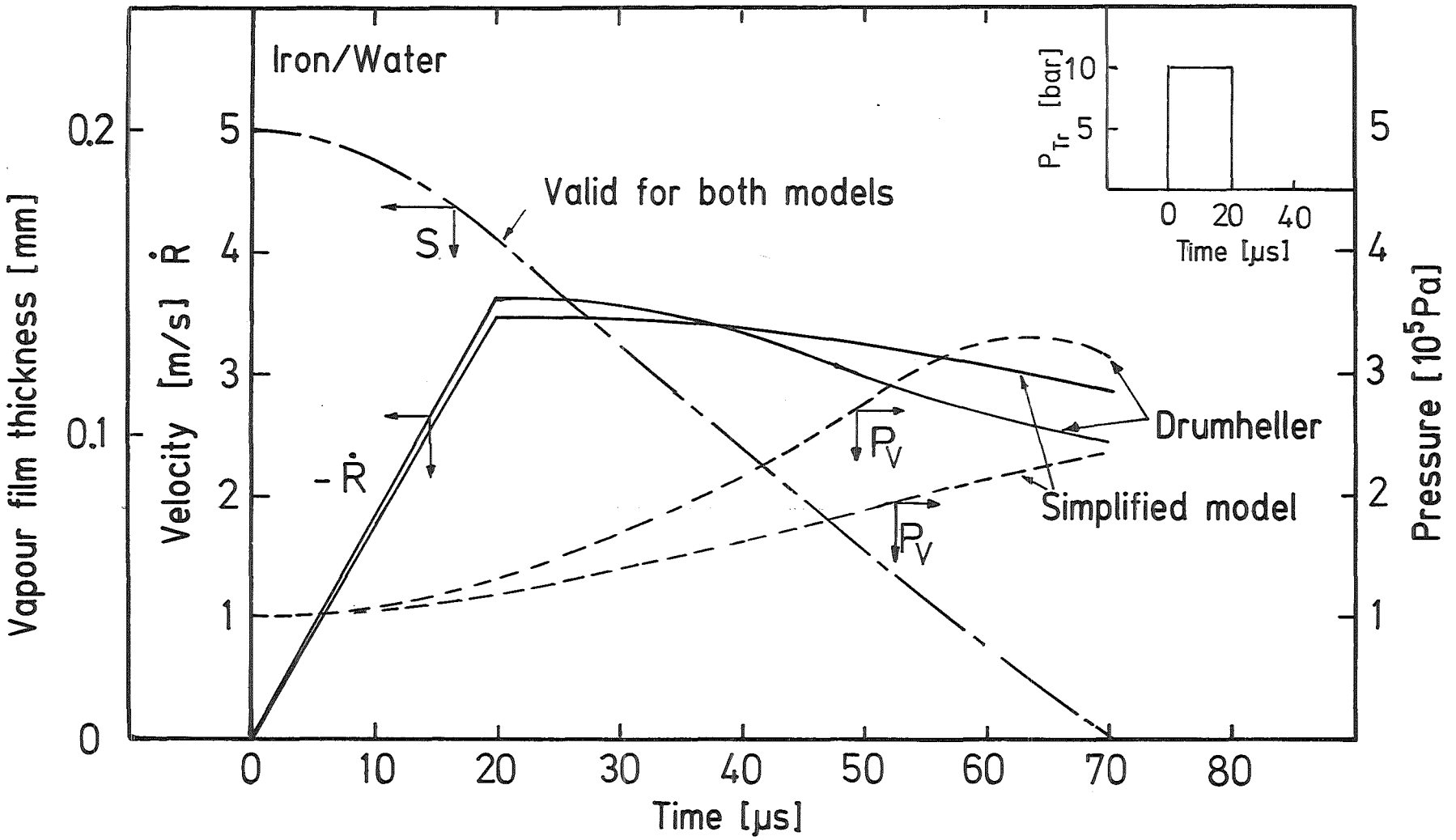

Fig.30 Calculated Example of the Vapour Film Collapse Process for Iron and Water as Compared with the Calculations presented by Drumheller /47/

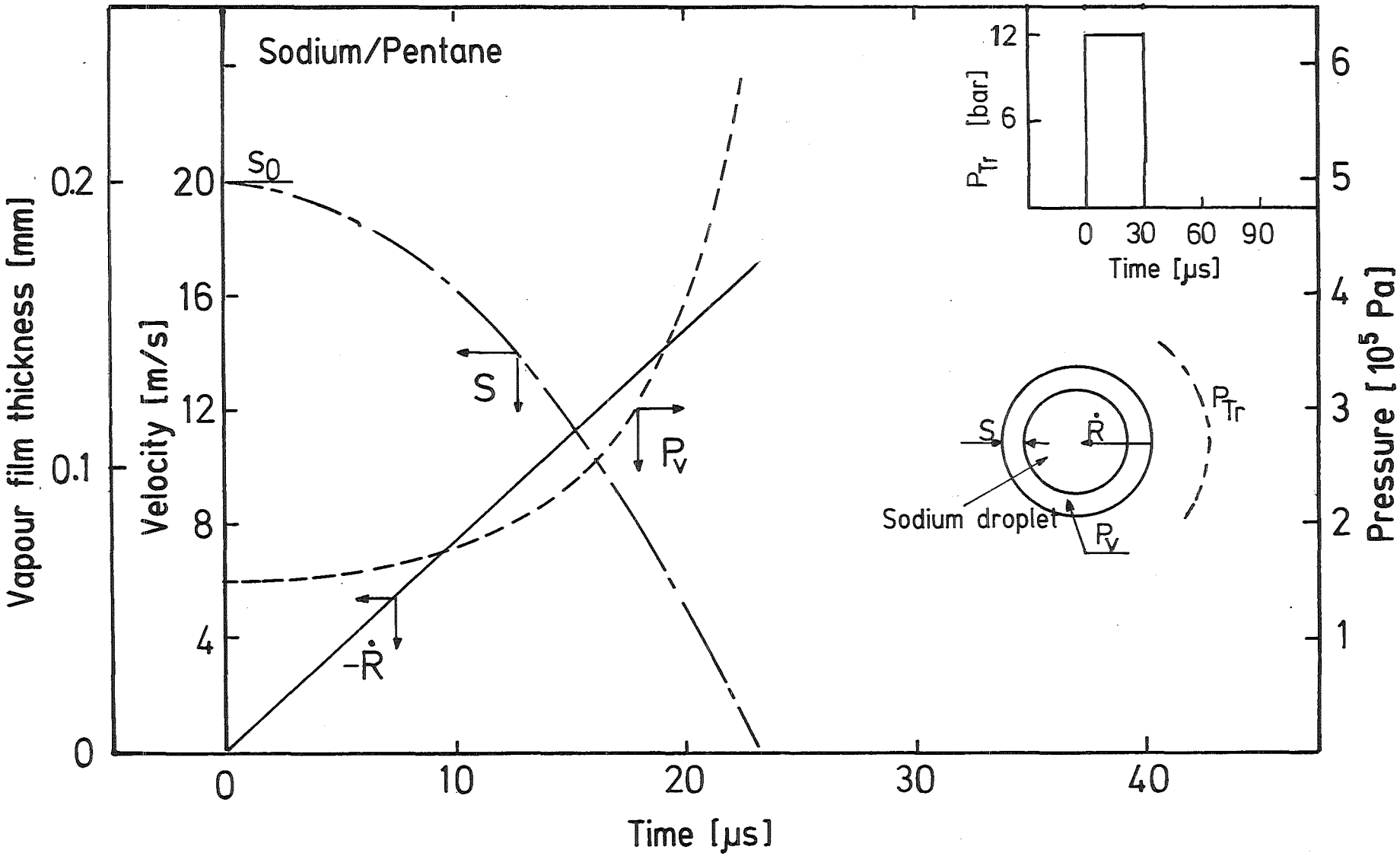

Fig.31 Calculated Vapour Film Collapse Process in the Sodium/Pentane System

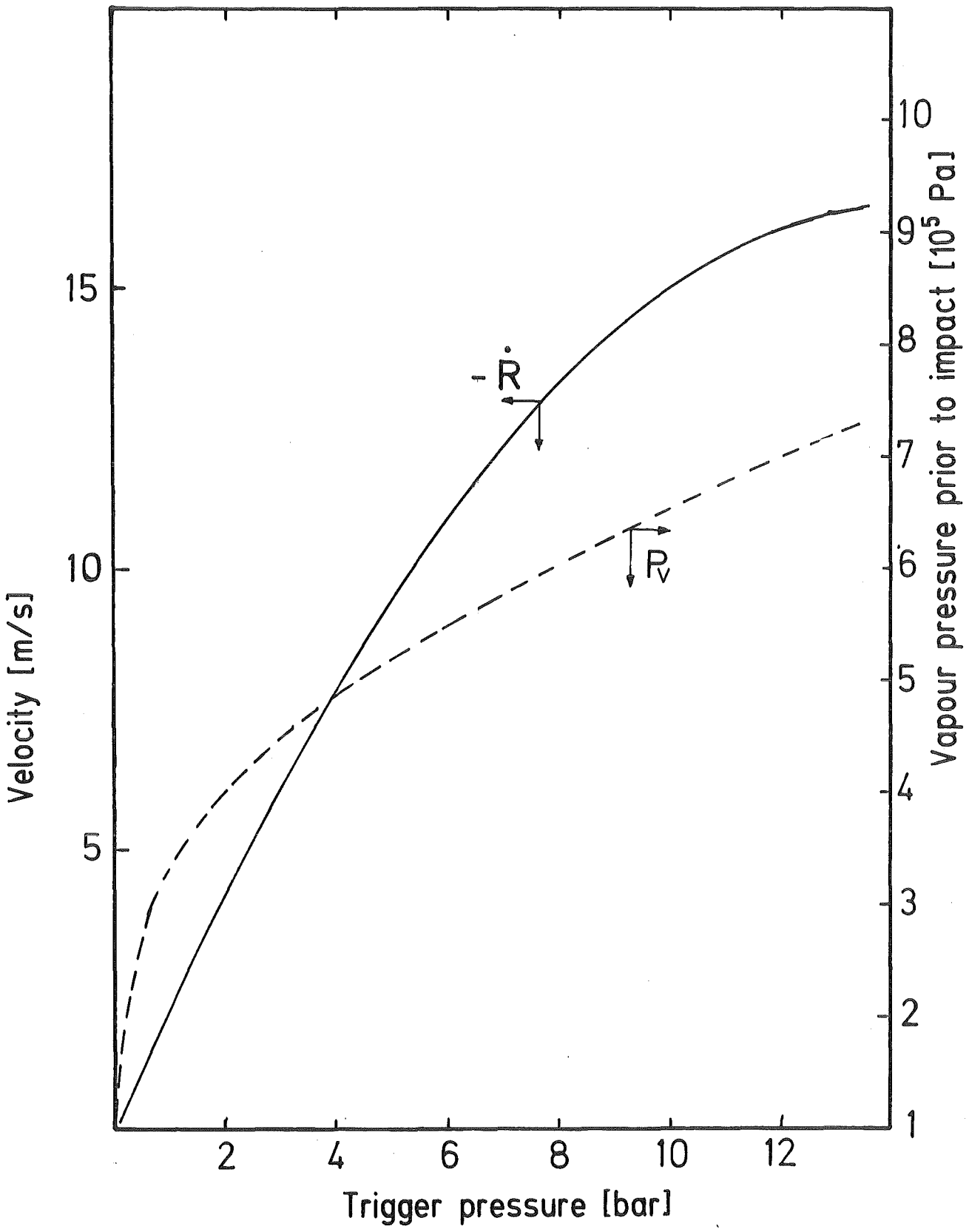

Fig. 32 Flow Velocity of the Liquid and Vapour Pressure before Impact on the Sodium Droplet

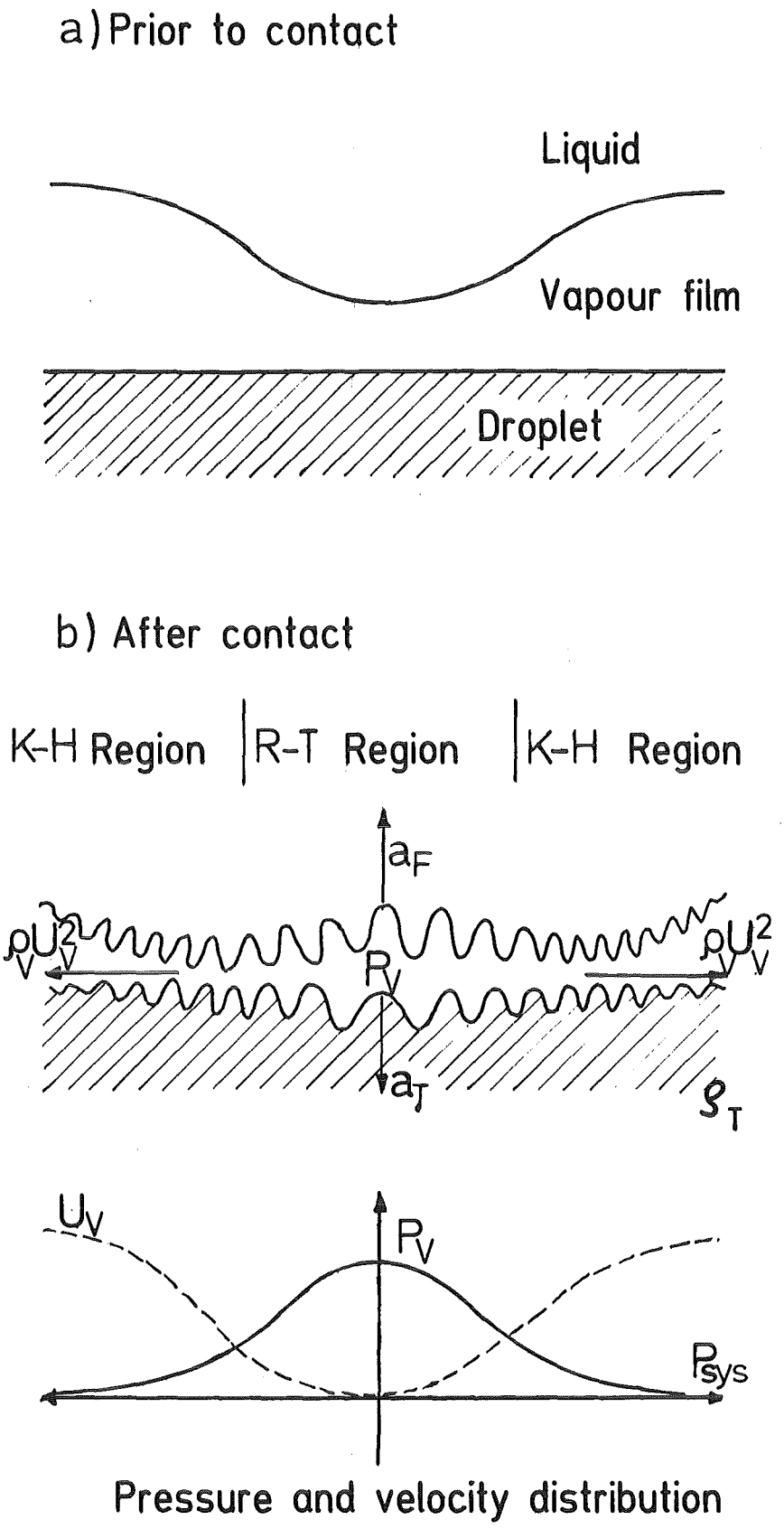

Fig. 33 Schematic Representation of the two Kinds of Instability in a Local Point of Contact

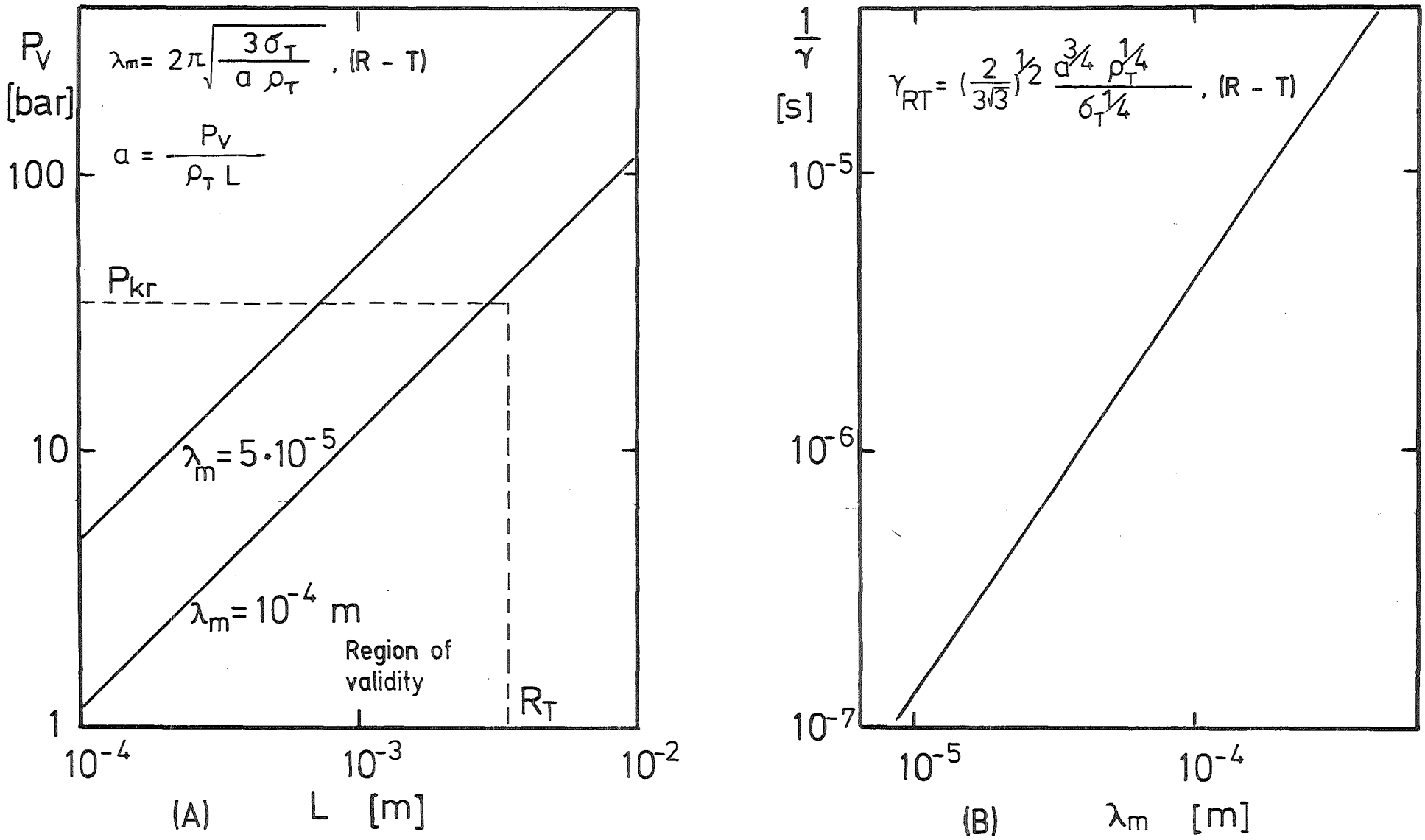

Fig.34 Fastest Growing Wavelength (A) and Growth Time Constant (B) for Rayleigh-Taylor Instability

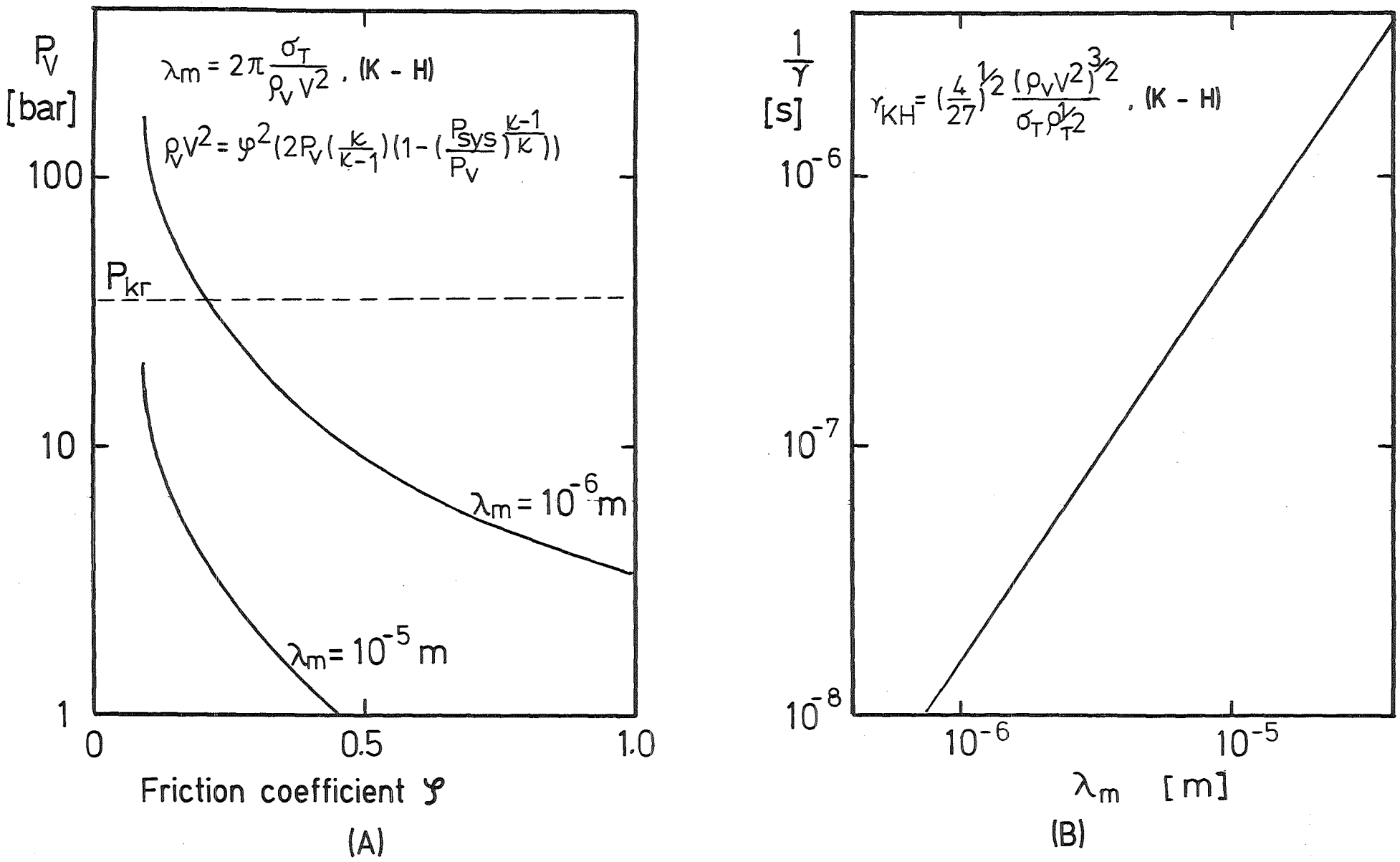

Fig.35 Fastest Growing Wavelength (A) and Growth Time Constant (B) for Kelvin-Helmholtz Instability

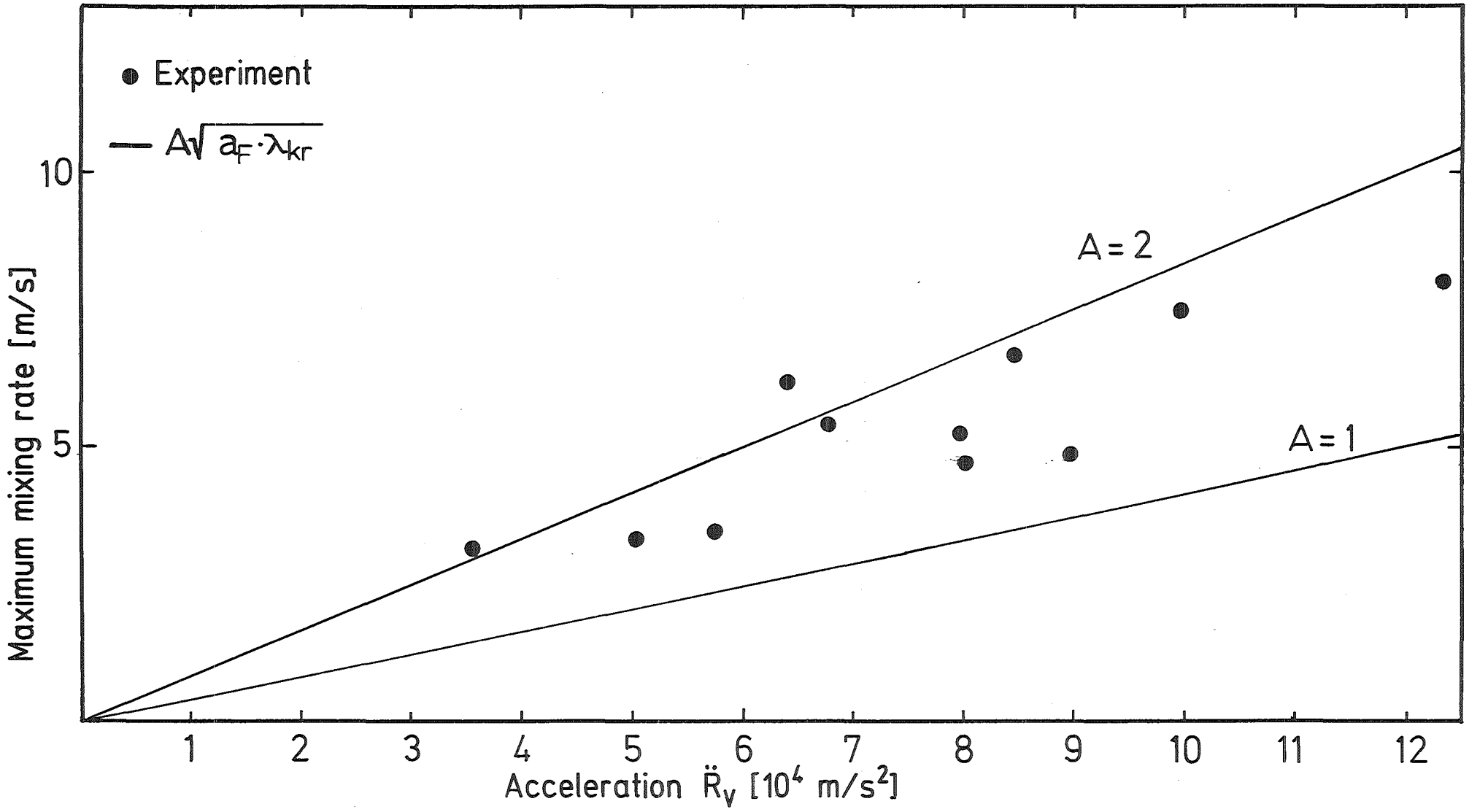

Fig.36 Maximum Mixing Rate of Liquid in the Experiments as Compared with Calculations

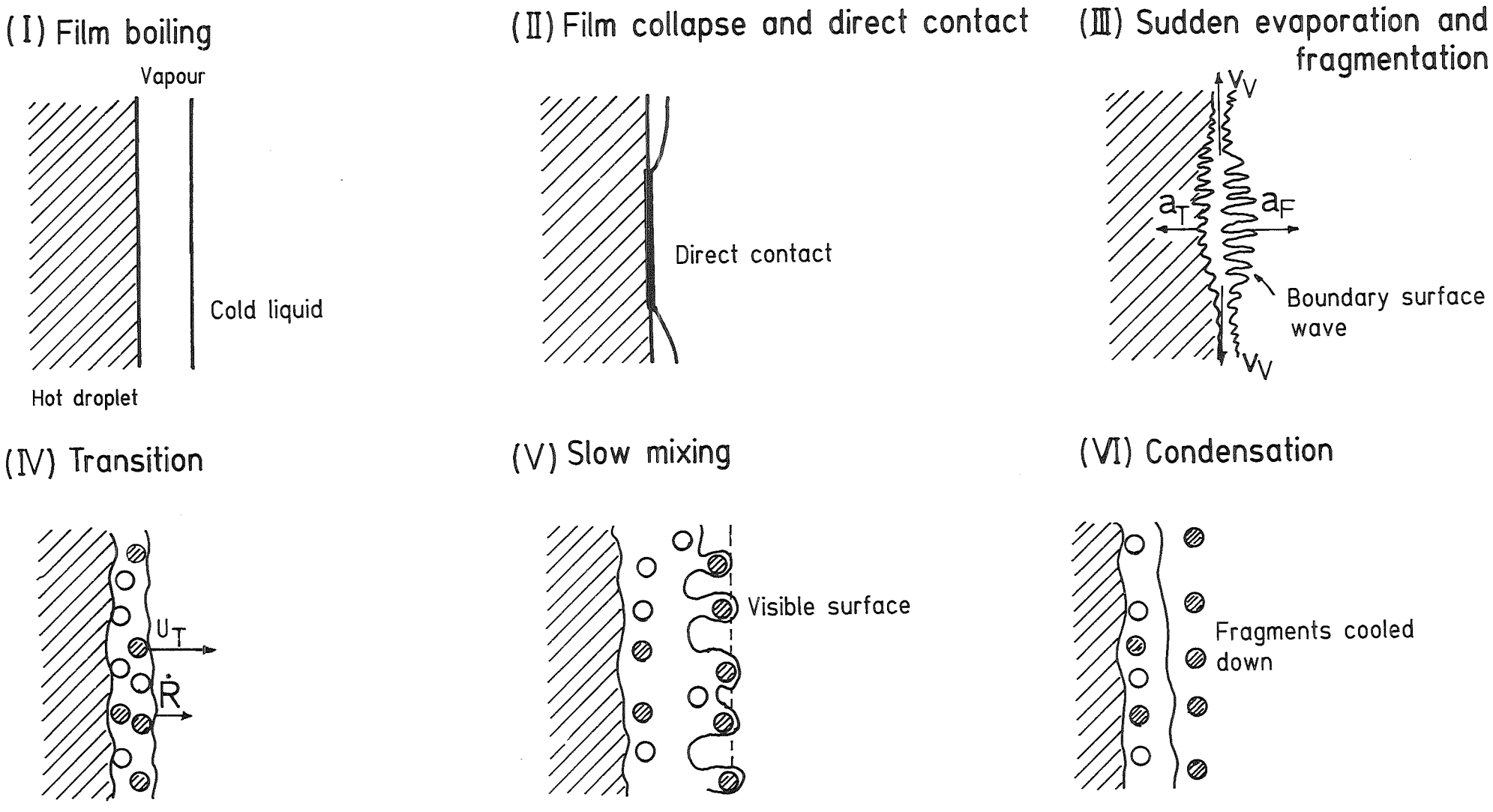

Fig.37 Schematic Fragmentation Model

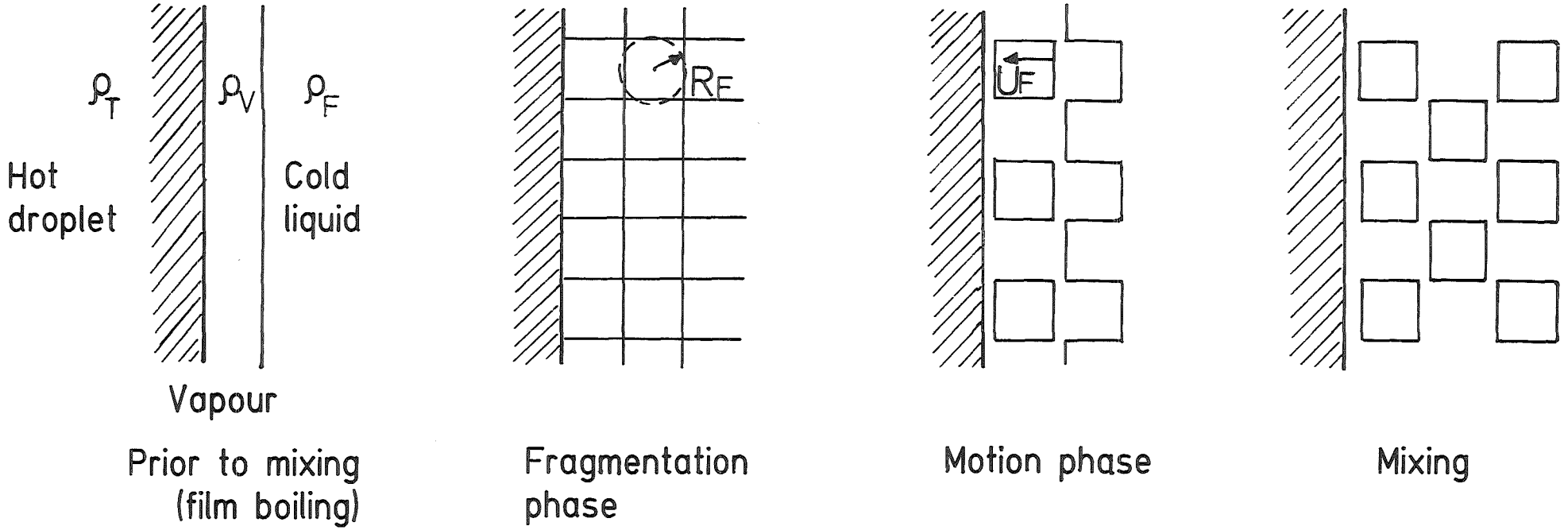

Fig. 38 Scheme for Assessment of the Mixing Energy

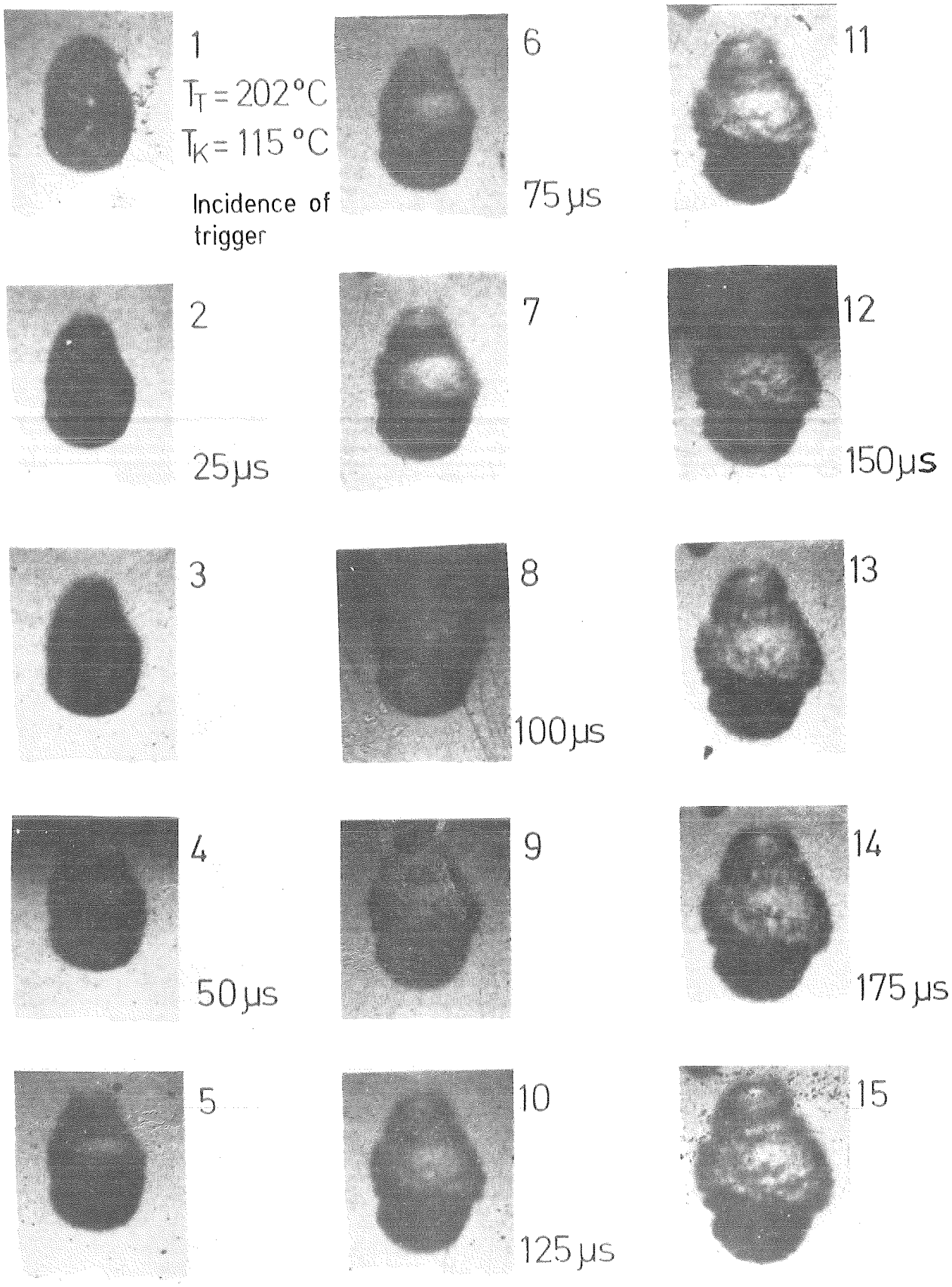

Silicone oil/Pentane P_{Tr} = 2 bar

Fig. 39 High-Speed Pictures Recorded for the Silicone Oil/Pentane System (1)

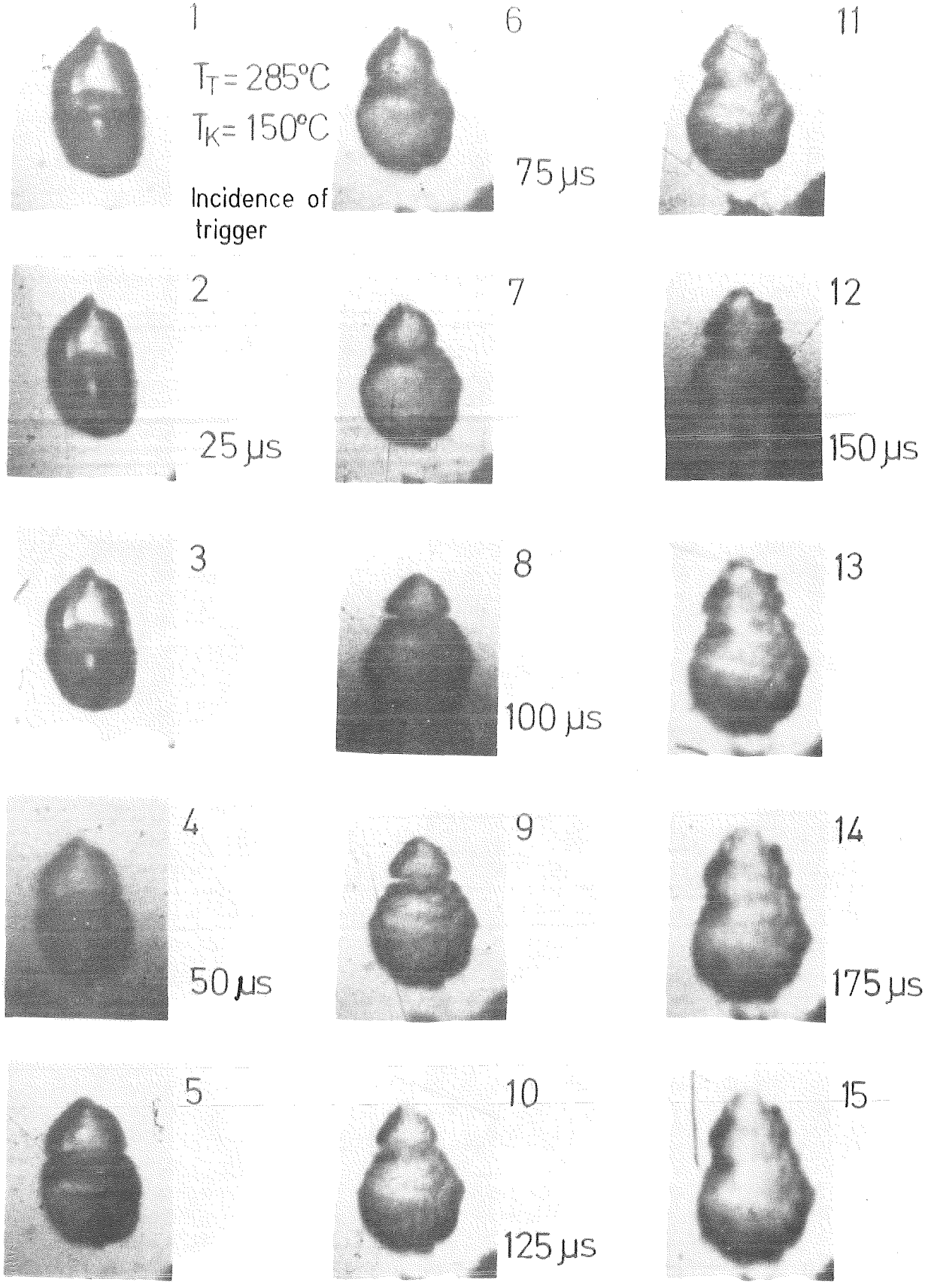

Silicone oil/Pentane P_{Tr} = 1.5 bar

Fig. 40 High-Speed Pictures Recorded for the Silicone Oil/Pentane System (2)

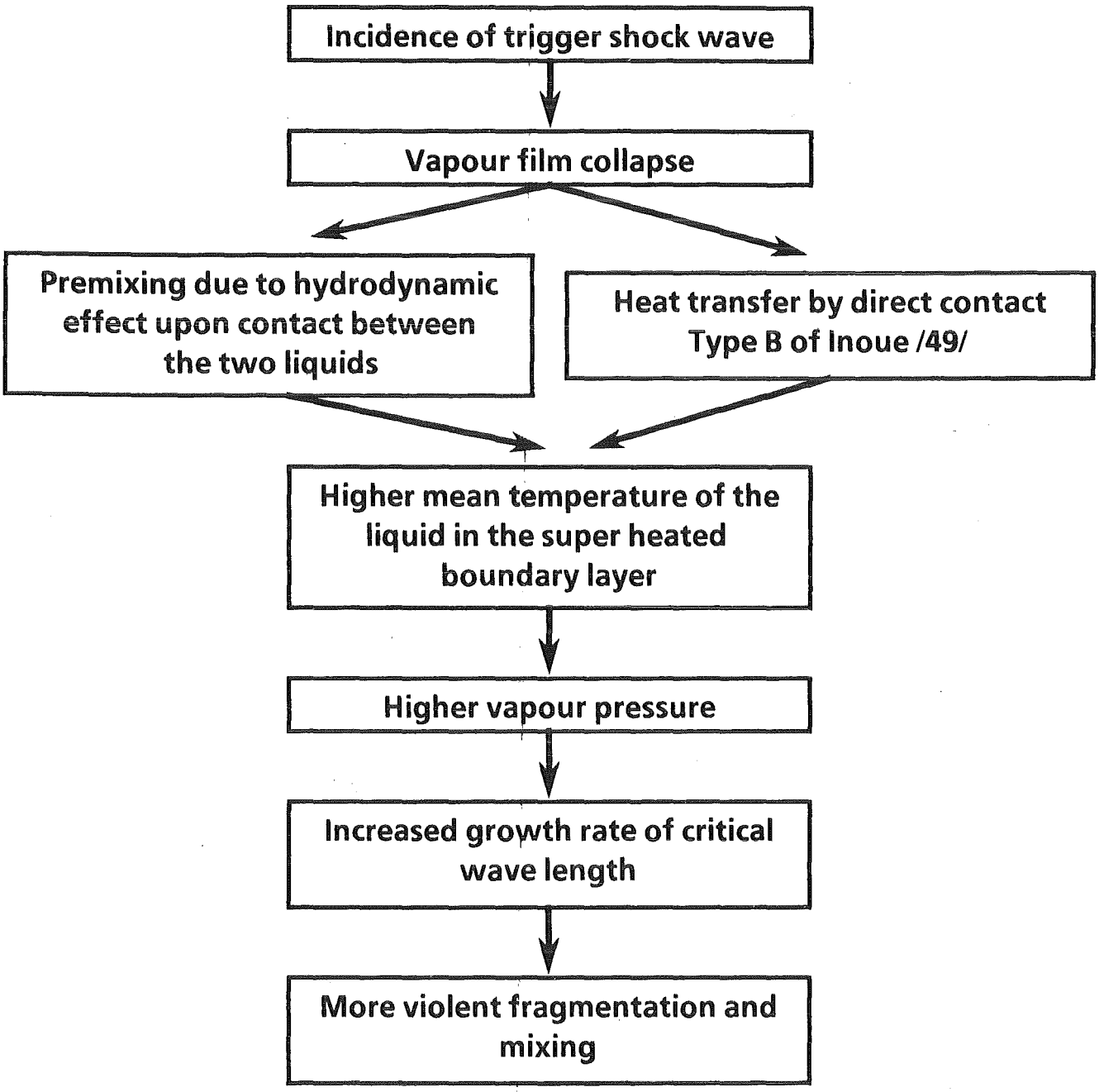

Fig. 41 Schematic Representation of the Mechanism of the External Trigger

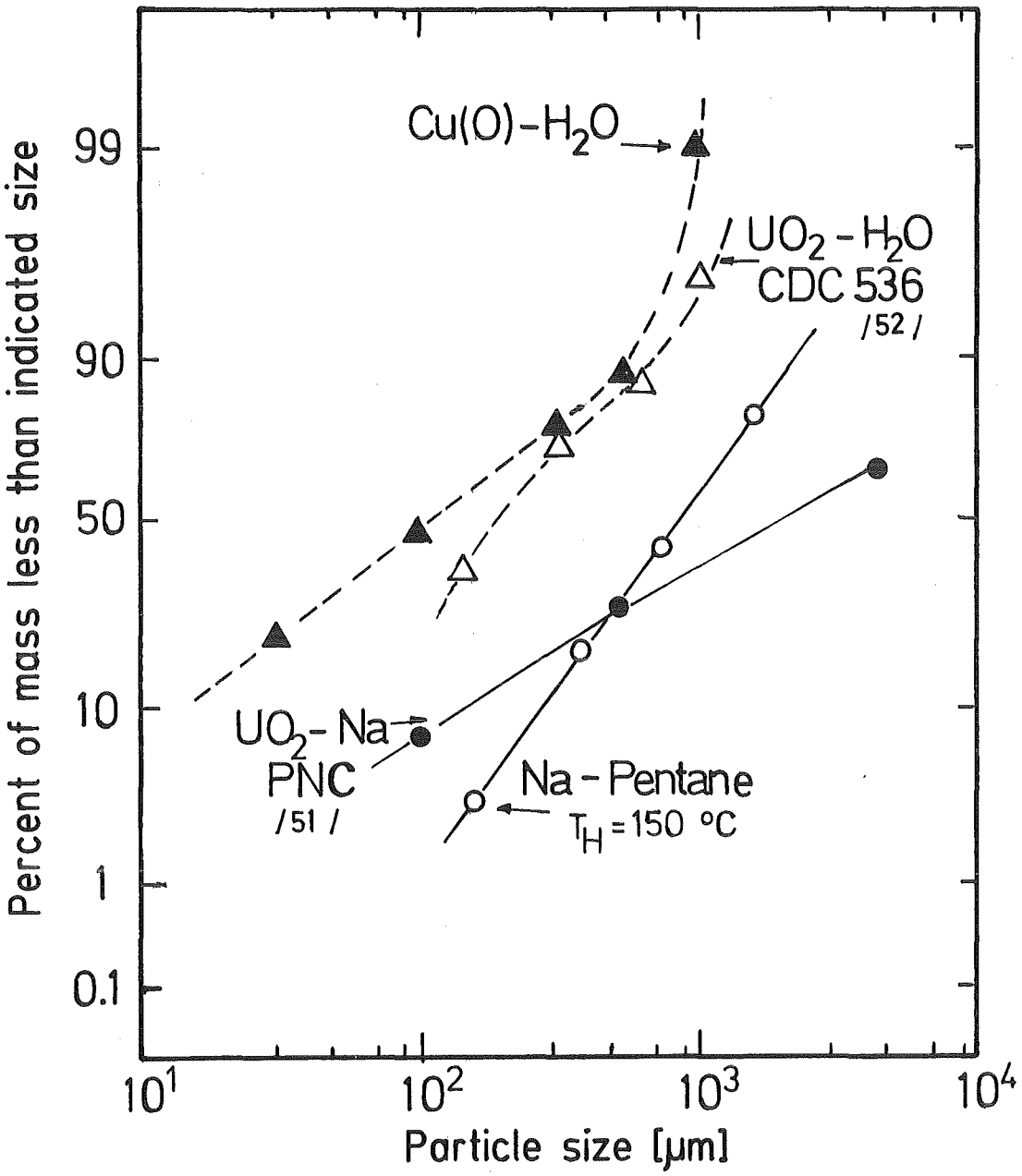

Fig. 42 Particle Size Distribution of Fragments for Different Systems of Materials

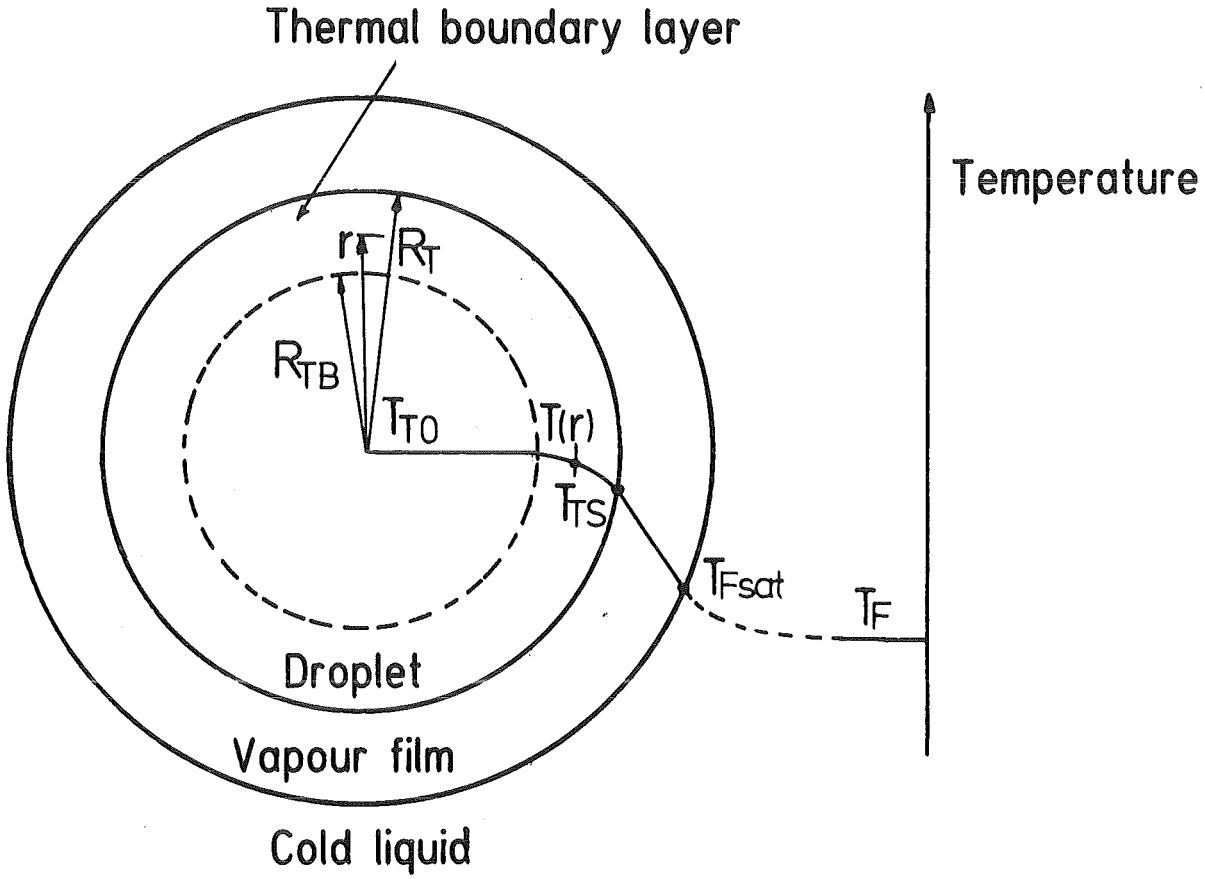

Fig. A-1 Schematic Temperature Distribution prior to Fragmentation

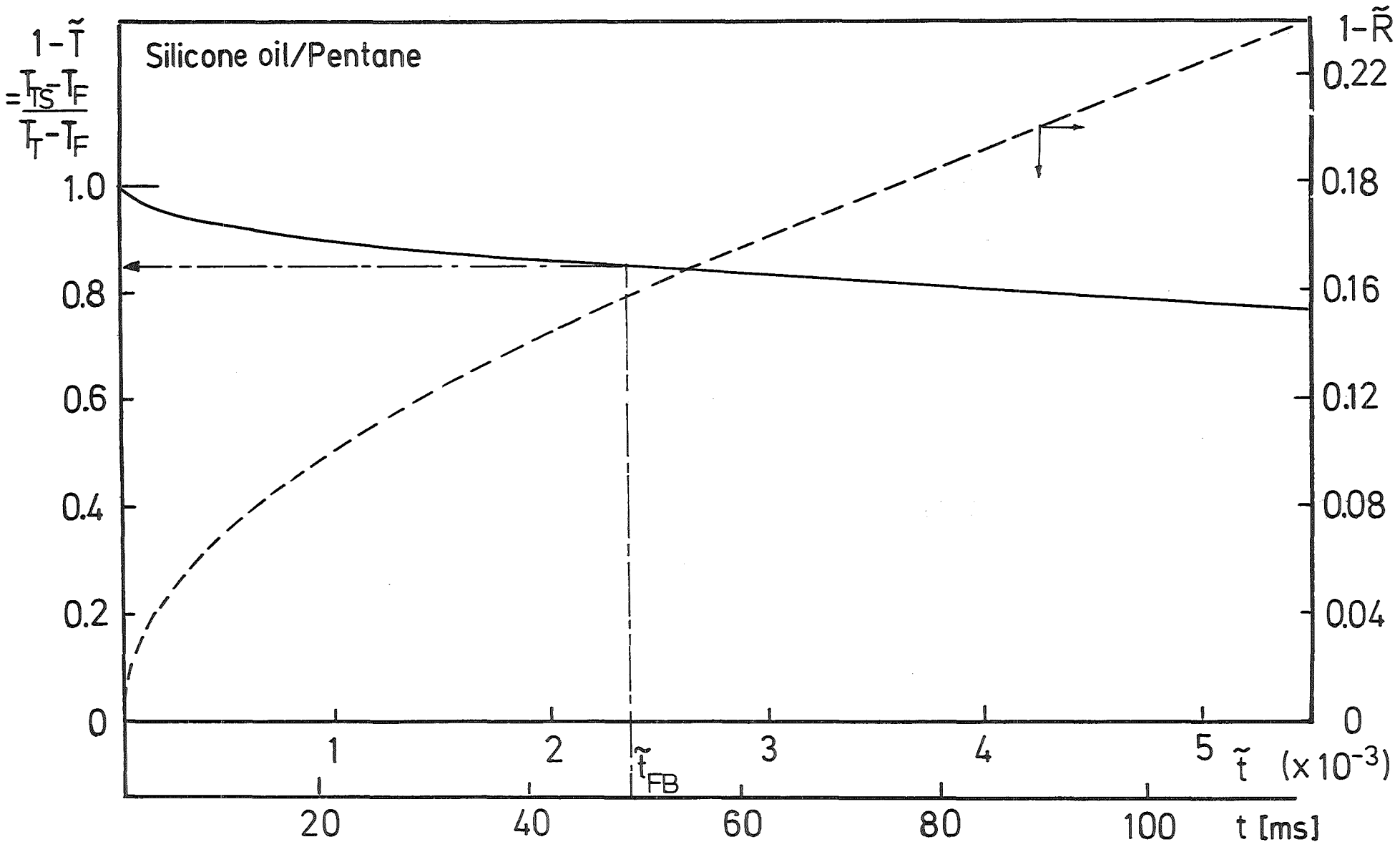

Fig.A-2 Time Curve of the Temperature and the Thermal Boundary Layer of the Droplet

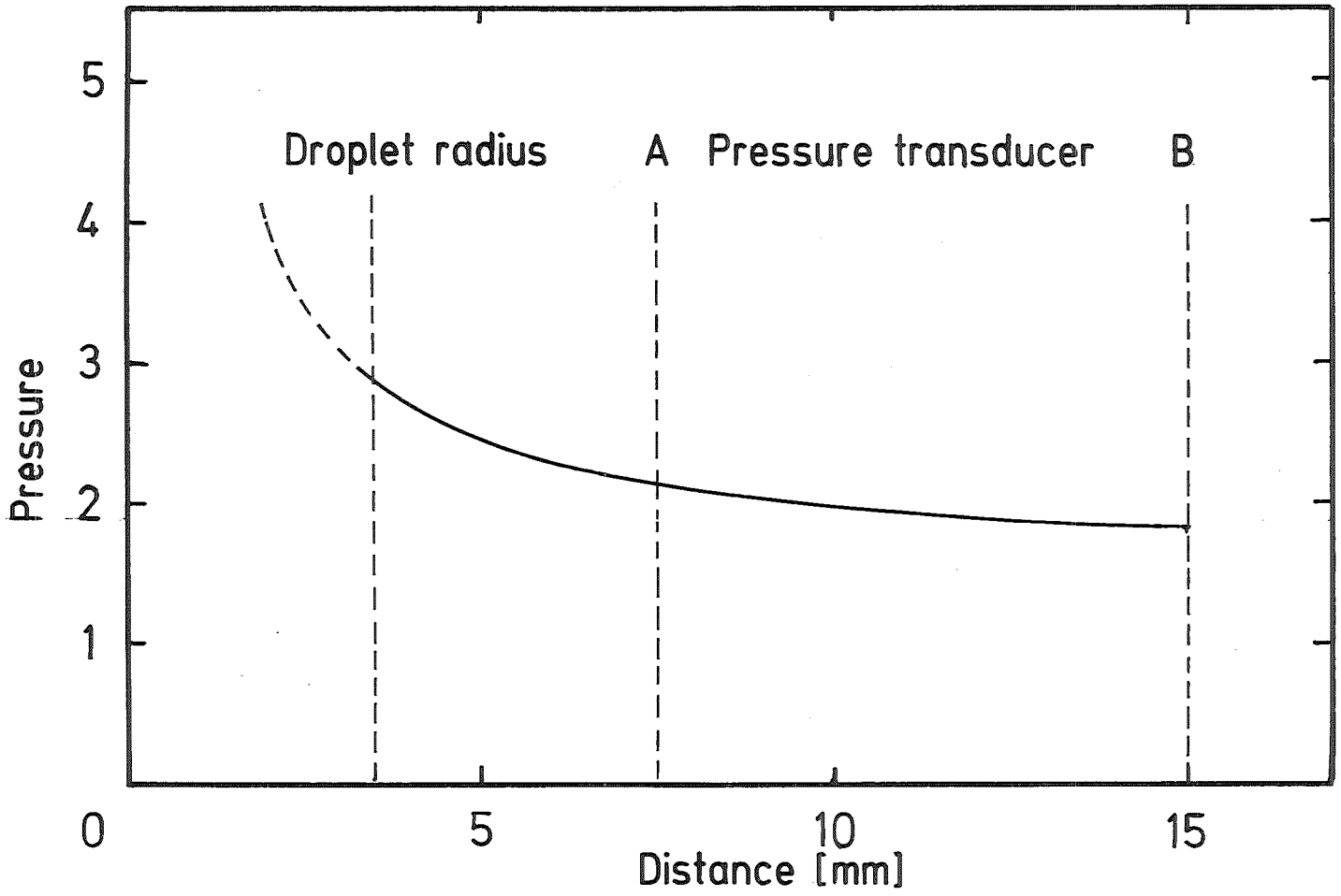

Fig.B-1 Radial Pressure Distribution in the Measuring Plane Calculated with the SING Code /54/